การสังเคราะห์อนุพันธ์เบนโซพอร์ไฟริน-ไทโอฟีนสำหรับการประยุกต์ทางอิเล็กทรอนิกส์เชิงแสง

นายวิทวัส แก้วส่องแสง

วิทยานิพนธ์นี้เป็นส่วนหนึ่งของการศึกษาตามหลักสูตรปริญญาวิทยาศาสตรมหาบัณฑิต
สาขาวิชาเคมี ภาควิชาเคมี
คณะวิทยาศาสตร์ จุฬาลงกรณ์มหาวิทยาลัย
ปีการศึกษา 2556

SYNTHESIS OF BENZOPORPHYRIN-THIOPHENE DERIVATIVES FOR OPTOELECTRONIC APPLICATIONS

Mister Wittawat Keawsongsaeng

A Thesis Submitted in Partial Fulfillment of the Requirements
for the Degree of Master of Science Program in Chemistry
Department of Chemistry
Faculty of Science
Chulalongkorn University
Academic Year 2013

Thesis Title	SYNTHESIS OF BENZOPORPHYRIN-THIOPHENE DERIVATIVES FOR OPTOELECTRONIC APPLICATIONS
By	Mister Wittawat Keawsongsaeng
Field of Study	Chemistry
Thesis Advisor	Assistant Professor Rojrit Rojanathanes, Ph.D.
Thesis Co-advisor	Assistant Professor Patchanita Thamyongkit, Ph.D.

Accepted by the Faculty of Science, Chulalongkorn University in Partial Fulfillment of the Requirements for the Master's Degree

……Dean of the Faculty of Science
(Professor Supot Hannongbua, Ph.D.)

THESIS COMMITTEE

……Chairman
(Assistant Professor Warinthorn Chavasiri, Ph.D.)

……Thesis Advisor
(Assistant Professor Rojrit Rojanathanes, Ph.D.)

……Thesis Co-advisor
(Assistant Professor Patchanita Thamyongkit, Ph.D.)

…… Examiner
(Assistant Professor Sumrit Wacharasindhu, Ph.D.)

……External Examiner
(Assistant Professor Nanthanit Wanichacheva, Ph.D.)

วิทวัส แก้วส่องแสง : การสังเคราะห์อนุพันธ์เบนโซพอร์ไฟริน-ไทโอฟีนสำหรับการประยุกต์ทางอิเล็กทรอนิกส์เชิงแสง (SYNTHESIS OF BENZOPORPHYRINS-THIOPHENE DERIVATIVES FOR OPTOELECTRONIC APPLICATIONS) อ . ที่ปรึกษาวิทยานิพนธ์หลัก : ผศ.ดร. โรจน์ฤทธิ์ โรจนธเนศ, อ. ที่ปรึกษาวิทยานิพนธ์ร่วม : ผศ.ดร. พัชณิตา ธรรมยงค์กิจ, 125 หน้า.

งานวิจัยนี้สังเคราะห์กลุ่มอนุพันธ์พอร์ไฟรินและเบนโซพอร์ไฟรินได้สำเร็จ ไทโอฟีนจำนวน 1 และ 2 วงถูกเติมในตำแหน่งมีโซของพอร์ไฟรินและเบนโซพอร์ไฟรินเพื่อเพิ่มการละลาย ขยายระบบคอนจูเกชัน และปรับปรุงสมบัติกายภาพเชิงแสงและเคมีไฟฟ้า พิสูจน์เอกลักษณ์ของสารประกอบที่สังเคราะห์ได้ทั้งหมดด้วยเอ็นเอ็มอาร์สเปกโทรสโคปี และมัลดิทอฟแมสสเปกโทรเมทรี สมบัติทางกายภาพเชิงแสงของสารสังเคราะห์ในรูปสารละลายและฟิล์มตรวจสอบด้วย ยูวี-วิสิเบิล และ ฟลูออเรสเซนส์สเปกโทรโฟโตเมทรี ข้อมูลทางสเปกโทรสโกปีแสดงให้เห็นว่าเมื่อจำนวนวงไทโอฟีนเพิ่มขึ้น จะพบการเคลื่อนที่ของค่าการดูดกลืนแสงและการคายแสงสูงสุดไปทางช่วงแสงสีแดงเนื่องจากระบบคอนจูเกชันที่ยาวขึ้น นอกจากนี้ไซคลิกโวลแทมเมทรีชี้ให้เห็นความเป็นไปได้ในการประยุกต์ใช้ในอุปกรณ์อิเล็กทรอนิกส์เชิงแสง โดยเฉพาะอย่างยิ่งเซลล์สุริยะ

ภาควิชา	เคมี	ลายมือชื่อนิสิต	
สาขาวิชา	เคมีอินทรีย์	ลายมือชื่อ อ.ที่ปรึกษาวิทยานิพนธ์หลัก	
ปีการศึกษา	2556	ลายมือชื่อ อ.ที่ปรึกษาวิทยานิพนธ์ร่วม	

5372331223 : MAJOR CHEMISTRY
KEYWORDS: BENZOPORPHYRINS/ THIOPHENE/ PHOTOACTIVE COMPOUND/ OPTOELECTRONICS APPLICATION

WITTAWAT KEAWSONGSAENG: SYNTHESIS OF BENZOPORPHYRINS-THIOPHENE DERIVATIVES FOR OPTOELECTRONIC APPLICATIONS. ADVISOR: ASST. PROF. ROJRIT ROJANATHANES, Ph.D., CO-ADVISOR: ASST. PROF. PATCHANITA THAMYONGKIT, Ph.D., 125 pp.

In this research, two series of *meso*-thiophene-linked porphyrin and benzoporphyrin derivatives were successfully synthesized. Mono- and bi-thiophene substituents were introduced into porphyrin and benzoporphyrin at the *meso*-positions in order to enhance the solubility, extend the conjugated system and improve photophysical and electrochemical properties. All synthesized compounds were characterized by NMR spectroscopy and MALDI-TOF mass spectrometry. Their optical properties were also investigated by UV-Vis and fluorescence spectrophotometry in both solution and film. The spectroscopic data revealed that with an increasing number of the thiophenyl rings, the red shift of absorption and emission maxima were observed due to the higher conjugation system. Moreover, cyclic voltammetry indicated the potential application in optoelectronic devices, especially solar cells.

Department: Chemistry Student's Signature .....

Field of study: Organic chemistry Advisor's Signature .....

Academic Year: 2013 Co-advisor's Signature .....

ACKNOWLEDGEMENTS

Firstly, the author would like to express his deepest gratitude to Assistant Professor Dr. Rojrit Rojanathanes and Assistant Professor Dr. Patchanita Thamyongkit for the extensive support, valuable advices and kindness in this project. The success of this thesis could not be achieved without one of them.

The author also wish to express appreciation to Assistant Professor Dr. Warinthorn Chavasiri, for serving as the chairman, Assistant Professor Dr. Sumrit Wacharasindhu and Assistant Professor Dr. Nantanit Wanichacheva for serving as the members of this thesis committee, respectively, for all of their valuable suggestion and comments in this research.

Finally, the author would like to thank his family for their fully support, care and encouragement for an entire of this course.

CONTENTS

Page

Page

LIST OF FIGURES

LIST OF SCHEMES

LIST OF ABBREVIATIONS

^{1}H-NMR	:	proton nuclear magnetic resonance spectroscopy
^{13}C-NMR	:	carbon-13 nuclear magnetic resonance spectroscopy
$CDCl_3$	:	deuterated chloroform
δ	:	chemical shift
s	:	singlet (NMR)
d	:	doublet (NMR)
m	:	multiplet (NMR)
dd	:	doublet of doublet (NMR)
td	:	triplet of doublet (NMR)
g	:	gram(s)
mg	:	milligram(s)
mmol	:	millimole(s)
equiv	:	equivalent(s)
mL	:	millilitre(s)
°C	:	degree Celcius
h	:	hour(s)
d	:	day(s)
rt	:	room temperature
eV	:	electron volt(s)
HOMO	:	highest occupied molecular orbital
LUMO	:	lowest unoccupied molecular orbital
E_{gap}	:	energy bandgap
λ	:	wavelength
λ_{ex}	:	excitation wavelength
λ_{abs}	:	absorption wavelength
λ_{emit}	:	emission wavelength
ε	:	molar absorptivity
MHz	:	megahertz (million Hertz)
TLC	:	thin layer chromatography

R_f	:	retardation factor
m/z	:	mass per charge ratio
obsd	:	observed
calcd	:	calculated

CHAPTER I

INTRODUCTION

Nowadays, the population and economic growth are highly increased every year thus the energy consumption is the first main crisis problem that needs to be considered. Approximately, the source of energy is made up of about 86% fossil fuels, 6% nuclear power, 6% hydroelectricity and a few fraction from biomass and solar energy [1]. Due to the byproducts of those non-renewable energy consumed processes such as greenhouse gases, i.e. CO, CO_2 and NO_x, carbon soot or even radioactive wastes, the environmental degeneration cannot be avoided. Consequently, the development of renewable and environmental friendly energy sources become an important topic in many research areas.

The sun is one of the best candidate energy resource due to its nearly unlimited lifetime, stable energy and availability everywhere on earth. Sun also creates energy through thermonuclear process converting about 650,000,000 tons [2] of hydrogen to helium every second which is higher than all of the energy used in human history. According to such advantages, development of efficient solar cell (also called photovoltaic cell) is one of the challenging topic of all time.

Solar cells are one of optoelectronic devices converting light energy directly to electricity by a photovoltaic effect, where voltage or electric current is created during the exposure of the material to light. Though inorganic semiconductor solar cells (crystalline and amorphous Si, CdTe and $CdIn_{1-x}Ga_xSe_2$ thin film [3]) are popular in present but, in fact, high-technology production is required in high cost [4]. Whilst, the interests in organic solar cells are increasing every year due to their flexibility, high efficiency and much lower cost compared to inorganic photovoltaic devices. The efficiency of the organic photovoltaic devices highly relies the photoactive compounds. Among all organic photosentisizer, porphyrinic compounds are in spotlight in recent years as photoactive compounds for optoelectronic applications [5] due to their extremely high absorption coefficients [6], high thermal and photo-stabilities [7]. Moreover, their electrochemical and photophysical properties can be

varied by changing the metal center and/or substituents at the macrocycle peripheral positions [8]. Porphyrins have also been reportedly useful of as photocatalysts, optical sensors [9], organic semiconductors [10], organic light-emitting diodes (OLEDs) or even as dye-sensitized solar cells (DSSCs) and bulk-heterojunction solar cells (BHJSCs) [11]. Recently, it has been reported that tetrabenzoporphyrin, porphyrin derivative with extended π-conjugated system (**Figure 1-1**), can be used as p-semiconductors in thin film solar cell providing up to 8.5% cell efficiency [12]. However, to the best of our knowledge, the impact of the substituents on the framework of the benzoporphyrin macrocycle has not been reported.

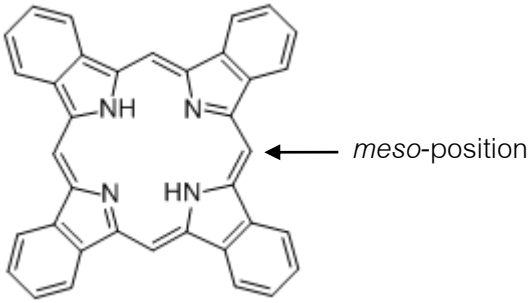

Figure 1-1: Structure of tetrabenzoporphyrin

In this research, we aim to synthesize a series of benzoporphyrinic compounds bearing oligothiophene moieties on their *meso*-positions. Thiophene and their oligomers, α-conjugated oligothiophenes, one of the most investigated π-conjugated systems in the field of material science due to their chemical stabilities in various redox forms, excellent charge transfer properties and their outstanding structural and electronic properties[13]. In this study, mono- and bithiophene moities were introduced onto the porphyrinic macrocycle. The target molecules are expected to exhibit better solubility, lower energy band gap and excellent photophysical and electrochemical properties, all of which are desirable features of the photoactive compounds in several efficient optoelectronic devices, esspecially DSSCs and BHJSCs.

1.1 Objectives of this research

Synthesis of novel benzoporphyrin-thiophene derivatives and investigation of their photophysical and electrochemical properties for potential used in optoelectronic devices.

1.2 Scope of this research

The scope of this research covers the synthesis of benzoporphyrins bearing mono- and bithiophene units at the *meso*-postions. All new compounds were fully characterized by spectroscopic techniques, *i.e.* mass spectrometry, ^{1}H-NMR and ^{13}C-NMR spectroscopy. Photophysical properties were investigated by UV-Visible and fluorescene spectrophotometry in both solution and film. Electrochemical studies were also employed to evaluate the potential used as donor/acceptor in successful optoelectronic devices.

CHAPTER II

THEORY AND LITERATURE REVIEWS

THEORY

2.1 Optoelectronic devices

Optoelectronics is a branch of electronics combining electric and optic together thus optoelectronic devices can interconvert between light and electricity in their operations [14]. There are many applications relating to optoelectronic field in two common processes. In photoconductive devices such as photo resistors, photodiode and phototransistor etc. can activate or deactivate electric circuits by the detection in the light intensities. On the other hand, Photovoltaic devices, i.e. solar cell, optical sensor, produce a voltage when these are exposed to light that corresponding to a potential difference between p-n junctions depended on the light intensity. Therefore, these devices are combined from two types of semiconductor, p-type and n-type, which act as electron acceptor and electron donor, respectively. The process of introducing impurities such as phosphorus, arsenic or boron to a pure semiconductor material such as germanium and silicon is called “doping” [15]. The resulting junction can be used in many optoelectronic devices and is known as p-n junction (**Figure 2-1**).

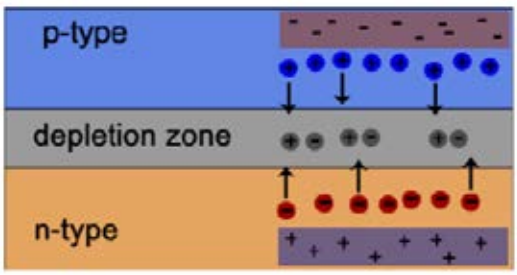

Figure 2-1: Schematic setup of p-n junction in optoelectronic device.

Organic optoelectronics is a new research area based on organic chemistry, physics, electronic engineering and materials science [16-18]. Organic optoelectronic devices, such as organic electroluminescent device (OLED), organic photovoltaic (OPV) and organic thin film transistors (OTFT), have attracted significant attention in both academic and industries due to their lower cost compared to inorganic-based devices and great application potential in flat-panel and flexible display [19]. Additionally, compared to the inorganic counterparts, the most important advantage of organic semiconductors is the possibility of tuning their properties by the structural modification.

The electronic structure of all organic semiconductors is based on conjugated π-system. The system is a connection of p-orbitals by delocalized electron along the path with alternating single and multiple carbon-carbon bonds causing the new wave functions over the conjugation backbone. The new π-orbitals are either filled (called occupied molecular orbital) or empty (called unoccupied molecular orbital). The difference of energy level between highest occupied molecular orbital (HOMO) and lowest unoccupied molecular orbital (LUMO) is called energy band gap (E_{gap}) altering difference in photophysical and electrochemical properties in such organic molecules.

In bulk heterojunction solar cells (BHJSCs), the p-type and n-type materials must have a good balance of the electronic levels [20], in theoretically, the LUMO of the donor must have an energy higher than the LUMO of the acceptor, and the HOMO of the acceptor must also have a lower energy of the HOMO donor to impede holes, transfer from the donor to the acceptor. The one of the most popular n-type organic materials is a fullerene derivative, [6.6]-phenyl C_{61}-butyrric acid methyl ester (PCBM), which has better solubility in several common organic solvents compared to fullerene C_{60}. The commonly used p-type organic materials are poly(3-hexylthiophene-2,5-diyl) (P3HT) and poly(p-phenylene vinylene) (PPV), which have a low E_{gap} with high mobility of the positive charges (holes mobility) [21].

Typically, the best performance in the BHJSCs is achieved by connecting of P3HT with PCBM. This system generates up to 5-10% cell efficiency [22]. **Figure 2-2** shows examples of well-known conjugated organic molecules in optoelectronic devices.

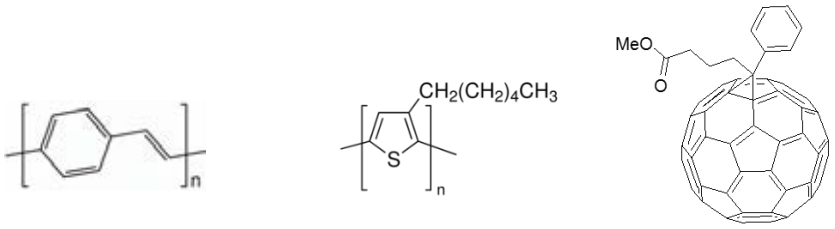

PPV P3HT PCBM

Figure 2-2: Chemical structures of PPV, P3HT and PCBM

2.2 Molecular design of organic photosentisizers

For organic optoelectronic devices, the molecular design of the organic photosentisizer comes to an important section for improving the device efficiency. In general, the organic photosentisizer should have all of the following properties:

(i) Long-term stability in working environment

(ii) Suitable physical properties for the desired devices

(iii) Photophysical properties : Wide absorption band
: High absorption coefficient

(iv) Electrocheical properties : Appropriate redox potentials
: High charge mobility

2.3 Jablonski energy diagram of organic molecule

Electronic transitions can be occured between the ground states and excited states energy levels. The several energy levels involved in the absorption and emission of light by a chromophore are normally presented by Jablonski energy diagram [23] (**Figure 2-3**).

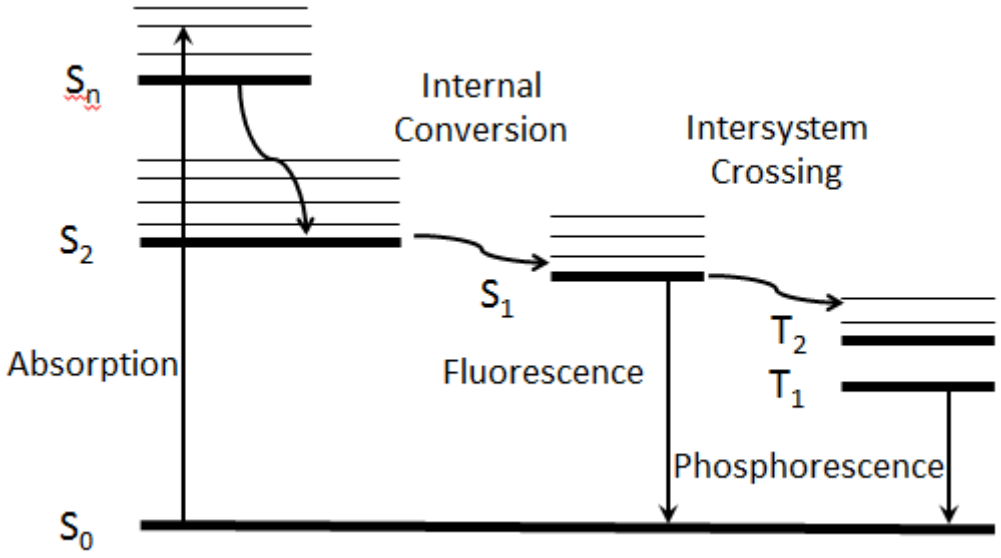

Figure 2-3: Simplified Jablonski diagram

The Jablonski diagram demonstrates a singlet ground state (S_0), and several excited singlet states (S_2, S_3 …) in horizontal lines. Different multiplicity states, triplet states, are represented by T_1, T_2, T_3.... The thicker lines denote electronic energy levels, while the thinner lines denote the various vibrational energy states. Straight arrows show electronic transitions associated with absorption or emission of photons. Curly arrows shows a molecular internal conversion or non-radiative relaxation processes [24].

The first transition is the absorbance of the photons by the molecule. Normally, the molecular absorption of the photons at a specific wavelength causes electronic excitation from the ground state to some vibrational level in the excited singlet state. If the absorbed photon has higher energy than that of necessary for a simple electronic transition, the excess energy is usually converted into vibrational or rotational energy. The broadening of absorption spectrum is resulted from the closely spaced of vibrational energy levels plus thermal motion that enable a range of the photon energy to match a particular transition. After that, several processes will occur with various probabilities, but the most likely to happen would be a relaxation to the lowest vibrational energy level of the first excited state (S_1). This process is known as internal conversion or vibrational relaxation. An excited molecule exists in the lowest excited singlet state for periods before finally relaxing to the ground state (S_1 to S_0). If

relaxation from this long-lived state is accompanied by the emission of a photon, the process is normally known as fluorescence. It is the reason that the fluorescence spectrum is always shifted to higher wavelength compared to the corresponding absorption spectrum (called stokes shift). If the phenomenon known as intersystem crossing occurred instead of a normal emission, the spin multiplicity of excited molecule will change from singlet to triplet state. This event is relatively rare, but eventually results in emission of a photon through phosphorescence (T_1 to S_0). Transitions from the triplet excited state to the singlet ground state are forbidden, resulting in rate constants for triplet emission is slower than those of fluorescence [25].

It should be noted that an emission spectrum of a chromophore is typically a mirror image of its absorption spectrum. This is due to the fact that electronic excitation does not significantly change the geometry of the molecule and the spacing of excited state vibrational levels is similar to that of the ground state. The overall result is that the fluorescence emission spectra recorded with the spectrophotometer often display similar, but reversed to those observed in the absorption spectra.

2.4 Porphyrin

2.4.1 Overview

Porphyrins (without any substituent, called “porphine”) and its derivatives are narurally occurring aromatic molecules, with composed of four pyrrole subunits connecting at each α-carbon atoms with methine (-CH=) bridges. The structure of porphine is shown in **Figure 2-4**.

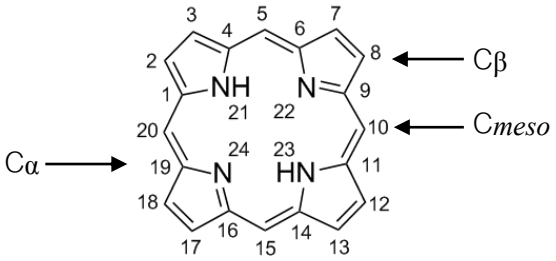

Figure 2-4 The structure of porphyrin (or porphine)

The *meso*-positions are numbered 5, 10, 15, 20 and the β-positions are numbered 2, 3, 7, 8, 12, 13, 17, 18. Two of the pyrrole rings in the porphyrin are in the oxidized state: the nitrogen atoms point their unshared electron pairs towards the center of the macrocycle.

The word "porphyrin" is derived from a Greek's word "porphura" which means purple [26]. Due to the large conjugated system, porphyrin typically has a very intense absorption band in visible region and always appear deeply colored. Although there are 22 π-electrons inside the porphyrin macrocycle, only 18 electrons are found to actually participate in delocalization pathway, which is consistent with Hückel's [4n+2] rule for aromaticity, where n = 4. The different 18 electron-delocalization pathways are shown in **Figure 2-5** [27].

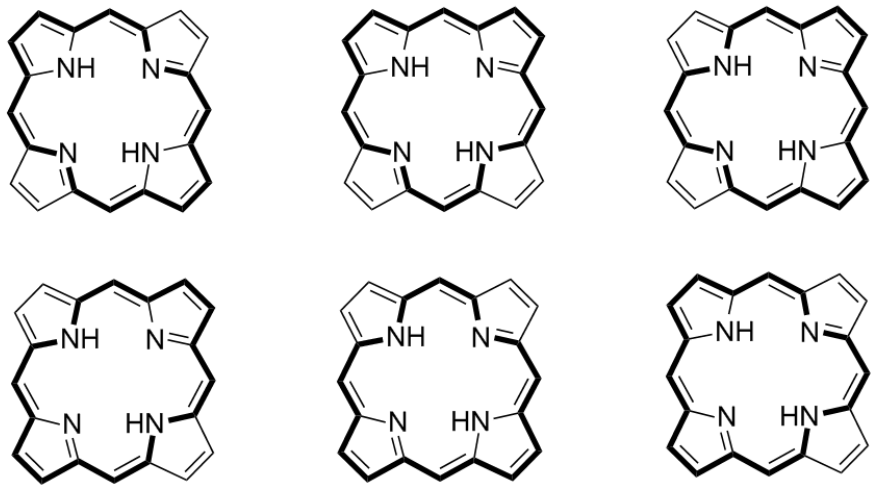

Figure 2-5: The delocalization of porphyrins, the six possible canonical forms of porphyrins are shown.

Porphyrin show important roles in many biological systems. Complexes of metal ions with various porphyrins are employed in specific purposes. Magnesium complexes in chlorophylls are found in green plants as photosynthetic reaction centers which convert light energy into chemical reaction [28]. Iron complexes are found in heme B and cytochrome C which is responsible for oxygen transport and as a single electron transporter in a redox catalytic reaction [29], respectively. (**Figure 2-6**)

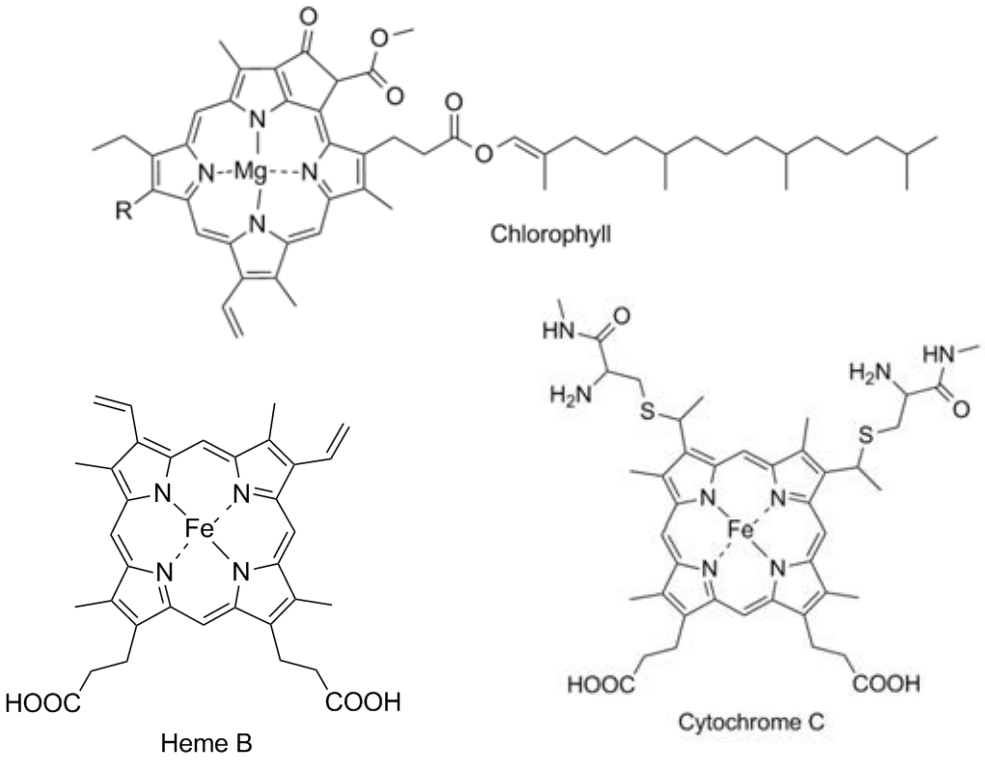

Figure 2-6: Structure of some natural porphyrins

Typically, porphyrin and its derivatives effectively absorb photons in a visible region around 420 nm with high molar extinction coefficient (about 10^5 $L \cdot cm^{-1}mol^{-1}$), also known as soret band or B-band. This absorption is mainly caused by electronic transition from the zeroth singlet ground state to second singlet excited state [30]. Another transition is from zeroth singlet ground state to first singlet excited state, resulting in several weaker absorption bands between 500-700 nm, also known as Q-bands (**Figure 2-7**). A modification in the peripheral substituents of the macrocycle normally results in a slightly changing of absorption maxima. However, as long as the main $18e^-$ conjugation system still exists, the soret band is the major characteristic band of the absorption spectra.

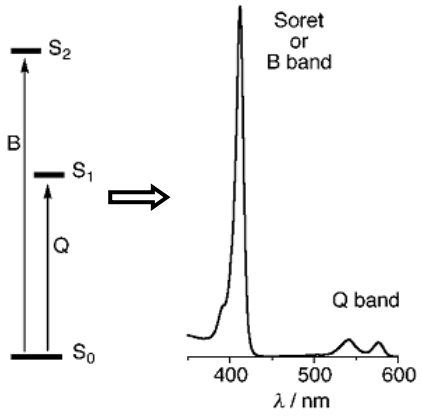

Figure 2-7: Electronic state and UV-Vis absorption spectrum of porphyrin.

2.4.2 Structural Modifications of Porphyrin

Porphyrin chemistry has progressed in great steps over the past years due to the potential applications of these compounds upon their physical and chemical properties. The main objectives of the structural modification of the porphyrin are listed below:

1. To obtain the desirable physical properties, e.g. solubility, chemical, thermal and electrical stability.
2. To tune photophysical properties, e.g. absorption and emission coefficient and redox potential
3. To achieve the appropriate molecular the orientation in the film beneficial for the particular

The main theme is extending π-conjugation system by introducing substituent groups into the peripheral positions of the macrocycle. The synthetic control over these substituent groups enables the porphyrin to be designed and tailored for specific applications. Two different patterns of substitution are shown in **Figure 2-8**

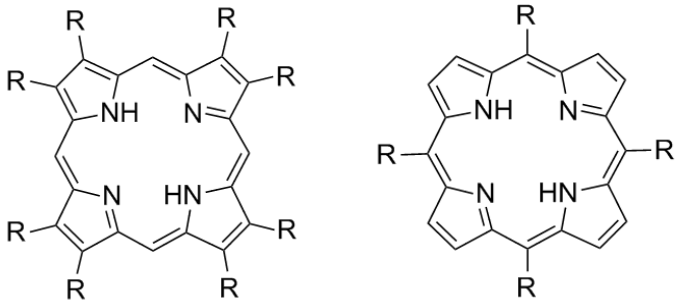

β-substituted porphyrin *meso*-substituted porphyrin

Figure 2-8: Structures of β- and *meso*-substituted porphyrins

The selection of a synthetic route to be used is based on the application of the porphyrin products. The *meso*-substituted porphyrins are widespread acceptance because of their ease of synthesis and flexibility toward synthetic modification. The wide availability and ease of manipulation of aldehydes starting materials enables various porphyrins to be synthesized. Substituents at *meso*-positions can be alkyl, aryl, heterocyclic or organometallic groups as well as other porphyrins. However, *β*-substituted porphyrins are more hardly to be synthesized due to the difficultly of the direct carbon-carbon bond formation on each pyrrolic group. Therefore, the synthesis of an appropriate pyyrole is required to be used as a starting material in porphyrin synthesis.

Another way to tune the photophysical and electrochemical properties of porphyrins could be achieved by coordination of various metal ions right at the center of the porphyrinic core (called metalloporphyrin). The pyrrole nitrogen atoms enable the N-metal σ-bonds formation (**Figure 2-9**). Coordination between metal ions and porphyrins is one of the most attractive areas in porphyrin chemistry [31].

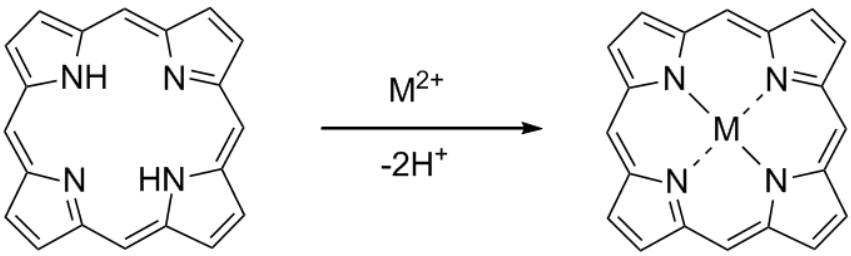

Figure 2-9: Formation of metalloporphyrins

2.4.3 Porphyrins synthesis

Porphyrin and their derivatives inspire chemists into synthesis, purification and characterization. One of the simplest porphyrins derivative is tetraphenylporphyrin (TPP) obtaining from a condensation of pyrrole and benzaldehyde in the presence of an acid. The first synthetic method was reported by Rothermund, P (**Scheme 2-1**) [32]. However, due to the high temperature is necessary in this method thus the low yield were realized.

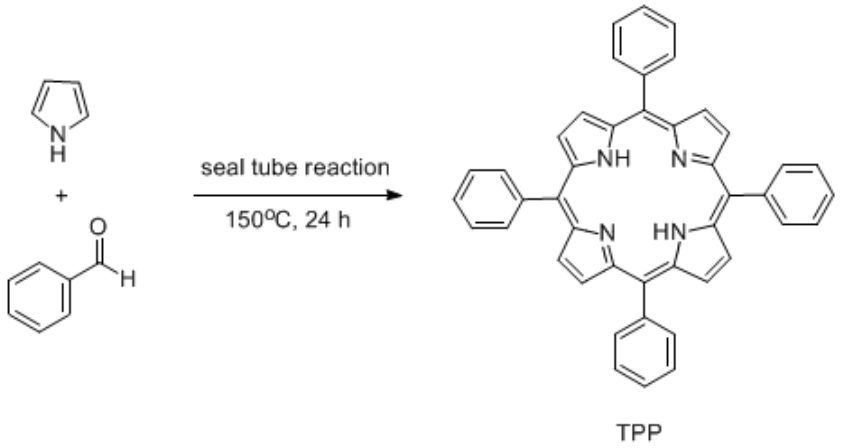

Scheme 2-1: Formation of TPP under Rothmund's condition.

Later on, Adler and their coworkers reported the use of refluxing propionic acid to obtain TPP and its derivatives in 20-25% yield (**Scheme 2-2**) [33].

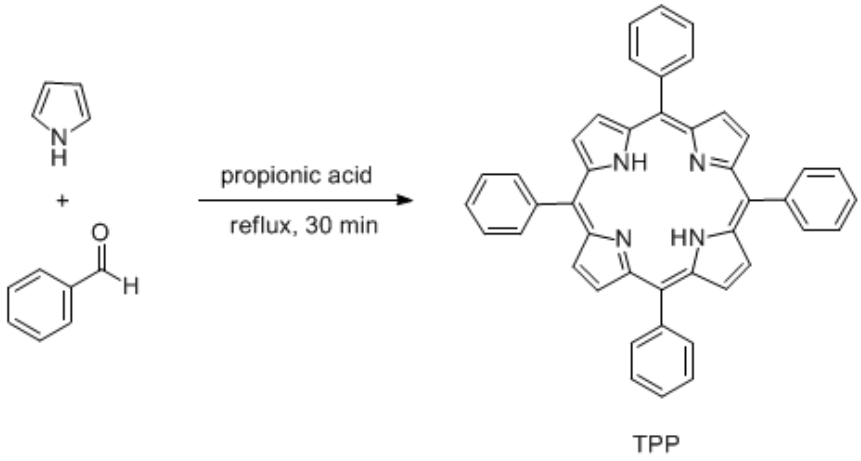

Scheme 2-2: Synthesis of TPP under Adler's condition.

A porphyrin synthetic route had been greatly developed by Lindsey's research group. A successful condensation was achieved in a mild conditions resulting in higher yield of *meso*-tetraarylporphyrin and similar derivatives [34]. Firstly, tetraarylporphyrinogen was formed by condensation between appropriate aldehyde and pyrrole in the presence of a mild acid, usually $BF_3{\cdot}OEt_2$ or TFA, at room temperature following by the irreversibly oxidation with a quinone derivatives in the second step (**Scheme 2-3**).

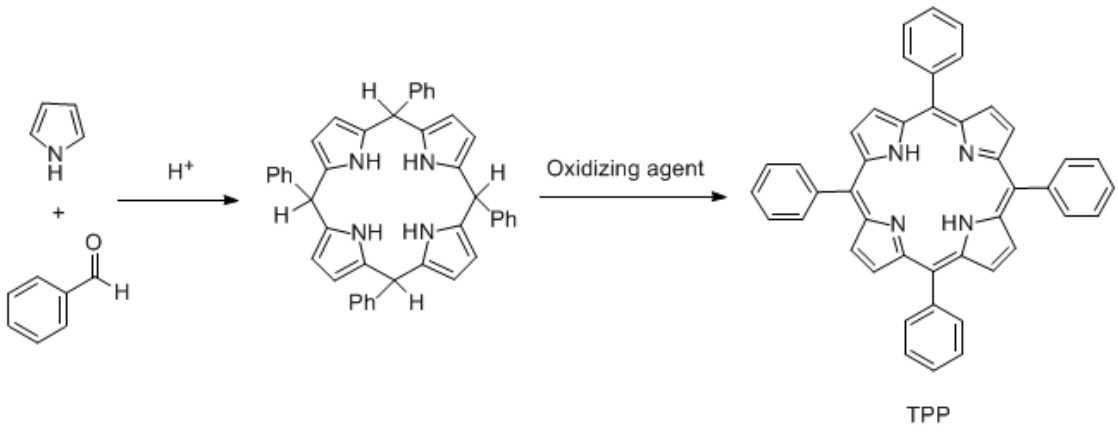

Scheme 2-3: Synthesis of TPP under Lindsey's condition

2.4.4 Uses and Application of Porphyrin Derivatives

According to such advantages from the previous section, the interest in porphyrin and its derivatives is continuously increased. There are a lot of interesting applications of porphyrin derivatives in chemical and medical fields, such as:

1. Organic-based optoelectronic devices such as solar cells and OLED [35]
2. Photocatalysts [36]
3. Organic semiconductors [37]
4. Optical sensors [38, 39]
5. Photodynamic therapy [40]

2.5 Benzoporphyrin

2.5.1 Overview

Porphyrins that were extended their π-conjugation with exocyclic aromatic rings have received high attention in recent years [41, 42]. Tetrabenzoporphyrin (TBP) is one of well-known porphyrin derivatives that has aromatic subunits fused directly onto the *β*-pyrolic positions as shown in **Figure 1.1**. In 1966, TBPs were the first discovered and separated from petroleum distillation processes in trace amounts [43]. Commonly, TBPs are chemically stable compounds with unique chemical, physical and spectroscopic properties that significantly different from those of porphyrins. Due to a larger π-conjugation system, TBPs exhibit significant red shift in absorption and emission spectra to the infrared region. Absorption in red region of spectrum is generally useful for biomedical applications such as photodynamic therapy (PDT) [44-46], and *in vivo* optical imaging and sensing [47-49]. Moreover, TBPs can also be used as optical emitter [50], nonlinear optical materials [51] as well as organic semiconductors [52-54], photovoltaic cells and near-IR labeling dye.

2.5.2 Benzoporphyrin Synthesis

Synthesis of unsubstituted TBP was first reported by Helberger and coworkers [55] and later by Linstead and coworkers [56]. The macrocycle was synthesized by self-condensation of *o*-cyanoacetophenone in the presence of a metal template at high temperature (**Scheme 2-4**, A). The metalated symmetrical benzoporphyrins were obtained with high impurity and required several steps in purification. A number of similar precursors, such as *ortho*-acetylbenzoic acid [57] (**Scheme 2-4**, B), phthalimides [58, 59] (**Scheme 2-4**, C), phthalimidines [60] (**Scheme 2-4**, D), were used to prepare variety of unsubstituted TBPs.

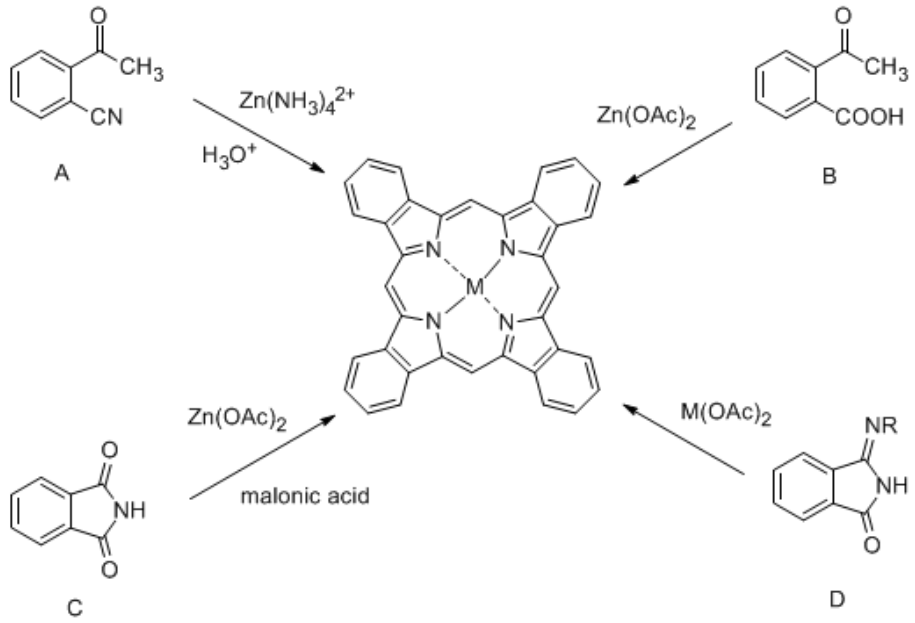

Scheme 2-4: Previous symmetrical benzoporphyrin synthetic routes

Later on, Vicente *et. al*. developed a modern synthetic route to prepare metalated symmetrical TBP (**Scheme 2-5**) [61]. Starting from self-condensation of pyrrole derivatives, which can be obtained from classical Barton-Zard reaction [62], followed by oxidation with DDQ. The mixture of isomers of phenylsulfonyl-substituted porphyrins was separated in 60% yield. TBP was achieved in 53% overall yield by elimination of phenylsulfonate under basic condition and subsequently oxidized by DDQ.

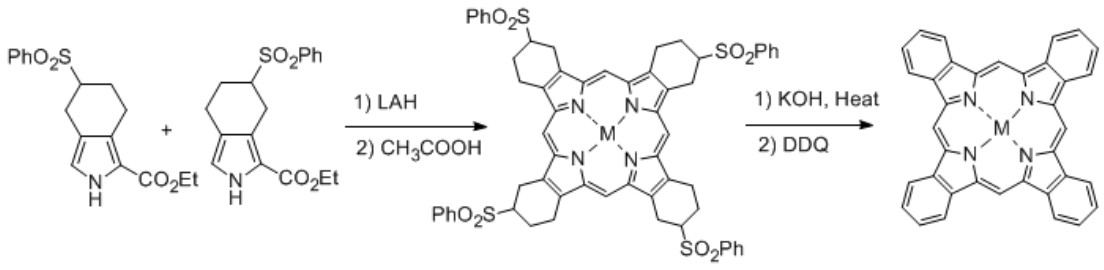

Scheme 2-5: Improved synthetic route of benzoporphyrins

Aside from low yields and a large number of byproducts, the template condensation approach suffers from an extremely harsh condition is required in

condensation step. Therefore, only a few TBPs with inert substituents could be synthesized using this method. Over the past decade, several new approaches to π-extended porphyrins had been developed, all of them were based on traditional porphyrin chemistry. Unfortunately, in the substituted TBP system, the directly using of standard methods of porphyrin chemistry – condensation of appropriate pyrrole with corresponding aldehydes – is not possible, as in this case the precursor pyrrole, 2*H*-isoindole, is a very unstable molecule (**Scheme 2-6**, A). Consequently, the only available approach was through imitating the phthalocyanine synthesis by a high-temperature template condensation of phthalimide or analogous compounds [63] resulting in complex mixtures of TBPs which required HPLC for separation [64].

To avoid dealing with an unstable precursor, two routes were simultaneously developed, starting from tetrahydroisoindole (**Scheme 2-6**, B) [65-67] and bicycle octadiene-fused pyrrole (**Scheme 2-6**, C) [68, 69]. Both of these routes had a serious drawback in the final aromatization step, which a harsh condition was required to generate four aromatic rings and as a consequence in a low yield (5-30%). To get rid of these disadvantage, recently, Filatov and coworker reported a new route for TBP synthesis based on isoindole-liked molecule, 4,7-dihydro-2*H*-isoindole (**Scheme 2-6**, D) [70], using as a precursor for *meso*-substituted TBP syntheses. This approach is available with various aromatic aldehydes through a mild reaction condition in the final aromatization step, which allows a readily synthesis of previously inaccessibly structures.

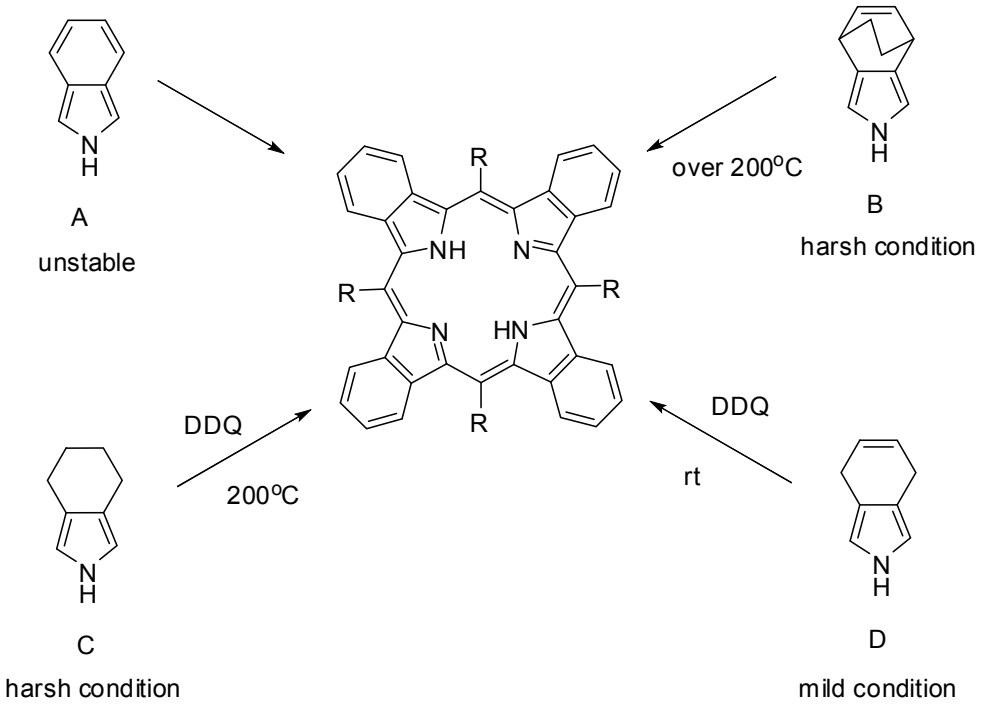

Scheme 2-6: General routes for *meso*-substituted tetrabenzoporphyrins.

2.6 Thiophene

Thiophene is a heterocyclic compound containing a sulfur in a corner of a five membered ring (**Figure 2-10**). The word "thiophene" derived from the word "*theion*", the Greek word for sulfur, and another Greek word "*phaino*" means shinning. Thiophene and their derivatives exist in petroleum or coal and also being obtainable as by-products from petroleum distillation. Thiophene has a structure analogous to pyrrole and due to π-conjugated system, it behaves as a higher reactive benzene derivatives.

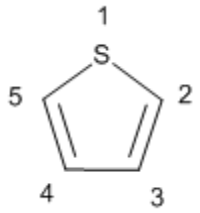

Figure 2-10: General structure of thiophene

Thiophene belongs to the most studied compound in many research areas: it is easy to process, chemically and electrically stable and its synthetic routes have been continuously developed for a long time. Thiophene and their derivatives have been employed in applications such as electronic and optoelectronic devices [71], biodiagnosis [72], block co-polymer self-assembled superstructures and conductivity-based sensory devices [73]. Moreover, oligo- and polythiophenes are among the best investigated and most often used as π-conjugated materials, in particular as a photoactive compound in organic optoelectronic devices and molecular electronics [74].

A major driving force behind the continuous development of thiophene-based materials is according to the attractive potential of structural variations which allow fine-tuning of the electronic properties over a wide range. Another reason is their outstanding chemical and physical properties. Thiophene and their derivatives are typically stable, both in the conducting and in the semiconducting state, and can be structurally characterized by many methods. Their unique electronic, optical, redox, charge transport and self-assembling properties are interesting, as well as their unique arrangement and stacking properties on solid surfaces and in the bulk. Furthermore, the high polarizability of sulfur atoms in thiophene rings leads to a stabilization of the conjugated chain and to excellent charge transfer properties, which make them as promising candidates for organic electronic devices.

LITERATURE REVIEWS

In 2011, Nguyen, T. *et. al.* reported the first use of benzoporphyrin (BP) as a donor material in bulk heterojunction organic solar cell and the film study were also investigated [75]. The precursor to BP, 1,4:8,11:15,18:22,25-tetraethano-29*H*,31*H*-tetrabenzo[*b,g,l,q*]porphyrin (CP), is a solution processable from organic solvents, and the resulting film can be converted to BP (p-layer) by thermal processing. Once the conversion takes place, the BP film is polycrystalline and insoluble in various organic solvents. Due to the alignment of the highest occupied molecular orbital (HOMO) of the donor material as shown in **Figure 2-11**, which made this architecture as a hole only device.

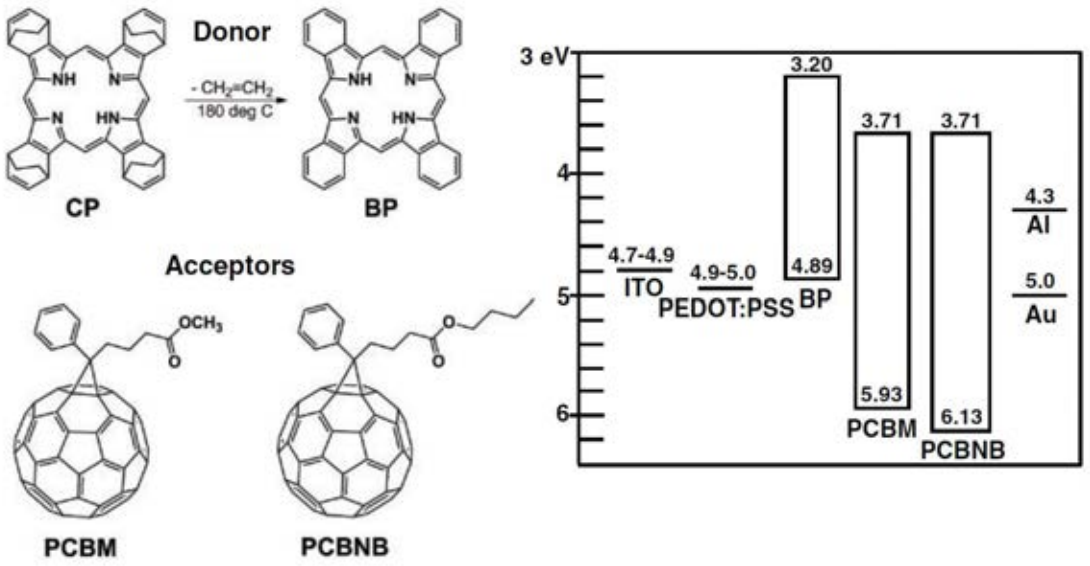

Figure 2-11: Chemical structures of the precursor, donor and acceptor materials and work functions of electrodes (based on ultraviolet photoelectron spectroscopy (UPS) measurements) and energy levels of benzoporphyrin (BP), PCBM, and PCBNB.

Later on, Mitsubishi Chemical Corporation [12] also reported a novel organic photovoltaic cell producing by adding two coatings of organic compounds to a film substrate with 8.5% cell conversion efficiency (**Figure 2-12**). This cell was fabricated with benzoporphyrin, acts as a p-semiconductor, and a fullerene, as a n-semiconductor. As this unnecessary renders glass substrates, each layer can be of nanosize thickness, enabling the production of extremely thin, highly flexible and surprisingly bendable photovoltaic cells. This broadens the range of potential applications for organic photovoltaic cells.

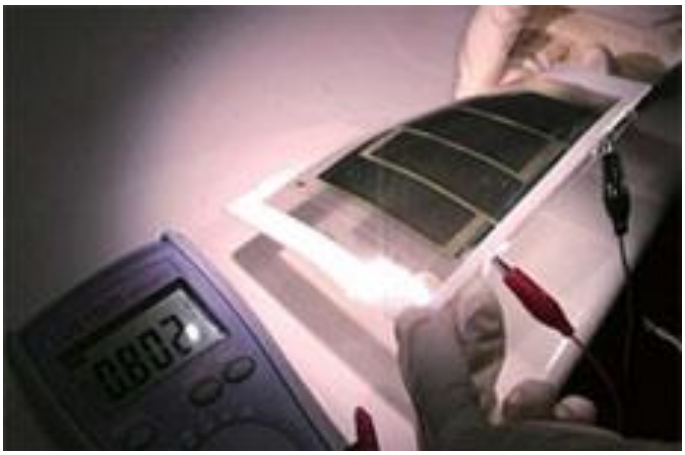

Figure 2.12: An organic photovoltaic cell passes a conductivity test in a bent position. (Image: Mitsubishi Chemical Corp.)

Tan, S. *et*. *al*. described the used of three novel thiophene-linked porphyrin dyes with donor–π–acceptor structure in dye-sensitized solar cells (**Figure 2-13**) [76]. The absorption bands of $\mathbf{P_{Zn}}$**-T**, $\mathbf{P_{Zn}}$**-hT** and $\mathbf{P_{Zn}}$**-oT** in $CHCl_3$ were broadened and slightly red-shifted compared with those of the starting material, 5-(4-bromophenyl)-10,15,20-tris(4-methylphenyl)porphyrinatozinc ($\mathbf{P_{Zn}}$). Among these porphyrin dyes, $\mathbf{P_{Zn}}$**-hT** exhibited the maximum power conversion efficiency up to 5.14%. The results suggested that a thiophene π-conjugation unit can improve the light harvesting capability of a porphyrin dye, the length and the alkyl chain of this unit influence the electron transport efficiency, both of which are crucial for photovoltaic performance in DSSCs.

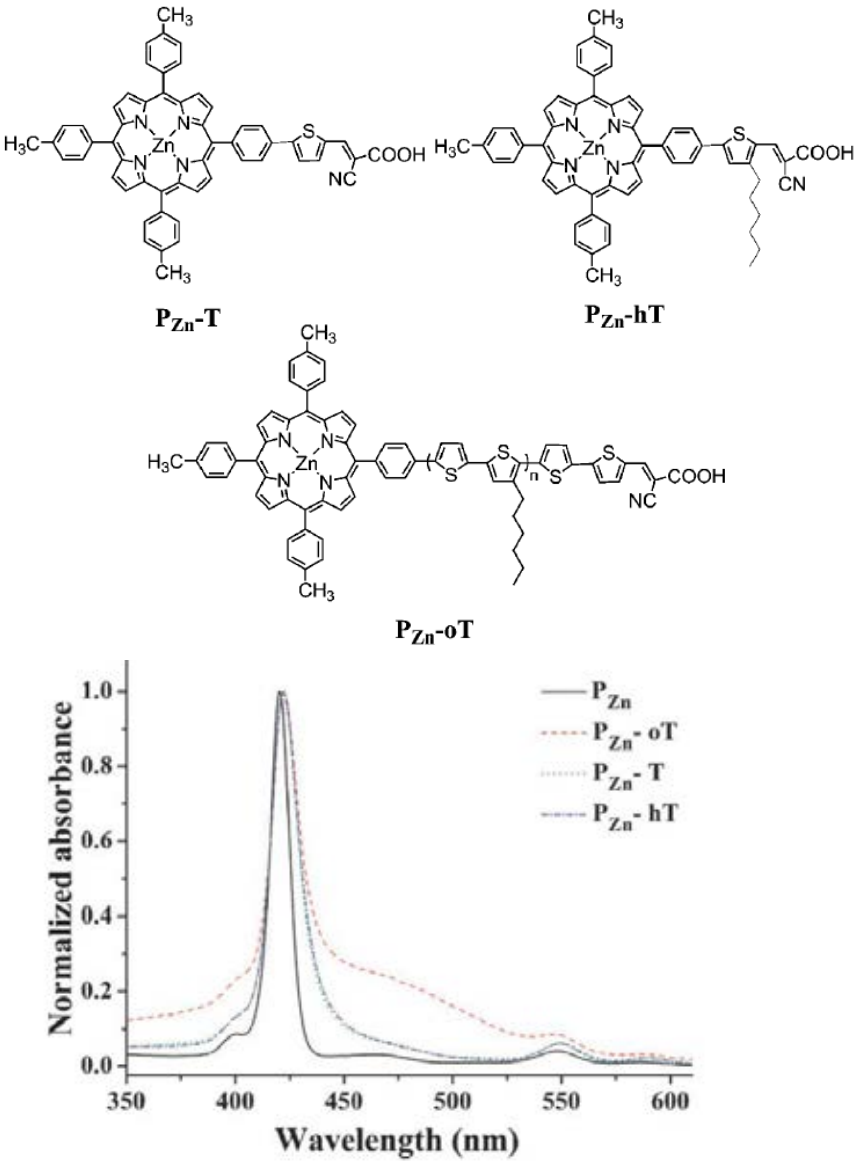

Figure 2-13: Structure of porphyrin dyes and their absorption spectrum in $CHCl_3$

Afterward, Tan, S. *et*. *al*. [77] reported a development of their previous work. Four porphyrin dyes (**Figure 2-14**), incorporating multi-alkylthienyl appended porphyrins as the electron donor, the 2-cyanoacrylic acid as the electron acceptor, and different π-conjugated spacers, were synthesized for dye-sensitized solar cells (DSSCs). All the porphyrin dyes studied in this work showed red-shifted and broadened electronic spectra compared to reference, P_{Zn}. In the presence of thiophenyl groups at the *meso*-positions of porphyrin rings, the energy levels of E_{ox} (excited-state oxidation potentials) are significantly shifted to the positive compared with the reference P_{Zn}, indicating a decreased E_{gap}. The highest power conversion efficiency of the four dyes based on DSSCs reached 5.71% under AM 1.5 G irradiation.

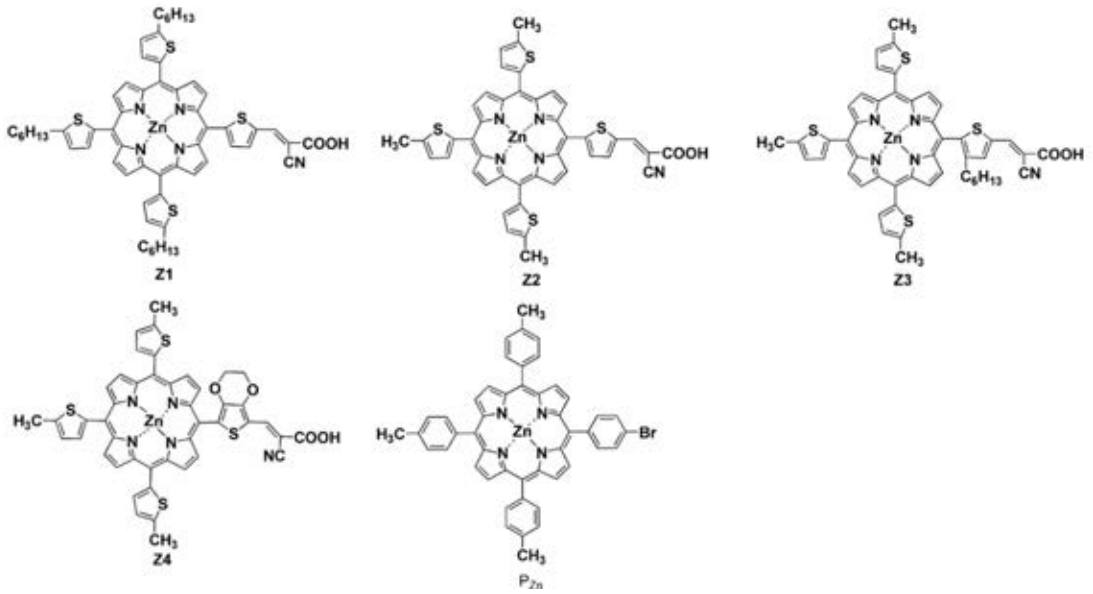

Figure 2-14: Molecular structures of the porphyrin dyes Z_1-Z_4 and P_{Zn}.

Investigating the cause of red shifting in absorption spectra of *meso*-substituted thiophenyl porphyrins. Brückner *et. al.* [78] described the used of density functional theory (DFT) to calculate the energy of three porphyrin derivatives as a function of rotation of a single meso aryl group. Five membered ring system of thiophene exhibit less steric hindrance compared to the larger six membered ring system of phenyl group. Additionally, the thiophen-2-yl group lacks one *ortho*-phenyl hydrogen to *β*-pyrrole H interaction (**Figure 2-15**), allowing free rotation of the thiophen-2-yl porphyrins and also a more slightly facile rotation for the thiophen-3-yl porphyrins. The computed rotational barriers of H_2P_1 and H_2P_2 are 50 and 75% lower, respectively, compared to that of H_2TPP, thus allowing the thienyl groups to adopt more co-planar organization to the porphyrin ring with respect to phenyl-substituted porphyrin.

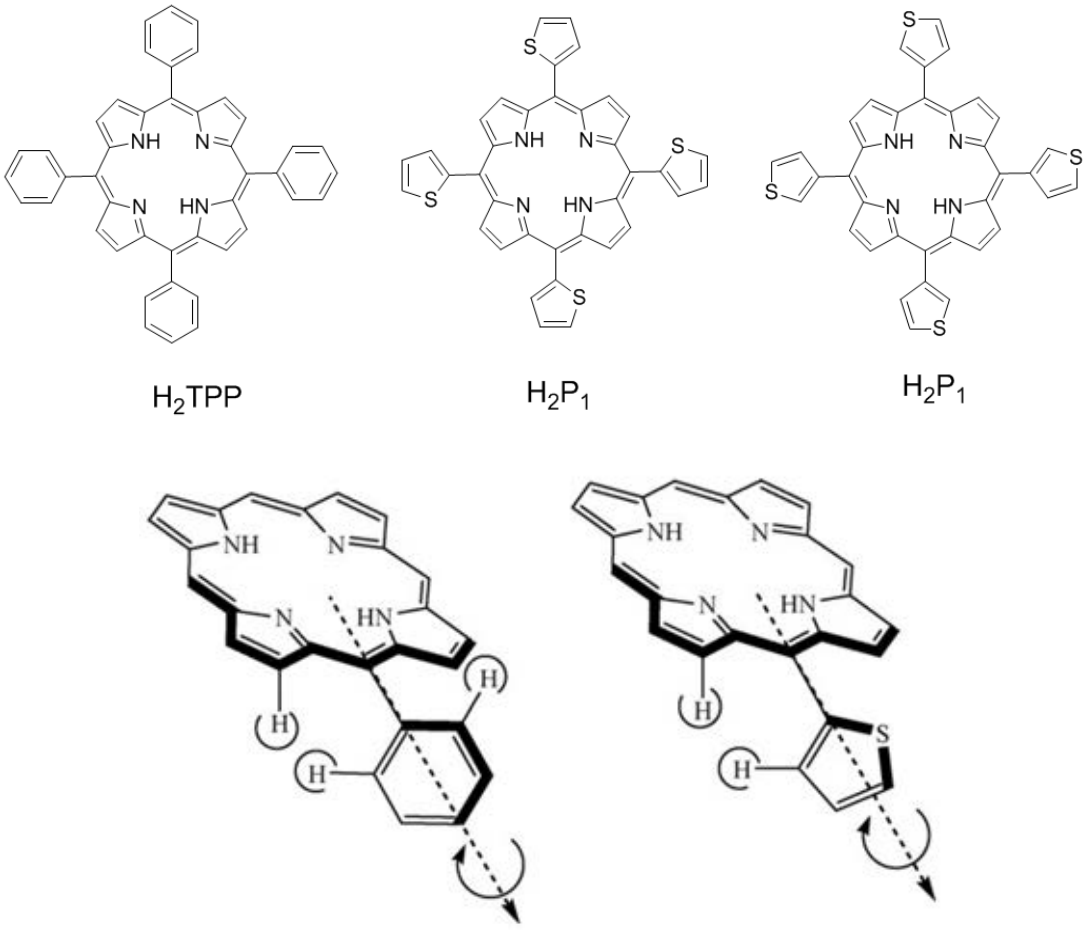

Figure 2-15: Structure and schematic of rotation for phenyl and thiophenyl meso substituent at the porphyrin ring.

According to the abovementioned literatures, benzoporphyrin derivatives showed promising properties to be used as a photoactive compound in optoelectronic devices. Thiophene and their oligomers have a potential to enhance the absorptivity and charge mobility of porphyrins.

In this study, the molecular design of the target molecules are expected to achieve the following beneficial features;

1. The appearance of thiophene units at the meso-positions of benzoporphyrin will tune the photophysical and electrochemical properties of target molecules for using in light-harvesting applications.
2. Thiophene will improve the solubility of benzoporphyrin in common organic solvent
3. Thiophene will be a good assistant in molecular charge transfer processes.

All of which are desirable features of photoactive compounds in successful organic optoelectronic devices such as BHJ-SCs and DSSCs.

CHAPTER III

EXPERIMENTAL

3.1 Chemicals

All chemicals are purchased from commercial sources and used as received, unless noted otherwise.

1. Bis(trimethylsilyl)acetylene : Sigma-Aldrich
2. 4-toluenesulfonyl chloride ($C_7H_7SO_2Cl$) : Sigma-Aldrich
3. Aluminium chloride ($AlCl_3$) : Merck
4. Sodium fluoride (NaF) : Merck
5. Ethanol (CH_3OH) : Merck
6. Ethyl isocyanoacetate ($C_2H_5OCOCH_2NC$) : Merck
7. Potassium *tert*-butoxide ($(CH_3)_3COK$) : Merck
8. Potassium hydroxide (KOH) : Merck
9. Ethylene glycol ($HOCH_2CH_2OH$) : Merck
10. Pyrrole : Sigma-Aldrich
11. Benzaldehyde (C_6H_5CHO) : Merck
12. 2-thiophene carboxaldehyde : Sigma-Aldrich
13. 2,2′-bithiophene-5-carboxaldehyde : Sigma-Aldrich
14. Boron trifluoride etherate ($BF_3 \cdot OEt_2$) : Merck
15. 2,3-dichloro-5,6-dicyano-1,4-benzoquinone (DDQ) : Sigma-Aldrich
16. Tetrachloro-1,4-benzoquinone (*p*-chloranil) : Sigma-Aldrich
17. Zinc acetate dihydrate ($Zn(OAc)_2 \cdot 2H_2O$) : Merck
18. Sodium sulfate (Na_2SO_4) : Merck
19. Silica gel : Merck
20. Methylene chloride (CH_2Cl_2) : Distilled from commercial grade
21. Tetrahydrofuran : Lab-Scan

22. Toluene ($C_6H_5CH_3$) : Merck
23. Sodium sulfite (Na_2SO_3) : Carlo Erba
24. Sodium chloride (NaCl) : Merck
25. Deuterated chloroform ($CDCl_3$) : Cambridge isotope
26. Deuterated toluene ($C_6D_5CD_3$) : Cambridge Isotope

3.2 Analytical instruments

^{1}H-NMR and ^{13}C-NMR spectra were obtained in $CDCl_3$ at 400 MHz for ^{1}H nuclei and 100 MHz for ^{13}C nuclei (Varian Company, USA) unless noted otherwise. Chemical shifts (δ) are reported in parts per million (ppm) relative to the residual $CHCl_3$ peak (7.26 ppm for ^{1}H-NMR and 77.0 ppm for ^{13}C-NMR). Coupling constant (*J*) are reported in Hertz (Hz).

Mass spectra were obtained using high resolution electrospray ionization (HR-ESI), and matrix-assisted laser desorption ionization (MALDI) mass spectrometry with dithranol as a matrix.

Absorption spectra were recorded in toluene by a Hewlett-Packard 8453 spectrophotometer and absorption extinction coefficient (ε) were reported in L/mol·cm. Fluorescence spectra were measured in toluene using a Perkin-Elmer LS45 luminescence spectrophotometer. Absorption and emission spectra of the solutions were measured in toluene at room temperature, and those of the films were obtained from the drop-casted films on a glass substrate.

3.3 Experimental procedure

Part 1: Synthesis of porphyin-thiophene derivatives

3.3.1 [5,10,15,20-tetraphenylporphyrinato]zinc (ZnTPP)

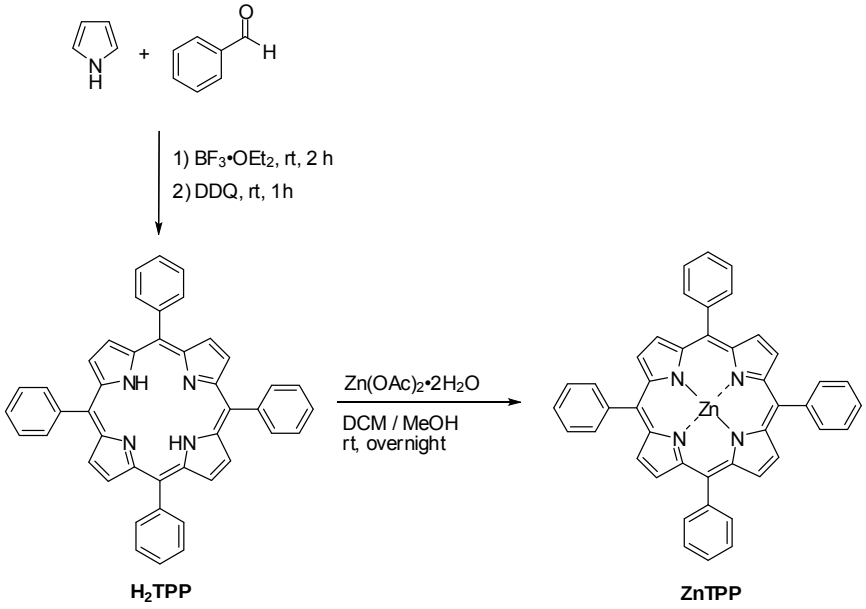

Following a previously published procedure [79], pyrrole (0.090 mL, 1.3 mmol) and benzaldehyde (0.132 mL, 1.30 mmol) were dissolved in dichloromethane (130 mL) and the solution was treated with $BF_3 \cdot OEt_2$ (16.5 μL, 0.130 mmol) in one portion. The resulting solution was stirred at room temperature for 1 h. Then 2,3-dichloro-5,6-dicyano-1,4-benzoquinone (DDQ) (221 mg, 0.97 mmol) was added and stirring was continued for additional 2 h. After removal of the solvent, the crude product was purified by a silica column using 1% TEA in dichloromethane as an eluent to give 5,10,15,20-tetraphenylporphyrin (**H_2TPP**) as a purple solid (114 mg, 25%). ^{1}H-NMR δ –2.77 (s, 2H), 7.71-7.83 (m, 12H), 8.22 (d, J = 6.0 Hz, 8H), 8.85 (s, 8H) (**Figure A-1**); MALDI-TOF-MS m/z obsd 615.660 [M^+], calcd 614.247 [M = $C_{44}H_{30}N_4$] (**Figure A-2**). Other spectroscopic data are consistent with those subscribed in the literature.

Zinc complex of **H_2TPP** was obtained by a standard metallation method [80]. Compound **H_2TPP** (97 mg, 0.16 mmol) was dissolved in chloroform (40 mL) and

then reacted with a solution of $Zn(OAc)_2 \cdot 2H_2O$ (176 mg, 0.800 mmol) in methanol (5 mL) at room temperature for 12 h. After removal of the solvent, the reaction mixture was redissolved in CH_2Cl_2 (50 mL), washed with water (50 mL), dried over anhydrous Na_2SO_4, and concentrated to dryness. Purification by column chromatography [silica, 1% TEA in CH_2Cl_2] followed by sonicating-centrifugating in hexanes and methanol to give [5,10,15,20-tetraphenylporphyrinato]zinc (**ZnTPP**) as a purple powder (96 mg, 93%). ^{1}H-NMR δ 7.78 (s, 12H), 8.23 (d, J = 6.8 Hz, 8H), 8.96 (s, 8H) (**Figure A-3**); MALDI-TOF-MS m/z obsd 675.422 [M^+], calcd 676.160 (M = $C_{44}H_{28}N_4Zn$) (**Figure A-4**); λ_{abs} (ε) 429 (5.7×10^5), 561, 600 nm (**Figure B-1**, **B-2**); λ_{em} (λ_{ex} = 429 nm) 607, 660 nm (**Figure B-3**). Other spectroscopic data are consistent with those subscribed in the literature.

3.3.2 [5,10,15,20-tetra(thiophen-2-yl)porphyrinato]zinc (ZnTTP)

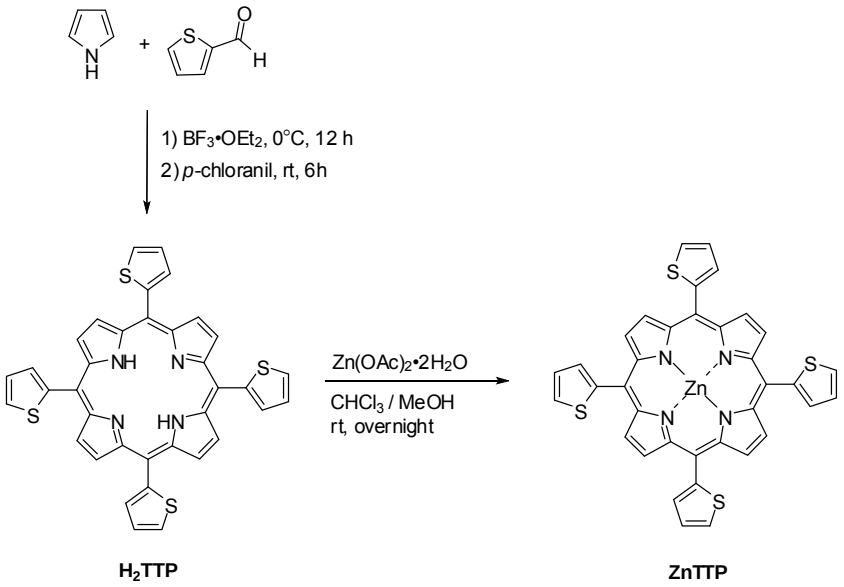

H_2-TTP was readily prepared *via* a modified version of Lindsey's method for synthesis of *meso*-substituted porphyrins [81]. Pyyrole (0.35 mL, 5.0 mmol) and 2-thiophenecarboxaldehyde (0.47 mL, 5.0 mmol) were dissolved in dichloromethane (200 mL) and the solution was purged with nitrogen for 15 min. The reaction mixture was cooled to 0°C, treated with $BF_3 \cdot OEt_2$ (63.4 μL, 0.50 mmol) and stirred at room temperature for 12 h under nitrogen atmosphere. Then tetrachloro-1,4-benzoquinone (*p*-chloranil) (922 mg, 3.75 mmol) was added to the mixture and stirring was

continued for additional 6 h. After removal of the solvent, the crude product was purified by a silica column using 1.5% TEA in dichloromethane as an eluent to give 5,10,15,20-tetra(thiophen-2-yl)porphyrin (**H_2TTP**) as a purple solid (145 mg, 18%). ^{1}H-NMR δ –2.63 (s, 2H), 7.51 (dd, *J* = 3.2, 5.2 Hz, 4H), 7.86 (dd, *J* = 0.8, 5.2 Hz, 4H), 7.92 (dd, *J* = 0.8, 3.2 Hz, 4H), 9.04 (s, 8H) (**Figure A-5**); MALDI-TOF-MS obsd 637.942 ([M^+]), calcd 638.852 ([M^+]; M = $C_{36}H_{22}N_4S_4$) (**Figure A-6**). Other spectroscopic data are consistent with those subscribed in the literature.

Zinc complex of **H_2TTP** was obtained by a standard metallation method [80]. **H_2TTP** (102 mg, 0.160 mmol) was dissolved in chloroform (40 mL) and then reacted with a solution of $Zn(OAc)_2 \cdot 2H_2O$ (176 mg, 0.800 mmol) in methanol (5 mL) at room temperature for 12 h. After removal of the solvent, the reaction mixture was redissolved in CH_2Cl_2 (50 mL), washed with water (50 mL), dried over anhydrous Na_2SO_4, and concentrated to dryness. Purification by column chromatography [silica, 1.5% TEA in CH_2Cl_2] followed by sonicating-centrifugating in hexanes to give [5,10,15,20-tetra(thiophen-2-yl)porphyrinato]zinc (**ZnTTP)** as a purple solid (103 mg, 93%). ^{1}H-NMR δ 7.43 (dd, *J* = 3.2, 5.2 Hz, 4H), 7.78 (d, *J* = 5.2 Hz, 4H), 7.85 (d, *J* = 3.2 Hz, 4H), 9.08 (s, 8H) (**Figure A-7**); ^{13}C-NMR δ 113.2, 125.9, 127.4, 132.2, 133.5, 143.3, 151.4 (**Figure A-8**); HR-ESI-MS m/z obsd 722.9737 ($(M+Na)^+$), calcd 722.9760 ($[M+Na]^+$; M = $C_{36}H_{20}N_4S_4Zn$) (**Figure A-9**); λ_{abs} (ε) 436 (4.4×10^5), 567, 610 nm (**Figure B-4**, **B-5**); λ_{em} (λ_{ex} = 436 nm) 626, 665 nm (**Figure B-6**).

3.3.3 [5,10,15,20-tetra(2,2′-bithiophen-5-yl)porphyrinato]zinc (Zn-TBP)

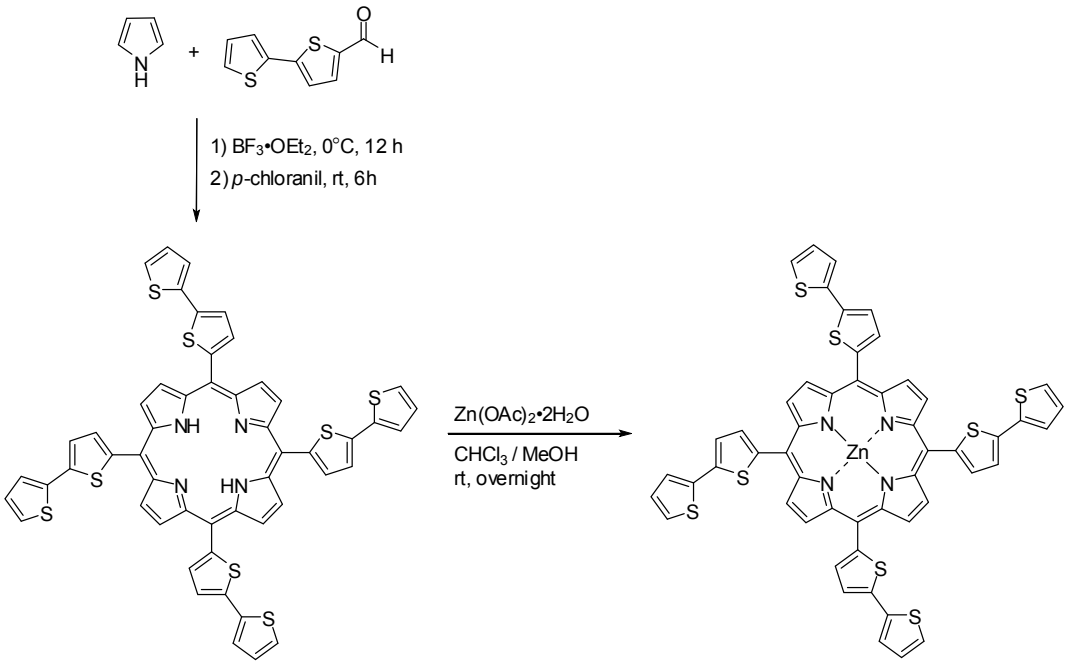

Following a published procedure with a slight modification [81], pyyrole (0.35 mL, 5.0 mmol) and 2,2′-bithiophene-5-carboxaldehyde (971 mg, 5.00 mmol) were dissolved in dichloromethane (200 mL) and the solution was purged with nitrogen for 15 min. The reaction mixture was cooled to 0°C, treated with $BF_3 \cdot OEt_2$ (63.4 μL, 0.50 mmol) and stirred under nitrogen atmosphere at room temperature for 12 h. Then, tetrachloro-1,4-benzoquinone (*p*-chloranil) (922 mg, 3.75 mmol) was added to the mixture and stirring was continued for additional 6 h. After removal of the solvent, the crude product was purified by a silica column using 1.5% TEA in dichloromethane as an eluent to give 5,10,15,20-tetra(2,2′-bithiophen-5-yl)porphyrin (**H_2TBP**) as a deep purple solid (145 mg, 12%). ^{1}H-NMR ($CDCl_3$) δ –2.61 (s, 2H), 7.12 (dd, *J* = 3.6, 5.2 Hz, 4H), 7.34 (dd, *J* = 0.8, 5.2 Hz, 4H), 7.42 (dd, *J* = 0.8, 3.6 Hz, 4H), 7.58 (d, *J* = 3.6 Hz, 4H), 7.80 (d, *J* = 3.6 Hz, 4H), 9.17 (s, 8H) (**Figure A-10**); MALDI-TOF-MS obsd 966.386 [$(M+H)^+$], calcd 966.023 ([M^+]; M = $C_{52}H_{30}N_4S_8$) (**Figure A-11**). Other spectroscopic data are consistent with those subscribed in the literature.

Zinc complex of **H_2TBP** was obtained by a standard metallation method [80]. Compound **H_2TBP** (90 mg, 0.093 mmol) was dissolved in chloroform (30 mL) and then reacted with a solution of $Zn(OAc)_2 \cdot 2H_2O$ (101 mg, 0.46 mmol) in methanol (4 mL) at room temperature for 12 h. After removal of the solvent, the reaction mixture was redissolved in CH_2Cl_2 (30 mL), washed with water (30 mL), dried over anhydrous Na_2SO_4, and concentrated to dryness. Purification by column chromatography [silica, 1.5% TEA in CH_2Cl_2] followed by sonicating-centrifugating in hexanes to give [5,10,15,20-tetra(2,2′-bithiophen-5-yl)porphyrinato]zinc (**ZnTBP**) as a dark green solid (87 mg, 91%). ^{1}H-NMR (toluene-d_8) δ 6.75 (s, 4H), 6.85 (d, J = 4.4 Hz, 4H), 7.19 (s, 4H), 7.35 (d, J = 2.2 Hz, 4H), 7.62 (d, J = 2.2 Hz, 4H), 9.30 (s, 8H) (**Figure A-12**); ^{13}C-NMR (toluene-d_8) δ 112.8, 123.1, 124.1, 124.6, 128.3, 132.4, 134.4, 138.0, 140.0, 143.8, 151.7 (**Figure A-13**); HR-ESI-MS obsd 1029.9408 ($[M+2H]^+$), calcd 1029.9528 ($[M+2H]^+$; M = $C_{52}H_{28}N_4S_8Zn$) (**Figure A-14**); λ_{abs} (ε) 450 (3.5×10^5), 574, 620 nm (**Figure B-7**, **B-8**); λ_{em} (λ_{ex} = 450 nm) 671 nm (**Figure B-9**).

Part 2 : Synthesis of benzoporphyin-thiophene derivatives

3.3.4 *p*-Tolyl 2-(trimethylsilyl)ethynyl sulfone (1)

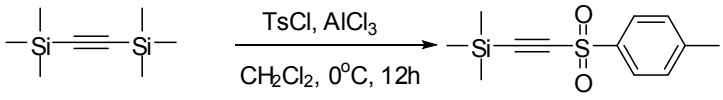

1

Following a previously published procedure [82], in a 250 mL, two-necked round-bottomed flask equipped with nitrogen inlet and septum, powdered anhydrous aluminium chloride (14.7 g, 0.11 mmol) was dissolved in dried dichloromethane (100 mL) and then treated with 4-toluenesulfonyl chloride (*p*-TsCl) (21.0 g, 0.11 mmol). The resulting yellow mixture was stirred at room temperature for 20 min.

To another 250 mL two-necked, round-bottomed flask equipped with nitrogen inlet and septum, bis(trimethylsilyl)acetylene (17.4 g, 0.1 mmol) was dissolved in dried dichloromethane (100 mL) and the solution was cooled to 0°C. Then, the above *p*-TsCl-$AlCl_3$ complex was slowly transferred to this solution *via* a cannula. After the addition was completed, the resulting mixture was stirred at room temperature for

additional 12 h. The mixture was hydrolyzed by pouring into a mixture of a 20% aqueous solution of hydrochloric acid (100 mL) and ice (100 g). The organic layer was separated, washed twice with water (75 mL) and brine (75 mL), and dried over anhydrous Na_2SO_4. After removal of the solvent, the crude product was recrystallized in hexane to give compound **1** (20.3 g, 80%) as a white crystal. ^{1}H-NMR δ 0.00 (s, 9H), 2.26 (s, 3H), 7.16 (d, J = 8.0 Hz, 2H), 7.67 (d, J = 8.0 Hz, 2H) (**Figure A-15**). Other spectroscopic data are consistent with those subscribed in the literature.

3.3.5 Ethynyl *p*-tolyl sulfone (2)

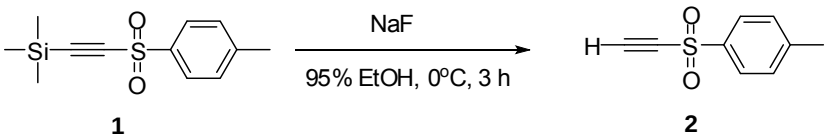

1 **2**

Following a previously published procedure [82], *p*-Tolyl 2-(trimethylsilyl)ethynyl sulfone (**1**) (18.7 g, 0.074 mol) was dissolved in 95% ethanol (400 mL) and the mixture was cooled to 0°C. A clear solution of sodium fluoride (10.0 g, 0.220 mol) in deionized water (150 mL) was added dropwise to the mixture by an additional funnel and the resulting mixture was stirred at room temperature for 3 h. The excess solvent was evaporated to prevent emulsion and the resulting mixture was extracted with dichloromethane (200 mL). The organic layer was washed with water (100 mL) and brine (200 mL), and dried over anhydrous Na_2SO_4. After removal of the solvent, the crude product was recrystallized in hexane to give compound **2** (11.6 g, 87%) as a white crystal. ^{1}H-NMR δ 2.47 (s, 3H), 3.44 (s, 1H), 7.39 (d, J = 8.0 Hz, 2H), 7.90 (d, J = 8.0 Hz, 2H) (**Figure A-16**). Other spectroscopic data are consistent with those subscribed in the literature.

3.3.6 1-Tosyl-1,4-cyclohexadiene (3)

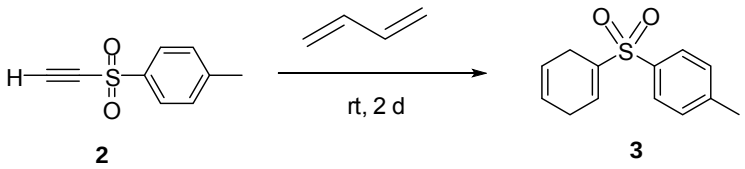

2 3

Following a previously published procedure [70], in a 100 mL heavy-walled sealed tube equipped with septum and gas inlet system, ethylnyl *p*-tolyl sulfone (**2**) (5.00 g, 27.7 mmol) was treated with condensed 1,3-butadiene (approximately 20 mL) at -78°C. The vessel was sealed and stirred at room temperature for 48 h. The excess amount of butadiene was evaporated, and the residue was purified by flash chromatography on a silica column using hexane:ethyl acetate (1:1) as an eluent. The product was recrystallized in hexane to give compound **3** (5.2 g, 80%) as a white crystal. ^{1}H-NMR ($CHCl_3$) δ 2.43 (s, 3H), 2.80 (t, J = 8.8 Hz, 2H), 2.94 (t, J = 8.8 Hz, 2H), 5.60-5.68 (m, 2H), 6.95-7.08 (m, 1H), 7.33 (d, J = 8.0 Hz, 2H), 7.75 (d, J = 8.0 Hz, 2H) (**Figure A-17**). Other spectroscopic data are consistent with those subscribed in the literature.

3.3.7 Ethyl 4,7-dihydro-2*H*-isoindole-1-carboxylate (4)

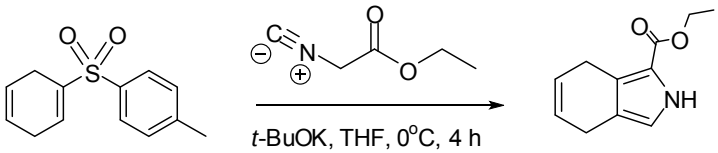

3 4

Following a previously published procedure [70] with a slight modification, ethyl isocyanoacetate (1.93 mL, 15.2 mmol) was added dropwise to a stirred suspension of potassium *tert*-butoxide (1.71 g, 15.2 mmol) in dried tetrahydrofuran (13 mL) at 0°C under nitrogen atmosphere. A solution of 1-tosyl-1,4-cyclohexadiene (3.24 g, 13.8 mmol) in dried tetrahydrofuran (13 mL) was then added dropwise, and the resulting mixture was stirred at room temperature for 4 h. The excess volume of solvent was evaporated by rotary evaporator and dichloromethane (70 mL) was

added. The organic layer was washed twice with water (50 mL) and brine (50 mL) and dried over anhydrous Na_2SO_4. The solvent was evaporated, and the residue was purified on a silica column using dichloromethane:hexane (4:1) as an eluent. The product was recrystallized in hexane to give compound **4** (1.83 g, 69%) as a colorless crystal. ^{1}H-NMR δ 1.36 (t, *J* = 7.2 Hz, 3H), 3.23 (s, 2H), 3.45 (s, 2H), 4.31 (q, *J* = 7.2 Hz, 2H), 5.89 (q, *J* = 11.2 Hz, 2H), 6.71 (d, *J* = 1.2 Hz, 1H), 9.00 (br s, 1H) (**Figure A-18**); ^{13}C-NMR δ 14.5, 22.4, 24.1, 59.8, 117.6, 118.4, 119.0, 123.8, 124.4, 124.9, 161.5 (**Figure A-19**).

3.3.8 4,7-dihydro-2*H*-isoindole

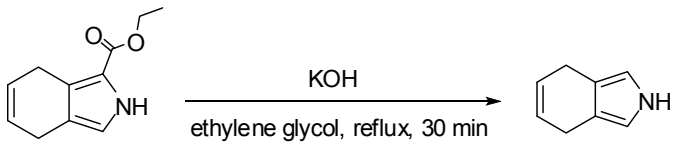

4 **5**

Following a previously published procedure [70], a mixture of ethyl 4,7-dihydro-2*H*-isoindole-1-carboxylate (**4**) (1.30 g, 6.82 mmol) and potassium hydroxide (1.91 g, 34.1 mmol) in ethylene glycol (20 mL) was refluxed under nitrogen atmosphere for 30 min. The mixture was cooled to 0°C and dichloromethane (80 mL) was added. The solution was washed with water (50 mL) and brine (50 mL) and dried over anhydrous Na_2SO_4. The excess solvent was evaporated in vacuo, and the residue was passed through a silica column using dichloromethane as an eluent. The yellow fraction was collected and concentrated to give compound **5** as a yellow oil (0.615 g, 75%). Due to low stability, this compound was used in the further step immediately or can be stored at -20°C up to 3 days.

3.3.9 [5,10,15,20-tetraphenyltetrabenzoporphyrinato]zinc (ZnTPBP)

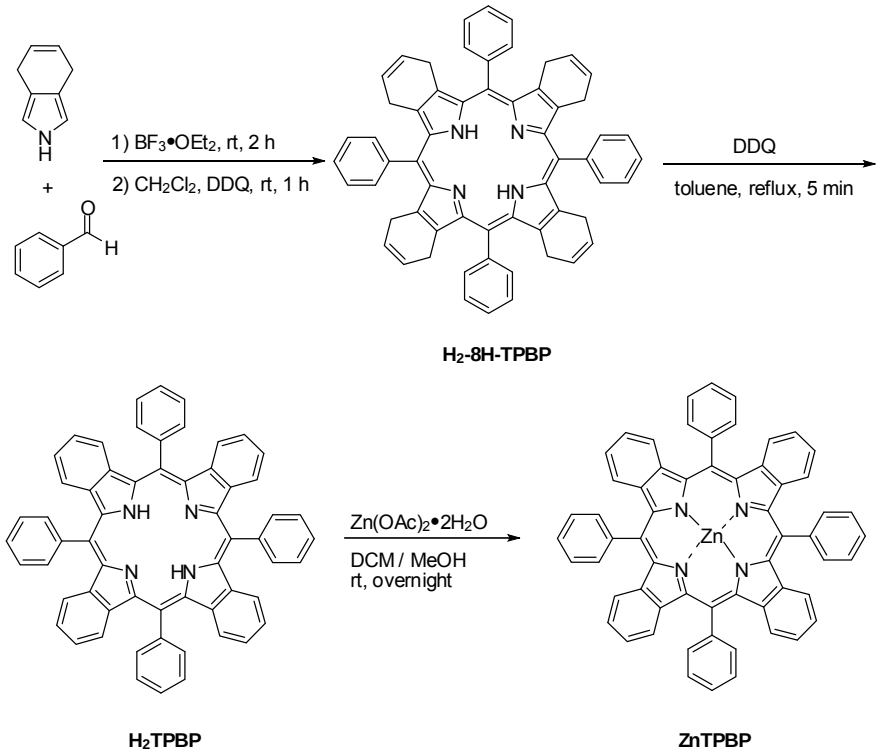

Following a previous published procedure [70], to a 250 mL round-bottomed flask equipped with a nitrogen inlet. 4,7-dihydro-2*H*-isoindole (0.30 g, 2.5 mmol) and benzaldehyde (0.26 mL, 2.5 mmol) were dissolved in dichloromethane (250 mL). The solution was stirred for 10 min in the dark at room temperature and then treated with $BF_3 \cdot OEt_2$ (63 μL, 0.50 mmol) in one portion. After 1 h, 2,3-dichloro-5,6-dicyano-1,4-benzoquinone (DDQ) (0.63 g, 2.8 mmol) was added to the solution and the reaction was stirred for additional 2 h. The resulting solution was washed with 10% sodium sulfite (100 mL), water (100 mL) and brine (100 mL) and dried over anhydrous sodium sulfate. After removal of the solvent, the crude product was purified by a silica column (dichloromethane to 10% ethyl acetate in dichloromethane as eluents to obtain 5,10,15,20-tetraphenyloctahydrotetrabenzoporphyrins (**H_2-8H-TPBP**) as a green solid (94 mg, 18%). MALDI-TOF-MS obsd 822.652 ([M^+]), calcd 822.372 ([M^+]; M = $C_{60}H_{46}N_4$) (**Figure A-20**). Other spectroscopic data are consistent with those subscribed in the literature.

Following to a published procedure [70], a solution of **H_2-8H-TPBP** (90 mg, 0.11 mmol) and dichloro-5,6-dicyano-1,4-benzoquinone (DDQ) (125 mg, 0.550 mmol) in toluene (18 mL) was refluxed for 5 min. The resulting solution was washed with 10% sodium sulfite (10 mL), water (10 mL) and brine (10 mL), and dried over anhydrous Na_2SO_4. After removal of the solvent, the crude product was purified by a silica column using dichloromethane then 10% ethyl acetate in dichloromethane as eluents to give 5,10,15,20-tetraphenyltetrabenzoporphyrins (**H_2TPBP)** as a green powder (86 mg, 96%). ^{1}H-NMR δ –1.17 (s, 2H), 7.02–7.07 (m, 4H), 7.09–7.16 (m, 4H), 7.73–7.97 (m, 16H), 8.06 (d, *J* = 7.2 Hz, 4H), 8.37 (d, *J* = 7.2 Hz, 8H) (**Figure A-21**). MALDI-TOF-MS obsd 814.592 ([M^+]), calcd 814.310 ([M^+]; M = $C_{60}H_{38}N_4$) (**Figure A-22**). Other spectroscopic data are consistent with those subscribed in the literature.

Zinc complex of **H_2TPBP** was obtained by a standard metallation method [80]. Compound **H_2TPBP** (80 mg, 0.098 mmol) was dissolved in dichloromethane (32 mL) and then reacted with a solution of $Zn(OAc)_2 \cdot 2H_2O$ (108 mg, 0.49 mmol) in methanol (4 mL) at room temperature for 12 h. After removal of the solvent, the reaction mixture was redissolved in dichloromethane (30 mL), washed with water (30 mL), dried over anhydrous Na_2SO_4, and concentrated to dryness. Purification by column chromatography [silica, CH_2Cl_2] followed by sonicating-centrifugating in hexanes to give [5,10,15,20-tetraphenyltetrabenzoporphyrinato]zinc (**ZnTPBP)** as a green powder (82 mg, 95 %). ^{1}H-NMR δ 7.17 (dd, *J* = 6.0, 3.2 Hz, 8H), 7.29 (dd, *J* = 6.0, 3.2 Hz, 8H), 7.87 (t, *J* = 7.2 Hz, 8H), 7.95 (t, *J* = 7.2 Hz, 4H), 8.31 (d, *J* = 7.2 Hz, 8H) (**Figure A-23**); MALDI-TOF-MS m/z obsd 875.598 [M^+], calcd 876.223 [M = $C_{60}H_{36}N_4Zn$] (**Figure A-24**); λ_{abs} (ε) 470 (1.9×10^5), 613, 656 nm (**Figure B-10**, **B-11**); λ_{em} (λ_{ex} = 470 nm) 666, 731 nm (**Figure B-12**). Other spectroscopic data are consistent with those subscribed in the literature.

3.3.10 [5,10,15,20-tetra(thiophen-2-yl)octahydro tetrabenzoporphyrinato]zinc (Zn-8H-TTBP)

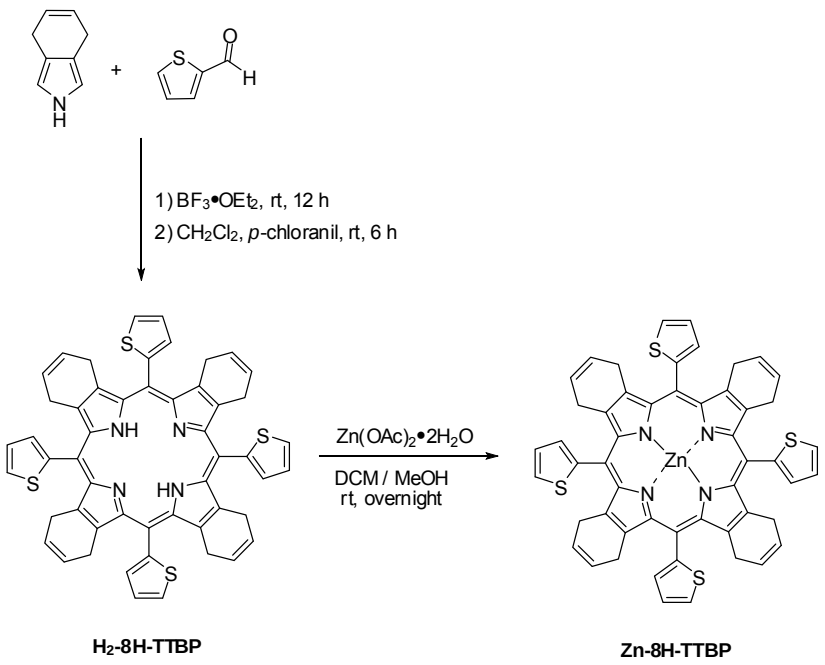

The target compound was synthesized according to a literature [81] with a slight modification and purified by a published method [70]. In a 100 mL round-bottomed flask equipped with a nitrogen inlet, 4,7-dihydro-2*H*-isoindole (0.24 mg, 2.0 mmol) and 2-thiophenecarboxaldehyde (0.19 mL, 2.0 mmol) were dissolved in dichloromethane (200 mL). The solution was stirred at 0°C for 10 min in the dark, treated with $BF_3 \cdot OEt_2$ (50 μL, 0.40 mmol) in one portion and then stirred for additional 12 h. After that, tetrachloro-1,4-benzoquinone (*p*-chloranil) (369 mg, 1.50 mmol) was added and the reaction mixture was stirred for 6 h. The resulting solution was washed with 10% sodium sulfite (80 mL), water (80 mL) and brine (80 mL), and dried over anhydrous Na_2SO_4. After removal of the solvent, the crude product was purified by a silica column using dichloromethane followed by 5-20% ethyl acetate in dichloromethane as eluents to obtain 5,10,15,20-tetra(thiophen-2-yl)octahydrotetrabenzoporphyrin (**H_2-8H-TTBP**). The resulting brown solid was used in next metallation step without further purification.

Zinc complex of **H_2-8H-TTBP** was obtained by a standard metallation method [80]. Compound **H_2-8H-TTBP** (85 mg, 0.10 mmol) was dissolved in dichloromethane (35 mL) and then reacted with a solution of $Zn(OAc)_2 \cdot 2H_2O$ (110 mg, 0.50 mmol) in methanol (4 mL) at room temperature for 12 h. After removal of the solvent, the reaction mixture was redissolved in dichloromethane (35 mL), washed with water (35 mL), dried over anhydrous Na_2SO_4, and concentrated to dryness. Purification by column chromatography [silica, CH_2Cl_2] followed by sonicating-centrifugating in hexanes and methanol to give [5,10,15,20-tetra(thiophen-2-yl)octahydrotetrabenzoporphyrinato]zinc (**Zn-8H-TTBP**) as a blue solid (66 mg, 15%). ^{1}H-NMR δ 3.20–3.55 (m, 16H), 5.62 (s, 8H), 7.14 (d, J = 29.2 Hz, 4H), 7.46 (t, J = 28.0 Hz, 4H), 7.80 (d, J = 19.2 Hz, 4H) (**Figure A-25**); MALDI-TOF-MS obsd 907.592 ([M^+]), calcd 908.111 ([M^+]; M = $C_{52}H_{36}N_4S_4Zn$) (**Figure A-26**).

3.3.10 [5,10,15,20-tetra(2,2′-bithiophen-5-yl)octahydrotetrabenzoporphyrinato]zinc (Zn-8H-TBBP)

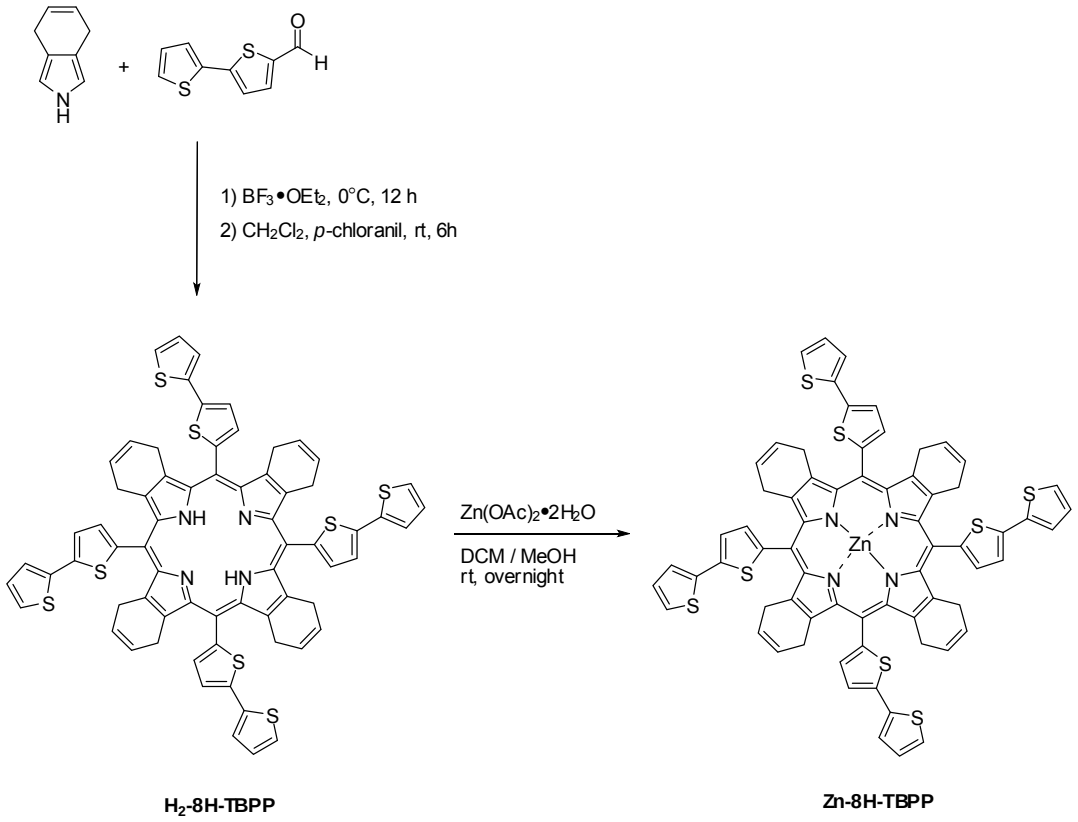

The target compound was synthesized according to a literature [81] with a slight modification and purified by a published method [70]. In a 100 mL round-bottomed flask equipped with a magnetic stirring bar and nitrogen inlet, 4,7-dihydro-2*H*-isoindole (0.24 mg, 2.0 mmol) and 2,2′-bithiophene-5-carboxaldehyde (388 mg, 2.00 mmol) were dissolved in dichloromethane (200 mL). The solution was stirred at 0°C for 10 min in the dark, treated with $BF_3 \cdot OEt_2$ (50 μL, 0.40 mmol) in one portion and then stirred for additional 12 h. After that, tetrachloro-1,4-benzoquinone (*p*-chloronil) (369 mg, 1.50 mmol) was added and the reaction mixture was stirred for an 6 h. The resulting solution was washed with 10% sodium sulfite (80 mL), water (80 mL) and brine (80 mL), and dried over anhydrous sodium sulfate. After removal of the solvent, the crude product was purified by a silica column using dichloromethane followed by 5-25% ethyl acetate in dichloromethane as eluents to obtain 5,10,15,20-tetra(2,2′-bithiophen-5-yl)octahydrotetrabenzoporphyrin (**H_2-8H-TBBP**). The resulting brown solid was used in next metallation step without further purification.

Zinc complex of **H_2-8H-TBBP** was obtained by a standard metallation method [80]. Compound **H_2-8H-TBBP** (85 mg, 0.078 mmol) was dissolved in dichloromethane (30 mL) and then reacted with a solution of $Zn(OAc)_2 \cdot 2H_2O$ (86 mg, 0.39 mmol) in methanol (4 mL) at room temperature for 12 h. After removal of the solvent, the reaction mixture was redissolved in dichloromethane (30 mL), washed with water (30 mL), dried over anhydrous Na_2SO_4, and concentrated to dryness. Purification by column chromatography [silica, CH_2Cl_2] followed by sonicating-centrifugating in hexane and methanol to give [5,10,15,20-tetra(2,2′-bithiophen-5-yl)octahydrotetrabenzoporphyrinato]zinc (**Zn-8H-TBBP**) as a deep red solid (67 mg, 11%). ^{1}H-NMR δ 3.45–3.82 (m, 16H), 5.78 (t, J = 12.0 Hz, 8H), 7.15 (s, 4H), 7.36 (t, J = 4.0 Hz, 4H), 7.46 (s, 4H), 7.56-7.64 (m, 4H), 7.67-7.82 (m, 4H) (**Figure A-27**); MALDI-TOF-MS obsd 1235.507 ([M^+]), calcd 1236.062 ([M^+]; M = $C_{68}H_{44}N_4S_8Zn$) (**Figure A-28**).

3.3.11 [5,10,15,20-tetra(thiophen-2-yl)tetrabenzoporphyrinato]zinc (ZnTTBP) and [5,10,15,20-tetra(2,2′-bithiophen-5-yl)tetrabenzoporphyrinato]zinc (ZnTBBP)

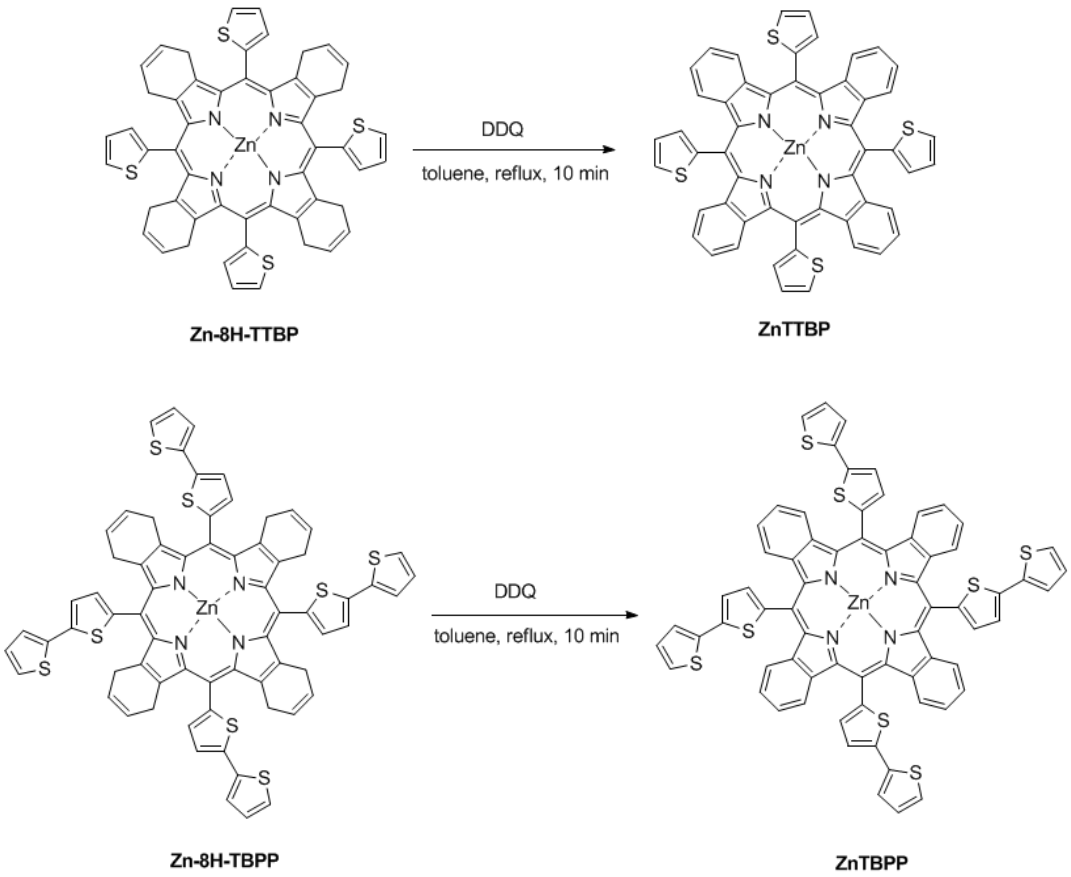

Following a previous published procedure [70] with a slight modification. T o a 25 mL round bottom-flask, **Zn-24H-TTBP** (60 mg, 0.066 mmol) or **Zn-24H-TBBP** (60 mg, 0.048 mmol) was reacted with dichloro-5,6-dicyano-1,4-benzoquinone (DDQ) (5 eq.) in toluene (10 mL) under reflux for 10 min. The resulting solution was washed with 10% sodium sulfite (10 mL), water (10 mL) and brine (10 mL), and dried over anhydrous sodium sulfate. After removal of the solvent, the crude product was purified by a silica column using dichloromethane as an eluent to give [5,10,15,20-tetra(thiophen-2-yl)tetrabenzoporphyrinato]zinc (**ZnTTBP**) or [5,10,15,20-tetra(2,2′-bithiophen-5-yl)tetrabenzoporphyrinato]zinc (**ZnTBBP**) as a blue or brown solid, respectively.

ZnTTBP (55 mg, 92%): ^{1}H-NMR ($CDCl_3$) δ 7.41 (s, 16H), 7.64 (t, *J* = 4.0 Hz, 4H), 7.92 (s, 4H), 8.00 (d, *J* = 5.2 Hz, 4H) (**Figure A-29**); ^{13}C-NMR δ 108.4, 124.9, 126.1, 127.9, 128.6, 132.4, 138.3, 144.8, 145.5 (**Figure A-30**); HR-ESI-MS m/z obsd 900.0561 [M^+], calcd 900.0488 ([M^+]; M = $C_{52}H_{28}N_4S_4Zn$) (**Figure A-31**); λ_{abs} (ε) 476 (2.0×10^5), 622, 667 nm (**Figure B-13**, **B-14**); λ_{em} (λ_{ex} = 476 nm) 677, 742 nm (**Figure B-15**).

ZnTBBP (56 mg, 94%): ^{1}H-NMR δ 7.17 (t, *J* = 3.6 Hz, 4H), 7.39 (d, *J* = 4.8 Hz, 4H), 7.47 (s, 12H), 7.70-7.88 (m, 16H) (**Figure A-32**); ^{13}C-NMR δ 108.2, 124.2, 124.3, 124.7, 126.4, 128.1, 133.4, 137.4, 138.1, 140.8, 144.2, 144.8 (**Figure A-33**); HR-ESI-MS m/z obsd 1229.9895 ([M+2H]$^+$), calcd 1230.0154 ([M+2H]$^+$; M = $C_{68}H_{36}N_4S_8Zn$) (**Figure A-34**); λ_{abs} (ε) 487 ($2.5\text{x}10^5$), 630, 673 nm (**Figure B-16**, **B-17**); λ_{em} (λ_{ex} = 487 nm) 684, 754 nm (**Figure B-18**).

3.4 Electrochemical Studies.

Electrochemical properties of all compounds were determined by cyclic voltammetry in acetonitrile containing 0.1 M Bu_4NPF_6 by using a ITO-coated glass working electrode, a Pt wire counter electrode and a Ag/AgCl quasi-reference electrode (QRE) with scan rate of 10 mV/s^{-1}. The resulting redox potentials were externally calibrated with a ferrocene/ferrocenium couple of which the potential value of 0.40 V versus NHE was used. The value of the NHE versus vacuum level used in this work is –4.75 eV.

CHAPTER IV

RESULTS AND DISCUSSION

The key concepts of molecular designing for organic photosensitizers in this research are based on the hypothesis that: (i) expansion of the porphyrinic macrocycle by introducing the fused benzo ring on the pyrrolic rings will extend the absorption range of the porphyrins in the near IR region, (ii) the introduction of thiophenyl and bithiophenyl unit to the meso positions will lead to the larger conjugation system and also enhanced charge transfer ability. Syntheses of these compounds are discussed as follow.

4.1 Synthesis and characterization

4.1.1 Synthesis of porphyrin-thiophene derivatives

According to the previously published procedure [79], synthesis of the benchmark 5,10,15,20-tetraphenylporphyrin (**H_2TPP**) was achieved by a common condensation between pyrrole and benzaldehyde under an acid-catalysed condition as shown in **Scheme 4-1**.

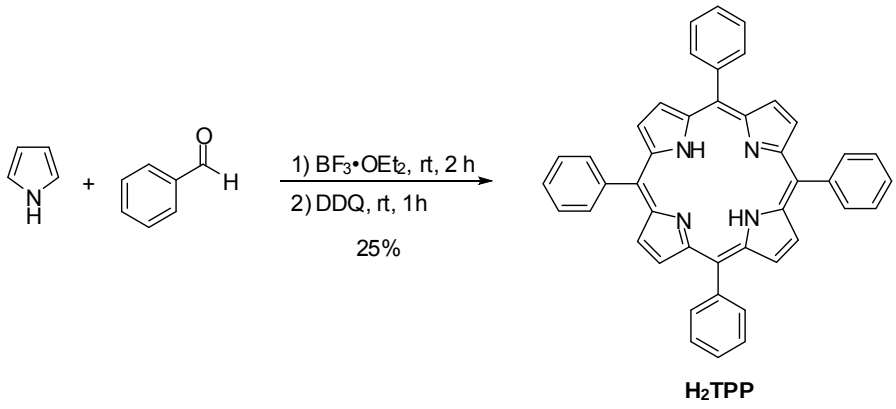

Scheme 4-1: Synthesis of **H_2TPP**.

Due to the low electrophilicity of carboxaldehyde group connected with thiophenyl ring resulting from the resonance effect from thiophenyl ring to carbonyl carbon, this method could not be used in the porphyrin-thiophene synthesis. Free-based porphyrin-thiophene derivatives were successfully synthesized using a modified Lindsey's condition involving a condensation of an appropriate α- carboxaldehyde-functionalized mono- and bithiophene with pyyrole under an acid catalyzed condition at 0°C for 12 h and subsequently oxidized by *p*-chloranil instead of DDQ [81]. This procedure yielded compound 5,10,15,20-tetra(thiophen-2-yl)porphyrin (**H_2TTP**) and 5,10,15,20-tetra(2,2'-bithiophen-5-yl)porphyrin (**H_2TBP**) in 18% and 12%, respectively (**Scheme 4-2**). Based on a thin layer chromatography (TLC), polymerization of pyrrole and the formation of other possible porphyrin by-products causes low yield of the desired product.

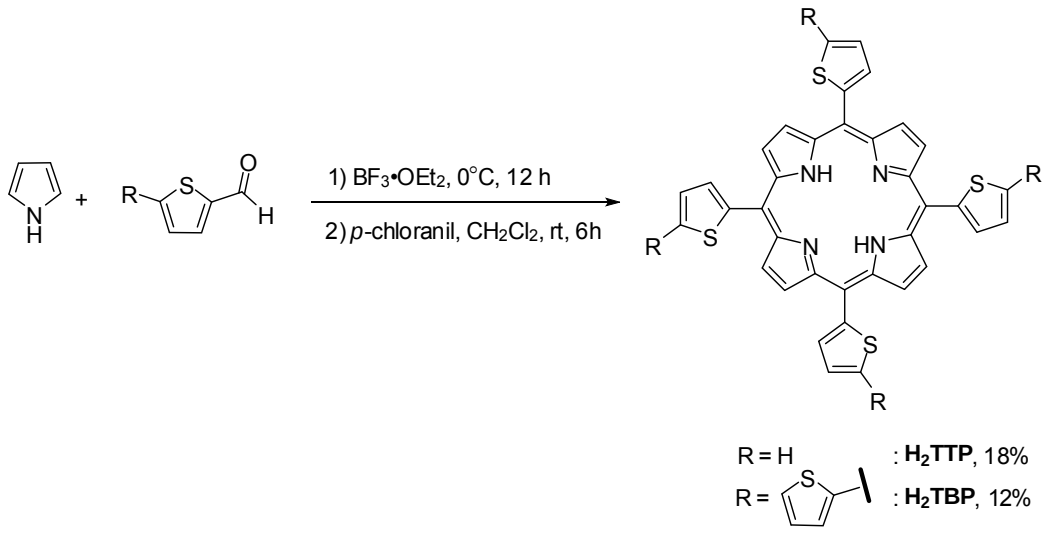

Scheme 4-2: Synthesis of **H_2TTP** and **H_2TBP**.

Based on ^{1}H-nuclear magnetic resonance (NMR) spectra, each of the *β*-pyrrolic protons exhibited identical magnetic environment as a sharp singlet signal around 8-9 ppm (**Figure 4.1**). Another singlet signal of **H_2TTP** and **H_2TBP** at –2.63 and –2.61 ppm was also observed, indicating their inner protons of both free-based porphyrin rings. These singlets occur at –2.77 ppm for **H_2TPP**, while a slightly downfield shift was observed in the **H_2TTP** and **H_2TBP** that consistent to previous literature reports [81, 83]. This phenomenon is resulted from the decreasing of the porphyrin ring current caused by the electron delocalization from porphyrin

macrocycle into the peripheral thiophene units [84]. Beside, mass spectra also confirmed the formation of compound **H_2TTP** and **H_2TBP** by showing their molecular ion peaks at m/z 637.942 and 966.992, respectively.

The subsequent metallation of these free-based porphyrins was performed by a reaction with $Zn(OAc)\cdot 2H_2O$ in $CHCl_3$/MeOH to give **ZnTPP**, **ZnTTP** and **ZnTBP** in excellent yields (**Scheme 4-3**). After purification, ^{1}H-NMR spectra showed the disappearance of the inner protons signal together with the absence of their free-based emission spectrum at about 720, 728 and 707 nm for **ZnTPP**, **ZnTTP** and **ZnTBP**, respectively. Good solubility of these compounds in various common organic solvent such as CH_2Cl_2, toluene, THF, etc. showed its usefulness for film preparation in wet processes.

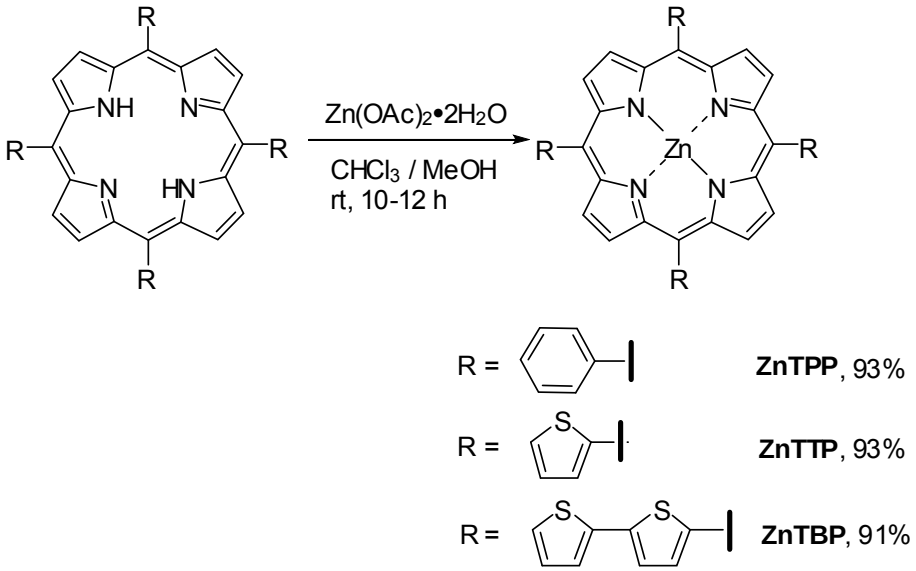

Scheme 4-3: Synthesis of **ZnTPP**, **ZnTTP** and **ZnTBP**.

4.1.2. Synthesis of benzoporphyrin-thiophene derivatives

According to the published reports [70], *meso*-substituted benzoporphyrin derivatives were successfully synthesized from isoindole derivatives. Due to the mild condition in final aromatization step, a commercially available starting material and the effective synthetic pathways, 4,7-dihydro-2*H*-isoindole is the precursor of choice for tetrabenzoporphyrin synthesis in this work.

Part 1: Synthesis of 4,7-dihydro-2*H*-isoindole

The synthesis started from a conventional preparation procedure of *p*-tolyl 2-(trimethylsilyl)ethynyl sulfone (**1**) using commercially available bis-(trimethylsilyl)acetylene [82] as shown in **Scheme 4-4**. The trimethylsilyl group was directly replaced by a tosyl group in the presence of a lewis acid, yielding compound **1** in 80%.

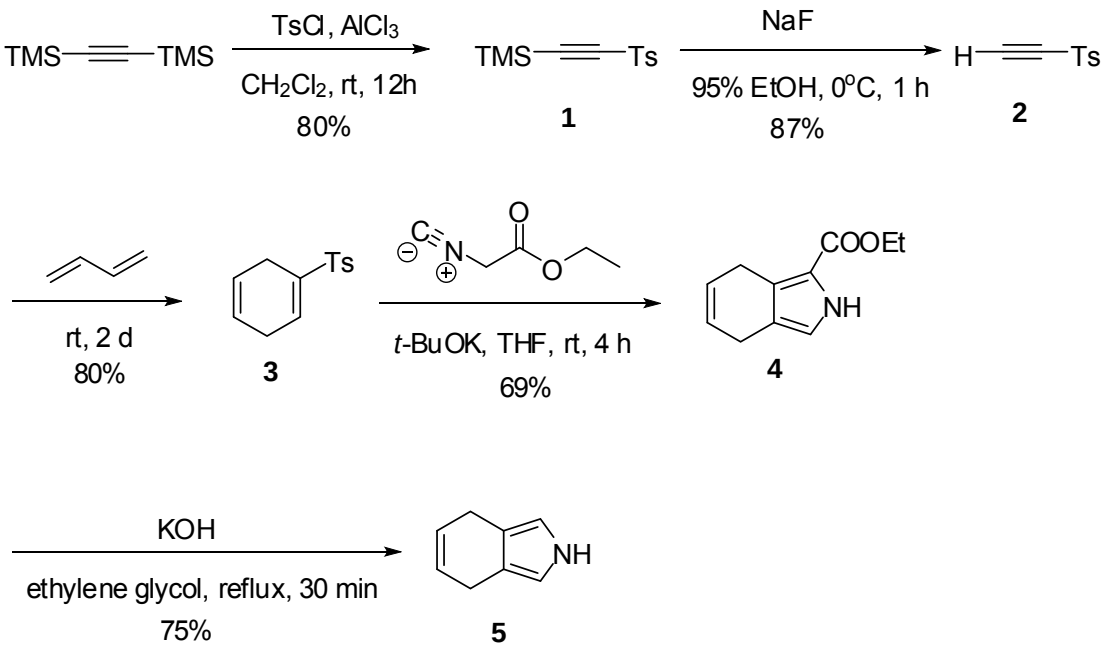

Scheme 4-4: Synthetic pathway of 4,7-dihydro-2*H*-isoindole (**5**).

Another trimethylsilyl group was readily detached from compound **1** by sodium fluoride in 95% ethanol, leading to tosylacetylene (**2)** in 87% yield. Compound **2** is regarded as a powerful dienophile [86]. From the published literatures [86, 87], **2** is usually employed in facile reactions with highly reactive, electron-rich cyclic dienes, such as *N*-acylpyrroles and furan. However, attempts to synthesize 1-tosyl-1,4-cyclohexadiene (**3**) *via* a common [4+2] cycloaddition reaction between **2** and 1,3-butadiene, *in situ* generated from the retro [4+1] cycloaddition of 3-sulfolene in various solvents were not successful (**Scheme 4-5**).

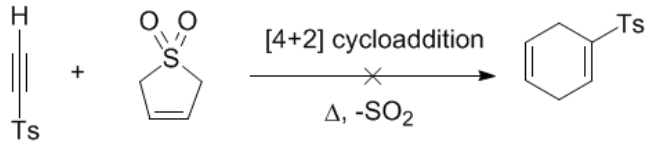

Scheme 4-5: Synthesis of 1-tosyl-1,4-cyclohexadiene (**3**) from 3-sulfolene.

Compound **3** was successfully prepared in 80% from a reaction of **2** with a large excess of butadiene gas at room temperature for 2 days in a thick-walled vessel. Compound **3** was used for the preparation of ethyl 4,7-dihydro-2*H*-isoindole-1-carboxylate (**4**) by a standard Barton–Zard reaction [88]. The reaction mechanism was shown in **Scheme 4-6**. Initially, an α-hydrogen of ethyl isocyanoacetate was deprotonated by potassium *tert*-butoxide (*t*-BuOK) and followed by Micheal addition of the resulting enolate and **3**. The resulting isocyanide intermediate was readily underwent a cyclization, and then aromatization to give corresponding ethyl 4,7-dihydro-2*H*-isoindole-1-carboxylate **(4)** in 69% yield.

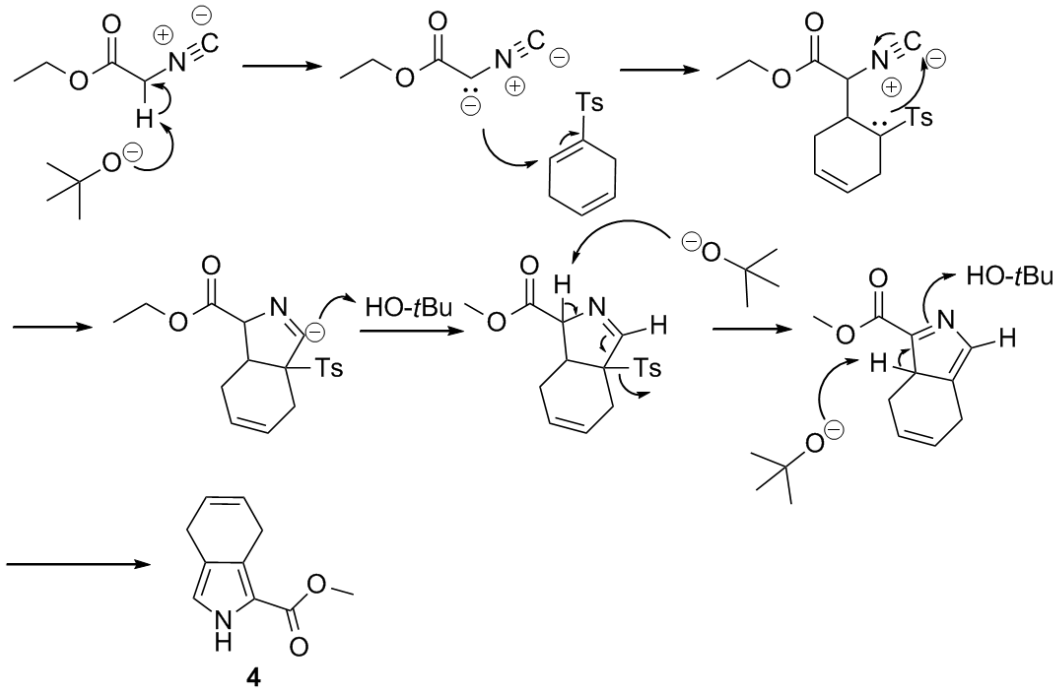

Scheme 4-6: Barton–Zard reaction mechanism of **4** synthesis.

In a ^{1}H-NMR spectrum of **4**, the doublet peaks of tosyl group at 7.33 and 7.75 ppm were disappeared and a broad singlet peak of a pyrrolic proton at 9.00 ppm was observed, indicating the successful reaction. It should be noted that the starting material in this step could be recovered in 15-20% from the crude product by a silica column chromatography using dichloromethane:hexane (3:1) as an eluent and subsequent recrystallization from hexane.

The target precursor, 4,7-dihydro-2*H*-isoindole (**5**), was obtained by performing the hydrolysis and decarboxylation reactions of **4** under basic condition in 75% yield. The mechanism was proposed and shown in **Scheme 4-7**. The unwanted migration of double bond was not observed even though the reaction was performed under reflux likely to be because of higher acidity and nucleophilicity of the pyrrolic nitrogen compared to those of the cyclohexene moiety involved in the awaited double bond migration [70]. Therefore, the pyrrolic ring serves to protect the double bond from the initiation of carbanionic shifts of the six-membered ring.

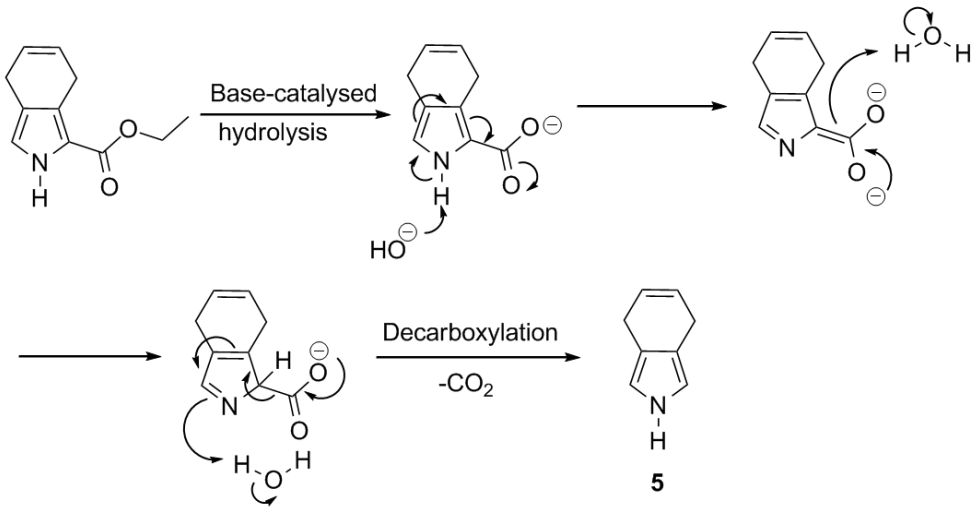

Scheme 4-7: Proposed mechanism of the synthesis of **5** under base-catalyzed condition.

Dihydroisoindole **5** is moderately stable and could be stored at -20°C up to 3 days, though its color rapidly got darken at room temperature similarly to other electron-rich *β*-substituted pyrroles. Therefore, its NMR spectra could not be obtained. This compound **5** was immediately used as a starting material for the *meso*-substituted tetrabenzoporphyrin synthesis.

Part 2: Synthesis of benzoporphyrin-thiophene derivatives

Dihydroisoindole **5** was further used as a starting material for the preparation of *meso*-tetraaryltetrabenzoporphyrins *via* the standard Lindsey's procedure [89]. Following to a literature [70], the first approach for benzoporphyrin synthesis was 5,10,15,20-tetraphenyltetrabenzoporphyrins (**H_2-TPBP**) synthesis as shown in **Scheme 4-8**.

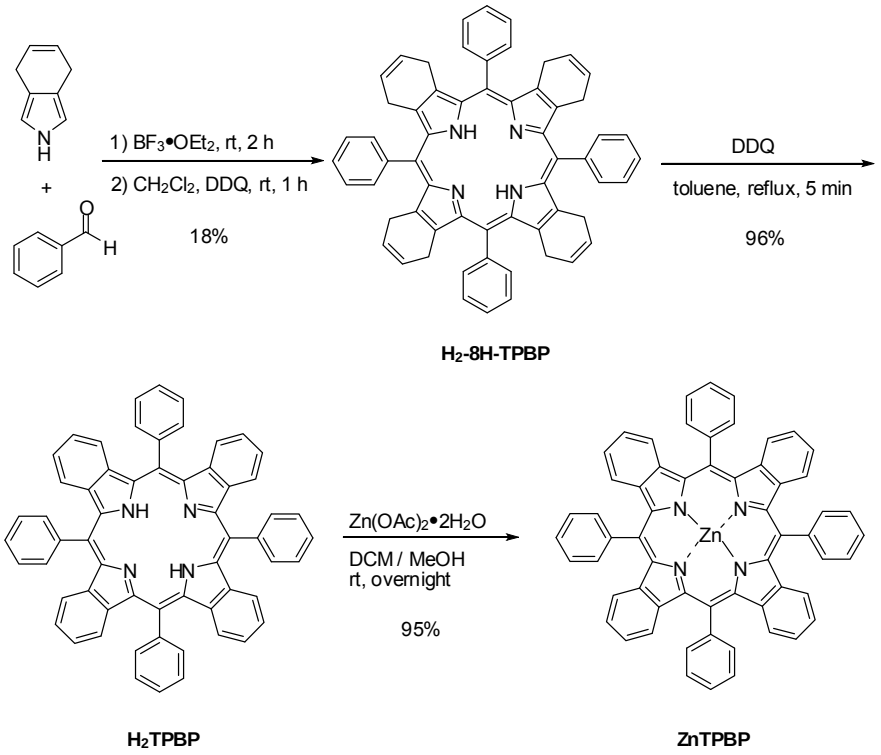

Scheme 4-8: Synthesis of 5,10,15,20-tetraphenyltetrabenzoporphyrins (**H_2-TPBP**).

According to ^{1}H-NMR spectrum, like other free-based porphyrins, **H_2-TPBP** showed a singlet signal of two inner protons at –1.17 ppm. Zinc complex of **H_2TPBP** was obtained by a reaction with $Zn(OAc)_2 \cdot 2H_2O$ in CH_2Cl_2/MeOH to give **ZnTPBP** in 16% overall yield. The absence of inner protons signal in ^{1}H-NMR spectra together with molecular ion peak at *m/z* 875.598 in mass spectra indicated the complete metallation of the benzoporphyrin ring.

Similar to porphyrin-thiophene derivatives, the benzoporphyrin-thiophene target molecules were successfully synthesized by a modified condition instead of a standard Lindsey's method. The synthesis started from condensation of **5** with corresponding α-carboxaldehyde-functionalized mono- and bithiophene under 0^{o}C for 12 h. Subsequently, oxidizing agent, *p*-chloranil, was carefully added in a stoichiometric ratio to prevent over oxidation (**Scheme 4-9**). Unfortunately, due to the high polarity of thiophene ring, free-based benzoporphyrin products could not be completely purified. To remove most of impurities prior to use, the crude product was flash chromatographed by a silica column using dichloromethane and then 5-20% ethyl acetate in dichloromethane as eluents. The resulting fraction containing **H_2-8H-TTB**P or **H_2-8H-TBBP** was directly reacted with $Zn(OAc)_2 \cdot 2H_2O$ in CH_2Cl_2/MeOH to give zinc-5,10,15,20-tetra(thiophen-2-yl) octahydrotetrabenzoporphyrins (**Zn-8H-TTBP**) or zinc-5,10,15,20-tetra(2,2'-bithiophen-5-yl)octahydrotetrabenzoporphyrins (**Zn-8H-TBBP**) in 15% and 11%, overall yield, respectively.

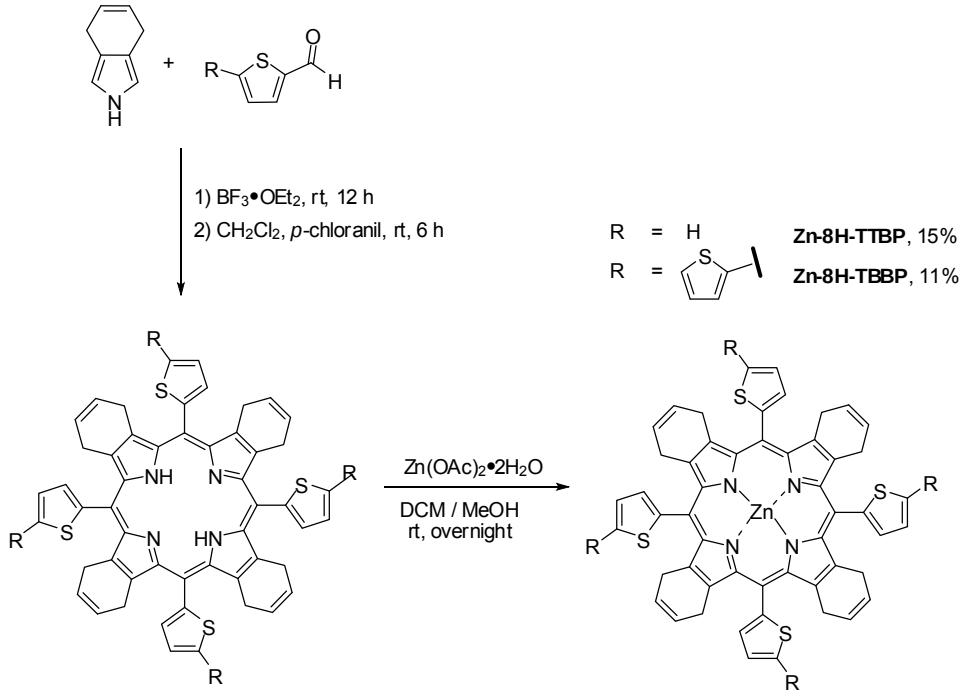

Scheme 4-9: Synthesis of **Zn-8H-TTBP** and **Zn-8H-TBBP**.

From ^{1}H-NMR spectra, **Zn-8H-TTBP** and **Zn-8H-TBBP** exhibited the signals of methylene (-CH_2-) units of β-fused periphery cyclohexene rings around 3.0-4.0 ppm. Mass spectrum also confirmed the formation of these compounds by the molecular ion peaks at *m/z* 907.592 for **Zn-8H-TTBP** and *m/z* 1229.068 for **Zn-8H-TBBP**.

Surprisingly, when **Zn-8H-TTBP** was kept in the dark at room temp for 2 days, it seems that only two cyclohexene ring were oxidized corresponding to its molecular ion peak at *m/z* 903.260. In comparison with the desired final product, **ZnTTBP**, mass spectrum and a proposed structure of undesired oxidized byproduct are shown in **Figure 4-1**.

This phenomena may be cause by the electron delocalization from porphyrin into thiophene units leads to the lower electron density in the macrocycle [84]. Therefore, **Zn-8H-TTBP** and **Zn-8H-TBBP** are easier to be partially oxidized by oxygen in the air compared to a stable molecule as previously reported, **Zn-8H-TPBP** [70].

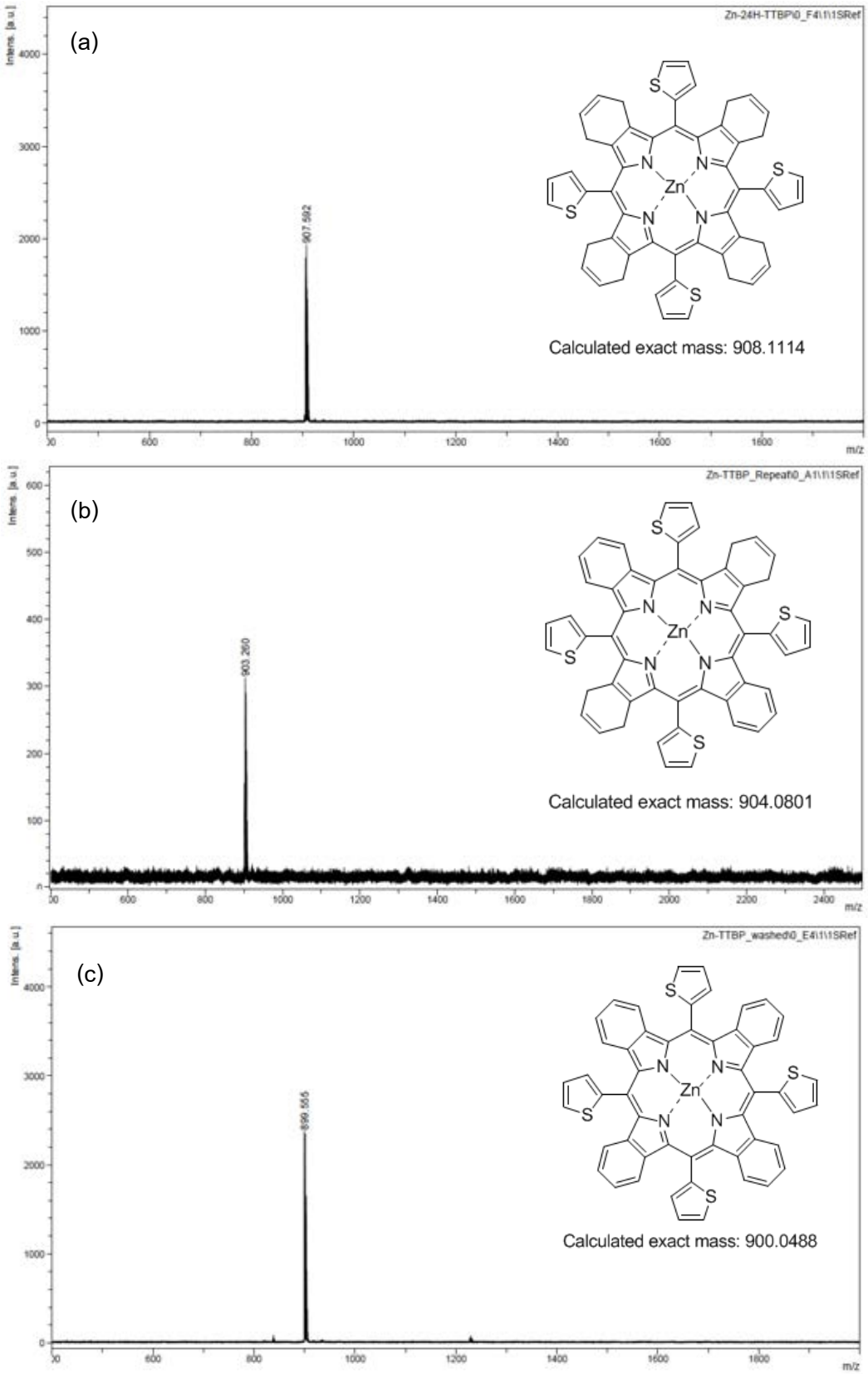

Figure 4-1: Mass spectrum and structure of (a) **Zn-8H-TTBP,** (b) partially oxidized **Zn-8H-TTBP** and (c) **ZnTTBP**.

Further aromatization of **Zn-8H-TTBP** and **Zn-8H-TBBP** was achieved even at room temperature by the reaction with DDQ for several days in the dark. Alternatively, the aromatization to give **ZnTTBP** and **ZnTBBP** can be accelerated by heating the solution in toluene with DDQ for 10 minutes. The reaction was monitored by mass spectroscopic analysis. No byproducts was observed.

Based on ^{1}H-NMR spectra, the signals of methylene (-CH_2-) units of cyclohexene rings that observed in **Zn-8H-TTBP** and **Zn-8H-TBBP** were disappeared together with the presence of extended aromatic-H signal at about 7-8 ppm, indicating the successful aromatization. High resolution mass spectra (HR-ESI-MS) also confirmed the formation of both **ZnTTBP** and **ZnTBBP** by showing their molecular ion peak at *m/z* 900.0561 and 1229.9895, respectively. Good solubility of these compounds in various common organic solvent such as CH_2Cl_2, $CHCl_3$, toluene, THF, etc. showed its usefulness for film preparation in wet processes.

4.2 Investigation of photophysical properties

As the two series of *meso*-thiophene-linked porphyrin and benzoporphyrin derivatives were successfully synthesized and characterized, the photophysical properties was investigated. This study was aimed to evaluate the potential application in optoelectronic devices.

4.2.1 Porphyrin-thiophene series

UV-Vis and fluorescence spectrophotometry were carried out with both solution in toluene and film of **ZnTPP**, **ZnTTP** and **ZnTBP**, resulting in the UV-Vis spectra shown in **Figure 4-2**.

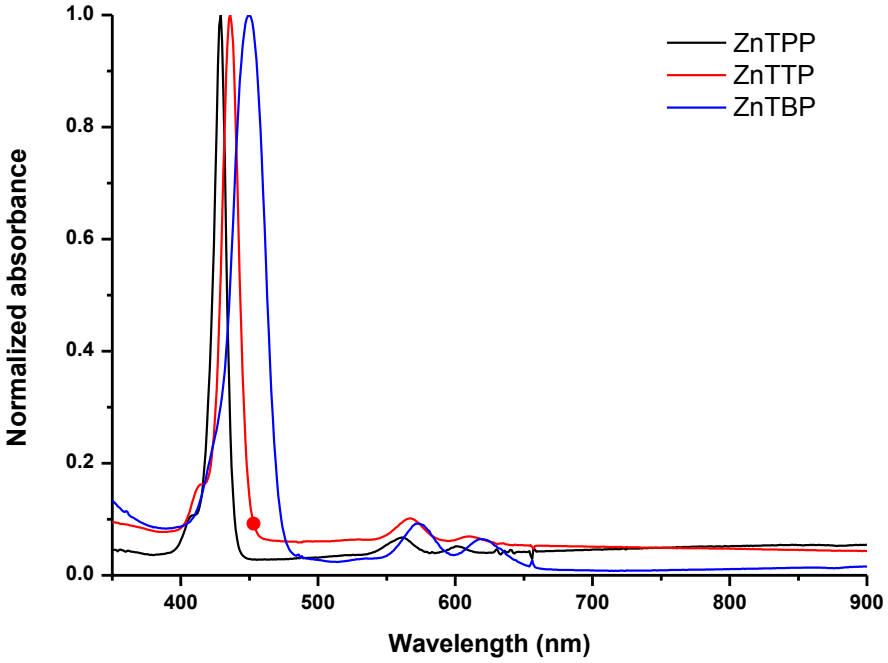

Figure 4-2: Normalized UV-Vis spectra of porphyrin-thiophene derivatives.

There have been many reports in the literature of electronic communication between a porphyrin ring and thiophene substituents at the *meso*-position of the macrocycle [90, 91]. The solution of **ZnTPP, ZnTTP** and **ZnTBP** exhibits a characteristic absorption pattern of a Zn-chelated porphyrin ring having intense B-band at 429, 436 and 450 nm, with the absorption coefficient around 5.7×10^5, 4.4×10^5 and 3.5×10^5 $M^{-1}\cdot cm^{-1}$, respectively. The Soret band was red-shifted by 7 nm for **ZnTTP** and 21 nm for **ZnTBP** with respect to **ZnTPP**. Similar changes were also observed for their Q-bands. These results indicate that the photophysical properties of the individual porphyrin macrocycle were significantly affected by the linking with the thiophene unit, which is consistent with a published report [92]. As reviewed previously [93], the steric hindrance caused by *meso*-thiophenyl ring on the porphyrin macrocycle is smaller than that caused by *meso*-phenyl group because there is only one thiophenyl *β*-hydrogen that can interact with the pyyrole *β*-hydrogen of the porphyrin compared to the two *o*-hydrogens of the phenyl ring. Consequently, the meso thiophenyl ring can rotate more freely than the meso phenyl ring, resulting in the higher π-π interaction between the macrocycle and thiophene substituents.

In addition, the molecular geometry of **ZnTPP** in solid state has also been investigated by B. Purushothaman and co-worker (**Figure 4-3**) [94].

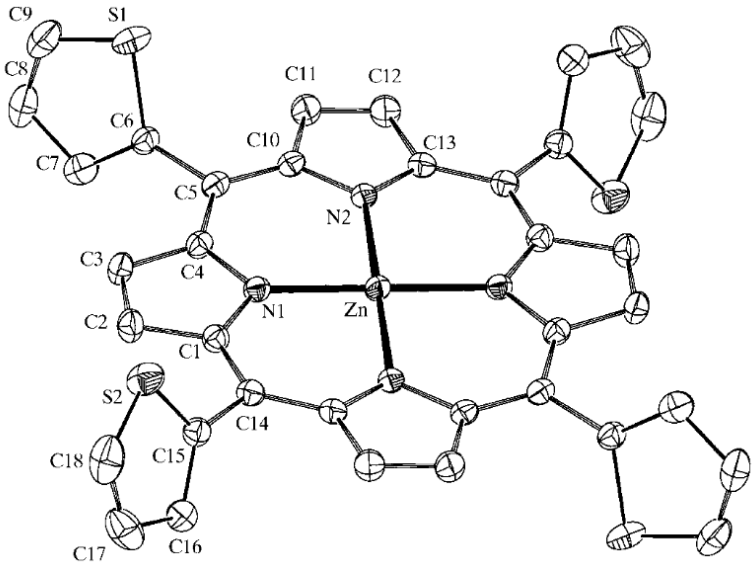

Figure 4-3: The molecular structure (ORTEP; Johnson, 1965) of **ZnTTP**, with the atom numbering scheme and 50% probability displacement ellipsoids. Only one of the two orientations of each of the disordered 2-thienyl rings is shown. H atoms have been omitted for clarity.

This study described that the thienyl groups adopt the typical near-perpendicular position. The average dihedral angle is of 62° between the thienyl group and porphyrin ring which commonly observed in *meso*-tetraarylporphyrins. Evidently, the thienyl groups seem not small enough to create a low-energy co-planar conformation with the porphyrin ring in a solid state. Though the *o*-carbon to *β*-carbon distances are slightly longer than those observed in the crystal structure of **ZnTPP**, the $C_{ortho} - C_{ipso} - C_{meso} - C_{\alpha}$ dihedral angles are similar. This suggests that the red shifting in UV-Vis spectrum of the thiophenyl substituted porphyrins may be caused by co-planarity conformers at the thermal equilibrium, enabling more π-overlaping between two aromatic systems compared to the more rigid rotational structure of the phenyl substituted **ZnTPP**.

Additionally, the red shift of the absorption maximum of **ZnTBP** compared with that of **ZnTTP** suggests that the increasing number of the thiophene ring at the

meso-position of porphyrin macrocycle does affect in electronic interaction between the two π-systems. The result is attributed to the extended conjugation system due to the introduction of the additional thiophene unit.

4.2.2 Benzoporphyrin-thiophene series

According to the literature review in chapter 2 [70], the *β*-extended π-conjugation porphyrin, benzoporphyrin, always show the significant red shift compared to those of the corresponding porphyrin. UV-Vis spectrum of benzoporphyrin-thiophene series synthesized herein in toluene are shown in **Figure 4-4**.

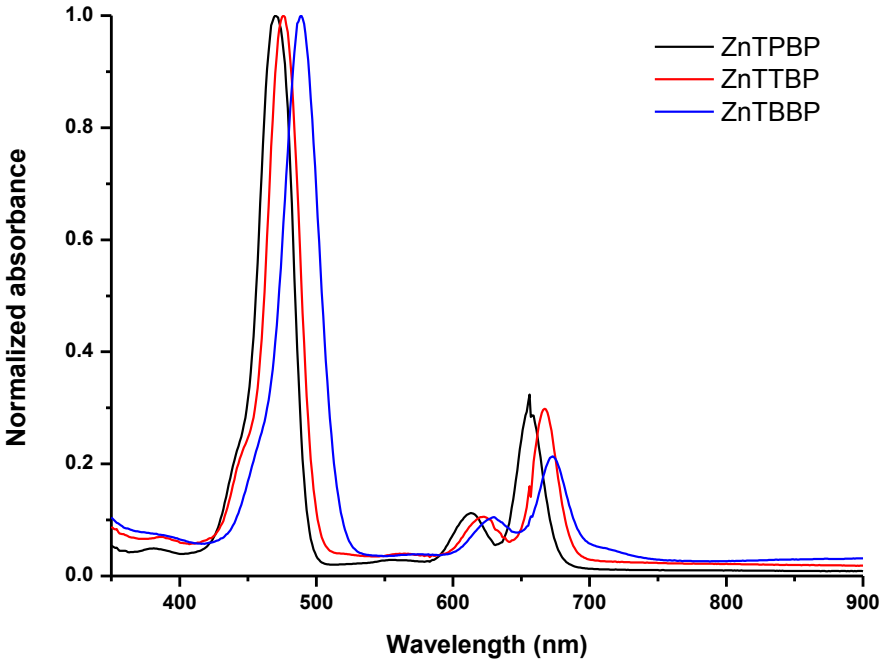

Figure 4-4: Normalized UV-Vis spectra of benzoporphyrin-thiophene derivatives.

Obviously, with the same *meso*-substituents, the absorption spectrum of each benzoporphyrin derivative showed the significant red shift compared to that of its corresponding porphyrin derivative. All benzoporphyrin derivatives exhibited a characteristic absorption pattern of porphyrin ring having intense B-band at 471, 476 and 489 nm for **ZnTPBP, ZnTTBP** and **ZnTBBP**, with the absorption coefficient

equal to $1.9x10^5$, $2.0x10^5$ and $2.5x10^5$ $M^{-1}\cdot cm^{-1}$, respectively. The B-band was red-shifted by 5 nm for **ZnTTBP** and 27 nm for **ZnTBBP** with respect to **ZnTPBP**. Similar changes are also observed for the Q bands. Clearly, in benzoporphyrin-thiophene series, the red shift causing by the delocalization from thiophene *meso*-substituents into benzoporphyrin macrocycle is still observed in the same pattern.

Comparison between both porphyrin series (**Figure 4-5**) suggests that the broadening of absorption peaks was also observed when the substituents group was changed from phenyl group to mono- and bi-thiophene, respectively. These results are consistent with those reported by Harriman *et al.* [95] describing that increasing the electronic interaction between the porphyrin macrocycle and the *meso*-substituents caused a red shift and band broadening due to the "intensity exchange" of the S_2 and S_1 electronic states. This result conforms that the thiophenyls appending on the macrocycles have positive effect on improving the UV-visible absorption of the porphyrin dyes.

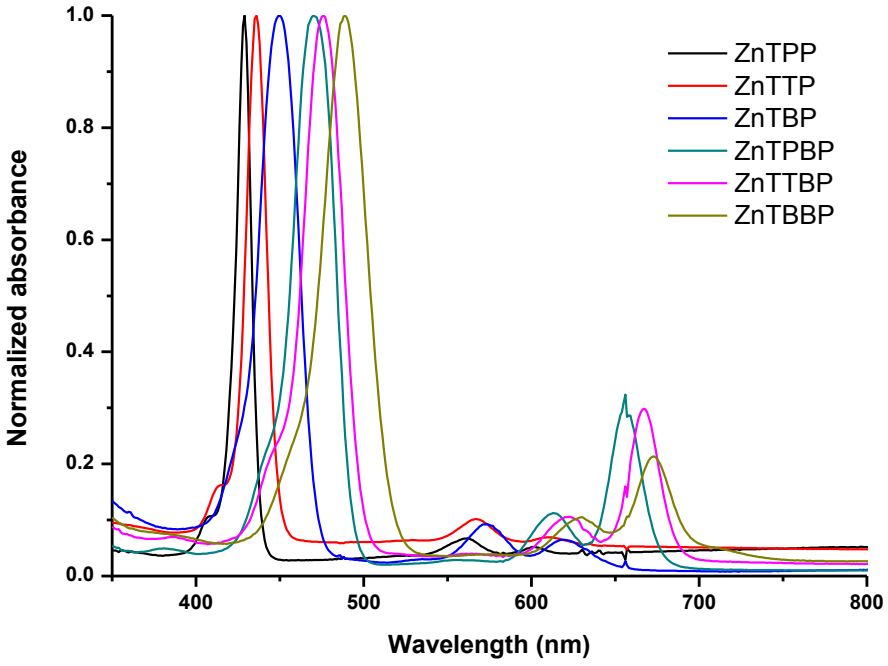

Figure 4.6: Normalized UV-Vis spectra of porphyrin- and benzoporphyrin-thiophene series.

4.3.3 UV-Vis absorption in a film state

The photophysical properties of all porphyrin derivaives were also investigated in form of film to evaluate the potential used in BHJ-SCs. Each porphyrin derivatives were fabricated on a glass substrate by a drop-casting technique. UV-Vis absorption spectra of the films are shown in **Figure 4-6**.

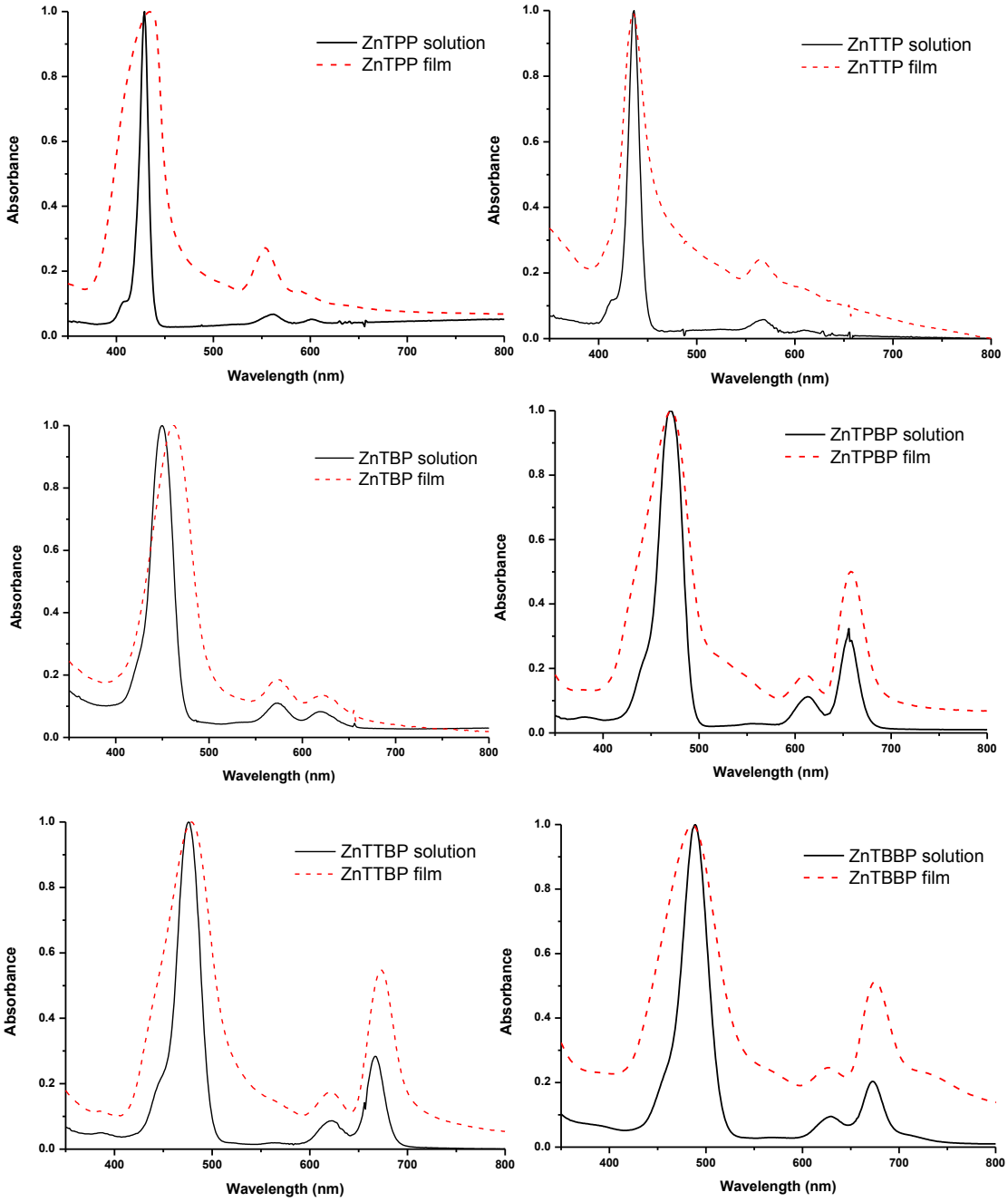

Figure 4-6: UV-Vis spectra of the solution (black line) and the film (red dashed line) porphyrin and benzoporphyrin derivatives.

As expected, the absorption patterns if the films of all porphyrin derivatives were consistent with those of their solutions except that the band were broader. This is attributed to the aggregation of the porphyrin macrocycle which commonly observed in solid state.

4.2.4 Emission spectra

The emission spectra of the solution of porphyrin-thiophene derivatives in solution are shown in **Figure 4-7**. Upon excitation at 436 nm, **ZnTTP** exhibited emission peaks at 627 and 667 nm. As for the emission of **ZnTBP**, the single broad peak at 670 nm was observed upon the excitation at its absorption maximum (450 nm). The maximum emission wavelength (λ_{em}) is red-shifted by 20 nm for **ZnTTP** and 63 nm for **ZnTBP** with respect to **ZnTPP**.

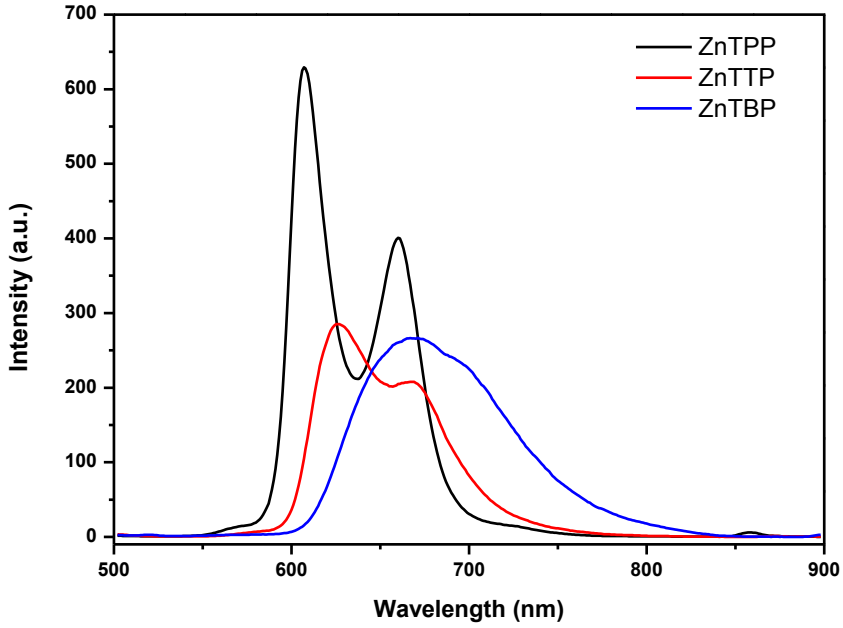

Figure 4-7: Emission spectra of the 10 μM solution of **ZnTPP** (black line), **ZnTTP** (red line) and **ZnTBP** (blue line) in toluene.

In a similar manner to their absorption spectra, the emission spectra of benzoporphyrin-thiophene derivatives exhibited the red shift when compared with those of porphyrins (**Figure 4-8**). Upon excitation at 470 nm, **ZnTPBP** exhibited emission peaks at 670 and 730 nm. The emission peaks of **ZnTTBP** were observed at

677 and 743 nm upon the excitation at its absorption maximum (476 nm). As for the emission of **ZnTBBP**, upon the excitation at 487 nm, the broader peak at 685 and 753 nm was observed. The maximum emission wavelength (λ_{em}) is red-shifted by 7 nm for **ZnTTBP** and 15 nm for **ZnTBBP** with respect to **ZnTPBP**. The observed red-shifts of λ_{em} should be attributed to the increase of the effective conjugation in **ZnTTBP** and **ZnTBBP** molecules compared to that of **ZnTPBP**. These results are obviously affected from the extending conjugation by the thiophene unit attached.

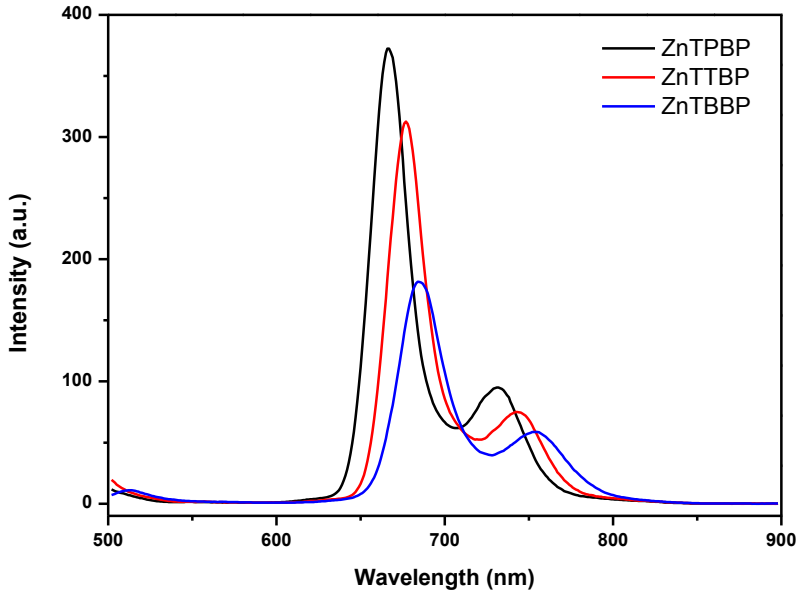

Figure 4-8: Emission spectra of the 10 μM solution of **ZnTPBP** (black line), **ZnTTBP** (red line) and **ZnTBBP** (blue line) in toluene.

It should be noted that the lower of emission intensities when the substituents group was changed from phenyl to mono- and to bithiophene group might be caused by the heavy atom effect due to the presence of additional sulfur atoms on the periphery of the porphyrin ring [78].

In order to prove the electronic communication when thiophene moieties connected with porphyrin macrocycle. Porphyrin and benzoporphyrin derivatives were excited at all of their observed absorption wavelengths (B- and Q-bands). The resulting emission spectra are shown in **Figure 4-10**

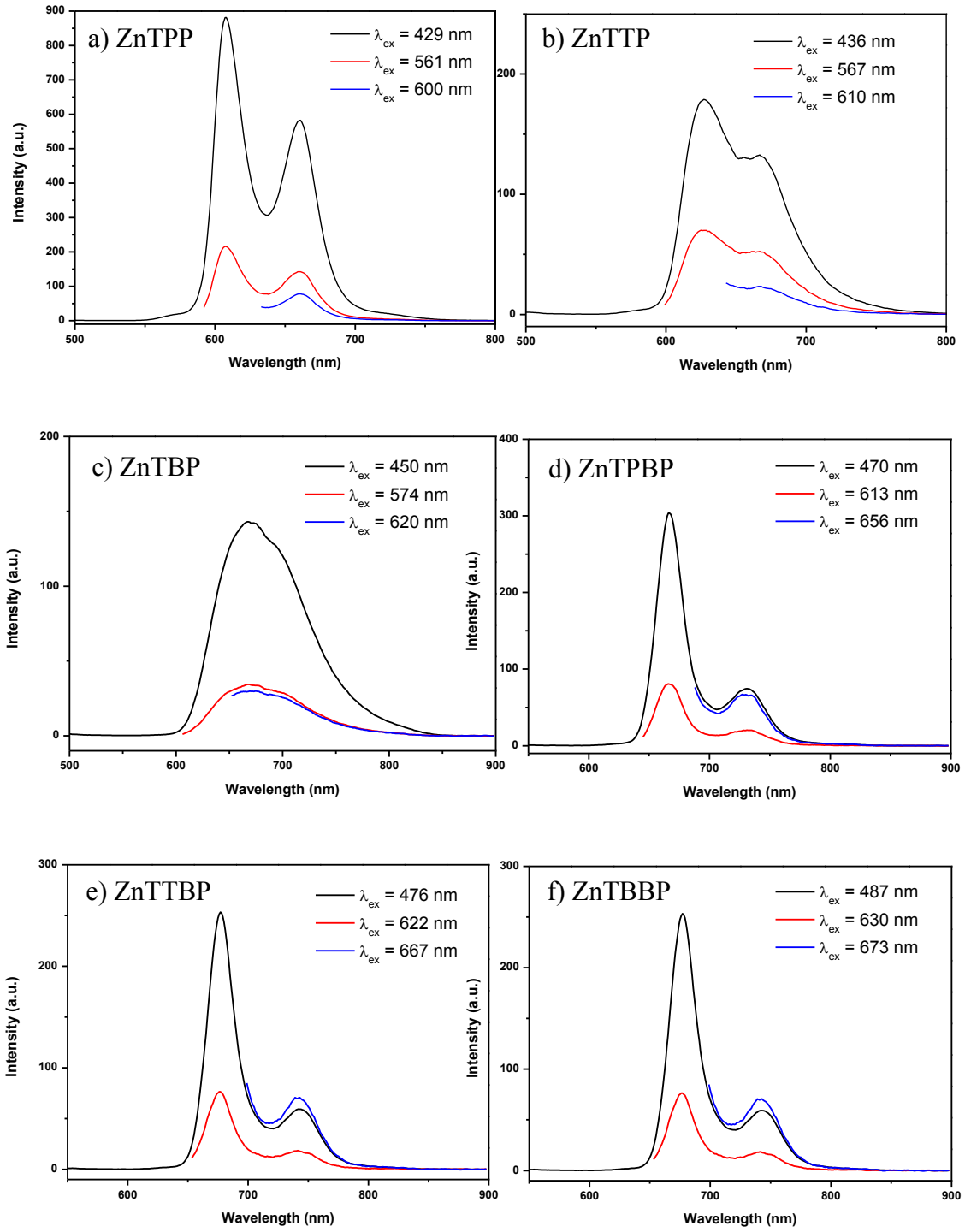

Figure 4-10: Emission spectra of (a) **ZnTTP** (b) **ZnTTP** (c) **ZnTBP** (d) **ZnTPBP** (e) **ZnTTBP** and (f) **ZnTBBP** upon excitation at their absorption wavelengths.

All of porphyrin derivatives still showed the same pattern of its emission spectra upon the excitation at different wavelengths, indicating the electronic corporation between porphyrin and thiophene as a single molecule. To confirm this conclusion, the back excitation were employed to observe the origin of each emission peak (**Figure 4-10**).

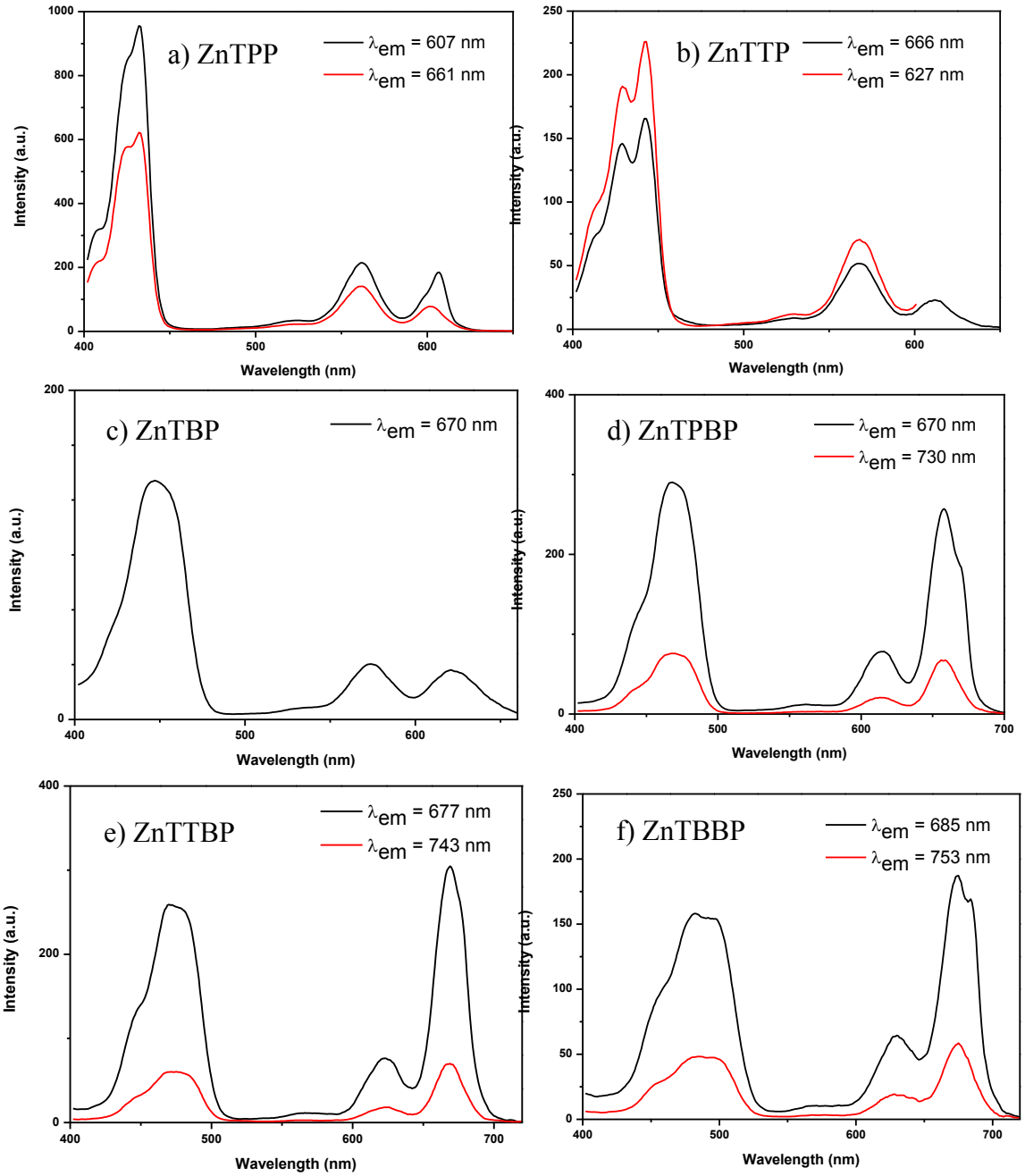

Figure 4-10: Excitation spectra of (a) **ZnTTP** (b) **ZnTTP** (c) **ZnTBP** (d) **ZnTPBP** (e) **ZnTTBP** and (f) **ZnTBBP**.

The results in **Figure 4-10** showed that all excitation spectra are consistent with their absorption spectra, confirming that the porphyrin or benzoporphyrin macrocycle and their *meso*-substituents have electronic communication and absorb light as a single molecule.

4.3 Investigation of electrochemical properties

Electrochemical properties of all compounds in film were determined by mean of cyclic voltammetry in MeCN containing Bu_4NPF_6 by using a ITO-coated glass working electrode, Pt wire counter electrode and Ag/AgCl quasi-reference electrode (QRE) with scan rate of 10 mV/s. The resulting redox potentials were externally calibrated with ferrocene/ferrocenium couple of which the potential of 0.40 V *vs* NHE was used. These values were used to determine an energy gap (E_{gab}), and Highest Occupied Molecular Orbital (HOMO) and Lowest Unoccupied Molecular Orbital (LUMO) energy levels (E_{HOMO} and E_{LUMO}, respectively) of compounds *versus* vacuum with an estimated energy of NHE of –4.75 eV *versus* vacuum [97, 98]. According to the equations:

$$E_g = E_{ox} - E_{red};$$

$$E_{HOMO} = -(Eox + 4.75)\ (eV);\ \text{and}$$

$$E_{LUMO} = -(Ered + 4.75)\ (eV);\ [99]$$

The calculated E_{gab} with E_{HOMO} and E_{LUMO} of compounds from cyclic voltammetry are described in **Table 4-1**.

Compound	E_{HOMO} (eV)	E_{LUMO} (eV)	E_{gab} (eV)
ZnTPP	**–5.6**	**–3.3**	**2.3**
ZnTTP	**–5.7**	**–3.6**	**2.1**
ZnTBP	**–5.6**	**–3.6**	**2.0**
ZnTPBP	**–5.3**	**–3.3**	**2.0**
ZnTTBP	**–5.5**	**–3.5**	**2.0**
ZnTBBP	**–5.3**	**–3.6**	**1.7**

Table 4-1: The estimated E_{HOMO}, E_{LUMO} and E_{gab}

The porphyrin series has comparable HOMO-LUMO levels in the range of –5.6 to –5.7 eV and –3.3 to –3.6 eV with energy band gap around 2.0-2.3 eV and benzoporphyrin derivatives also has the similar pattern with slightly narrower energy gap about at 1.7-2.0 eV. These narrowing energy band gap can be explained by π-π overlap of the macrocycle and thiophenyl structures resulting in the stabilization of both HOMO and LUMO orbitals. It should be noted that the difference of 0.1 eV was not quite significant as it is from the consideration of the onset point of the plot.

To determine whether compounds should be employed as a donor or acceptor in the BHJ-OSCs, the calculated HOMO-LUMO energy level were plotted with ITO conduction band (CB), PEDOT:PSS Fermi level (FL), HOMO-LUMO level of P3HT and PCBM and Al work function (WF), as shown in **Figure 4-11**.

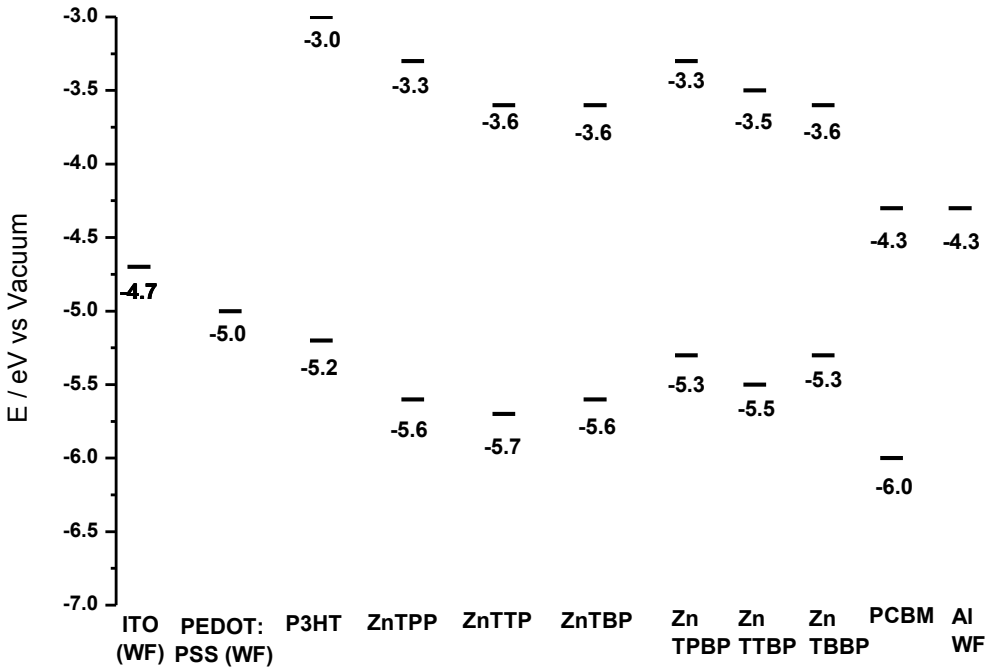

Figure 4-11: Comparative energy diagram of all derivatives based on BHJ-SC.

The plot reveals that the LUMO level of all porphyrin and benzoporphyrin derivatives were positioned at the lower level than that of P3HT. Therefore, the electron transfer from the excited P3HT molecule to those of porphyrins and then further to the Al electrode should be allowed. In addition, with the LUMO energy level of all derivative located above that of PCBM and the HOMO energy level lied below the WF of PEDOT:PSS, electron transfer from the excited molecules to PCBM and the charge transport from PEDOT:PSS to HOMO of compounds should be also possible. The further photoluminescence studies to confirm the use of these compounds as an electron acceptor for P3HT and as a donor for PCBM in the BHJ-OSCs will be performed and reported elsewhere.

CHAPTER V

CONCLUSION

Two series of zinc-metallated porphyrin and benzoporphyrin derivatives bearing thiophenyl and bithiophenyl at meso position were successfully synthesized from condensation between corresponding pyrrole and α-functionalized-carboxaldehyde thiophene in moderate yield (10-25%). The resulting compounds were characterized by spectroscopic techniques. All compounds showed characteristic absorption peaks at around 429 to 487 nm, and emission at around 604 to 684 nm upon the excitation at theirs maximum absorption. In comparison with benchmark phenyl-substituted porphyrin and benzoporphyrin, the spectrophotometric data of thiophene derivatives revealed that with an increasing number of the thiophenyl rings at the porphyrin meso positions, the red shift of absorption and emission maxima to the near-IR region were observed in both solutions and films due to the extended π-conjugated system. Good solubility of these compounds in various common organic solvent such as CH_2Cl_2, toluene, THF, etc. showed its usefulness for film preparation in wet processes. Moreover, based on cyclic voltammetry, the estimated energy band gaps and HOMO-LUMO energy levels of all derivatives are in the range allowing charge transport in the solar cells.

These results also confirm that the thienyls appending on both porphyrin and benzoporphyrin macrocycles can improves the photophysical and electrochemical properties for using in organic optoelectronic applications.

References

[1] World energy resources and consumption. Wikipedia [online]. 2010, Available from:http://en.wikipedia.org/wiki/World_energy_respurces_and_consumption [2010, May].

[2] Asimov, Isaac; *Understanding Physics: The Electron, Proton, and Neutron*; pg. 208.

[3] Wong, W. Y. and Ho, C. L. Organometallic photovoltaics: A new and versatile approach for harvesting solar energy using conjugated polymetallaynes. Accounts of Chemical Research. 43 (2010): 1246-1256.

[4] Bundgaard, E. and Krebs, F. C. Low band gap polymers for organic photovoltaics. Solar Energy Materials and Solar Cells. 91 (2007): 954-985.

[5] Ambroise, A., Wagner, R. W., Rao, P. D., Riggs, J. A., Hascoat, P., Diers, J. R., Seth, J., Lammi, R. K., Bocian, D. F., Holten, D. and Lindsey, J. S. Design and synthesis of porphyrin-based optoelectronic gates. Chemistry of Materials. 13 (2001): 1023-1034.

[6] Anderson, H. L. Building molecular wires from the colours of life: Conjugated porphyrin oligomers. Chemical Communications. (1999): 2323-2330.

[7] Krebs, F. C. and Spanggaard, H. Antibatic photovoltaic response in zinc-porphyrin-linked oligothiophenes. Solar Energy Materials and Solar Cells. 88 (2005): 363-375.

[8] K.M. Kadish, E.V. Caemelbecke and G. Royal In: K.M. Kadish, K.M. Smith and R. Guilard, Editors, *The Porphyrin Handbook*, **Vol.8,** Acedemic Press, New York (2000) ch. 55.

[9] Fang, Z. and Liu, B. A cationic porphyrin-based self-assembled film for mercury ion detection. Tetrahedron Letters. 49 (2008): 2311-2315.

[10] Kathiravan, A., Kumar, P. S., Renganathan, R. and Anandan, S. Photoinduced electron transfer reactions between meso-tetrakis(4-sulfonatophenyl)porphyrin and colloidal metal-semiconductor nanoparticles. Colloids and Surfaces A: Physicochemical and Engineering Aspects. 333 (2009): 175-181.

[11] Campbell, W. M., Jolley, K. W., Wagner, P., Wagner, K., Walsh, P. J., Gordon, K. C., Schmidt-Mende, L., Nazeeruddin, M. K., Wang, Q., Grätzel, M. and Officer, D. L. Highly efficient porphyrin sensitizers for dye-sensitized solar cells. Journal of Physical Chemistry C. 111 (2007): 11760-11762.

[12] The World's First Solution Conversion Type Organic Photovoltaic. Mitsubishi Chemical Group Science and Technology Research Center, Inc, 2011. Available from: http://www.mitsubishichemhd.co.jp/english/group/strategy/major_project/solar_cell.html [2011, Sep].

[13] P. Bäuerle In: K.G. Müllen, Editor, *Oligothiophenes in Electronic Materials: The Oligomer Approach,* Wegner, Wiley-VCH, Weinheim, Germany (1998), pp. 105–197.

[14] Casey, H. C. Jr., and Panish, M. B., *Heterostructure Lasers*, Academic Press, New York (1978).

[15] Robbins, D. J., Calcott, P. and Leong, W. Y. Electroluminescence from a pseudomorphic $Si_{0.8}Ge_{0.2}$ alloy. Applied Physics Letters. 59 (1991): 1350-1352.

[16] Tang, C. W. and Vanslyke, S. A. Organic electroluminescent diodes. Applied Physics Letters. 51 (1987): 913-915.

[17] Burroughes, J. H., Bradley, D. D. C., Brown, A. R., Marks, R. N., Mackay, K., Friend, R. H., Burns, P. L. and Holmes, A. B. Light-emitting diodes based on conjugated polymers. Nature. 347 (1990): 539-541.

[18] Kido, J., Kimura, M. and Nagai, K. Multilayer white light-emitting organic electroluminescent device. Science. 267 (1995): 1332-1334.

[19] Burn, P. L., Lo, S. C. and Samuel, I. D. W. The development of light-emitting dendrimers for displays. Advanced Materials. 19 (2007): 1675-1688.

[20] Keaens, D. and Calvin, M. Photovoltaic effect and photoconductivity in laminated organic systems. The Journal of Chemical Physics. 29 (1958): 950-951.

[21] Yu, G., Gao, J., Hummelen, J. C., Wudl, F. and Heeger, A. J. Polymer photovoltaic cells: Enhanced efficiencies via a network of internal donor-acceptor heterojunctions. Science. 270 (1995): 1789-1791.

[22] Yu, G., Wang, J., McElvain, J. and Heeger, A. J. Large-area, full-color image sensors made with semiconducting polymers. Advanced Materials. 10 (1998): 1431-1434.

[23] Jabłoństski, A. Efficiency of anti-stokes fluorescence in dyes [6]. Nature. 131 (1933): 839-840.

[24] Jaffé, H. H. and Miller, A. L. The fates of electronic excitation energy. Journal of Chemical Education. 43 (1966): 469-473.

[25] Tang, C. W. and Vanslyke, S. A. Organic electroluminescent diodes. Applied Physics Letters. 51 (1987): 913-915.

[26] Shirota, Y. Organic materials for electronic and optoelectronic devices. Journal of Materials Chemistry. 10 (2000): 1-25.

[27] Abraham, R. J., Medforth, C. J., Mansfield, K. E., Simpson, D. J. and Smith, K. M. Nuclear magnetic resonance spectra of porphyrins. Part 33.1 ring currents in nickel(II) hydroporphyrins derived from anhydromesorhodoporphyrin XV. Journal of the Chemical Society, Perkin Transactions 2. (1988): 1365-1370.

[28] Vicente, M. G. H., Jaquinod, L. and Smith, K. M. Oligomeric porphyrin arrays. Chemical Communications. (1999): 1771-1782.

[29] Thunell, S. Porphyrins, porphyrin metabolism and porphyrias. I. Update. Scandinavian Journal of Clinical and Laboratory Investigation. 60 (2000): 509-540.

[30] Anderson, H. L. Building molecular wires from the colours of life: Conjugated porphyrin oligomers. Chemical Communications. (1999): 2323-2330.

[31] Gouterman, M., Hanson, L. K., Khalil, G. E., Buchler, J. W., Rohbock, K. and Dolphin, D. Porphyrins. XXXI. Chemical properties and electronic spectra of d0 transition-metal complexes. Journal of the American Chemical Society. 97 (1975): 3142-3149.

[32] Rothemund, P. Formation of porphyrins from pyrrole and aldehydes [4]. Journal of the American Chemical Society. 57 (1935): 2010-2011.

[33] Adler, A. D., Longo, F. R., Finarelli, J. D., Goldmacher, J., Assour, J. and Korsakoff, L. A simplified synthesis for meso-tetraphenylporphin. Journal of Organic Chemistry. 32 (1967): 476.

[34] Lindsey, J. S., Schreiman, I. C., Hsu, H. C., Kearney, P. C. and Marguerettaz, A. M. Rothemund and Adler-Longo reactions revisited: Synthesis of tetraphenylporphyrins under equilibrium conditions. Journal of Organic Chemistry. 52 (1987): 827-836.

[35] Granström, M., Petritsch, K., Arias, A. C., Lux, A., Andersson, M. R. and Friend, R. H. Laminated fabrication of polymeric photovoltaic diodes. Nature. 395 (1998): 257-260.

[36] Rahiman, A. K., Rajesh, K., Bharathi, K. S., Sreedaran, S. and Narayanan, V. Catalytic oxidation of alkenes by manganese(III) porphyrin-encapsulated Al, V, Si-mesoporous molecular sieves. Inorganica Chimica Acta. 362 (2009): 1491-1500.

[37] Kathiravan, A., Kumar, P. S., Renganathan, R. and Anandan, S. Photoinduced electron transfer reactions between meso-tetrakis(4-sulfonatophenyl)porphyrin and colloidal metal-semiconductor nanoparticles. Colloids and Surfaces A: Physicochemical and Engineering Aspects. 333 (2009): 175-181.

[38] Fang, Z. and Liu, B. A cationic porphyrin-based self-assembled film for mercury ion detection. Tetrahedron Letters. 49 (2008): 2311-2315.

[39] Mizutani, T., Wada, K. and Kitagawa, S. Porphyrin receptors for amines, amino acids, and oligopeptides in water. Journal of the American Chemical Society. 121 (1999): 11425-11431.

[40] Fukushima, K., Tabata, K. and Okura, I. Photochemical properties of water-soluble fluorinated zinc phthalocyanines and their photocytotoxicity against HeLa cells. Journal of Porphyrins and Phthalocyanines. 2 (1998): 219-222.

[41] Lash, T. D. Modification of the porphyrin chromophore by ring fusion: Identifying trends due to annelation of the porphyrin nucleus. Journal of Porphyrins and Phthalocyanines. 5 (2001): 267-288.

[42] Vicente, M. G. H. and Smith, K. M. Porphyrins with fused exocyclic rings. Journal of Porphyrins and Phthalocyanines. 8 (2004): 26-42.

[43] Baker, E. W. Mass spectrometric characterization of petroporphyrins. Journal of the American Chemical Society. 88 (1966): 2311-2315.

[44] Bonnett, R. Photosensitizers of the porphyrin and phthalocyanine series for photodynamic therapy. Chemical Society Reviews. 24 (1995): 19-33.

[45] Brunner, H. and Schellerer, K. M. Benzoporphyrins and acetylene-substituted porphyrins as improved photosensitizers in the photodynamic tumor therapy with porphyrin platinum conjugates. Monatshefte fur Chemie. 133 (2002): 679-705.

[46] Moan, J. and Peng, Q. An Outline of the Hundred-Year History of PDT. Anticancer Research. 23 (2003): 3591-3600.

[47] Nyman, E. S. and Hynninen, P. H. Research advances in the use of tetrapyrrolic photosensitizers for photodynamic therapy. Journal of Photochemistry and Photobiology B: Biology. 73 (2004): 1-28.

[48] Young, S. W., Qing, F., Harriman, A., Sessler, J. L., Dow, W. C., Mody, T. D., Hemmi, G. W., Hao, Y. and Miller, R. A. Gadolinium (III) texaphyrin: A tumor selective radiation sensitizer that is detectable by MRI. Proceedings of the National Academy of Sciences of the United States of America. 93 (1996): 6610-6615.

[49] Vinogradov, S. A., Lo, L. W., Jenkins, W. T., Evans, S. M., Koch, C. and Wilson, D. F. Noninvasive imaging of the distribution in oxygen in tissue in vivo using near-infrared phosphors. Biophysical Journal. 70 (1996): 1609-1617.

[50] Liebsch, G., Klimant, I., Frank, B., Holst, G. and Wolfbeis, O. S. Luminescence lifetime imaging of oxygen, pH, and carbon dioxide distribution using optical sensors. Applied Spectroscopy. 54 (2000): 548-559.

[51] Rogers, J. E., Nguyen, K. A., Hufnagle, D. C., McLean, D. G., Su, W., Gossett, K. M., Burke, A. R., Vinogradov, S. A., Pachter, R. and Fleitz, P. A. Observation and Interpretation of Annulated Porphyrins: Studies on the Photophysical Properties of meso-

Tetraphenylmetalloporphyrins. Journal of Physical Chemistry A. 107 (2003): 11331-11339.

[52] Naga Srinivas, N. K. M., Venugopal Rao, S., Rao, D. V. G. L. N., Kimball, B. K., Nakashima, M., Decristofano, B. S. and Narayana Rao, D. Wavelength dependent studies of nonlinear absorption in zinc meso-tetra(p-methoxyphenyl)tetrabenzoporphyrin (Znmp TBP) using Z-scan technique. Journal of Porphyrins and Phthalocyanines. 5 (2001): 549-554.

[53] Martinsen, J., Pace, L. J., Phillips, T. E., Hoffman, B. M. and Ibers, J. A. (Tetrabenzoporphyrinato)nickel(II) iodide. A doubly mixed valence molecular conductor. Journal of the American Chemical Society. 104 (1982): 83-91.

[54] Liou, K., Ogawa, M. Y., Newcomb, T. P., Quirion, G., Lee, M., Poirier, M., Halperin, W. P., Hoffman, B. M. and Ibers, J. A. Preparation, characterization, and low-temperature transition of Cu(tatbp)I, a new porphyrinic conductor with local moments coupled to itinerant charge carriers. Inorganic Chemistry. 28 (1989): 3889-3896.

[55] Aramaki, S., Sakai, Y. and Ono, N. Solution-processible organic semiconductor for transistor applications: Tetrabenzoporphyrin. Applied Physics Letters. 84 (2004): 2085-2087.

[56] Helberger, J. H. and Hevér, D. B. Über die Bildung von Tetrabenzoporphin aus Isoindolderivaten. IV. Mitteilung zur Kenntnis der Benzoporphine. Justus Liebigs Annalen der Chemie. 536 (1938): 173-182.

[57] Barrett, P. A., Linstead, R. P., Rundall, F. G. and Tuey, G. A. P. Phthalocyanines and related compounds. Part XIX. Tetrabenzporphin, tetrabenzmonazaporphin and their metallic derivatives. Journal of the Chemical Society (Resumed). (1940): 1079-1092.

[58] Vogler, A., Kunkely, H. and Rethwisch, B. Tetrabenzporphyrin complexes of iron, palladium and platinum. Inorganica Chimica Acta. 46 (1980): Kopranenkov, V. N., Makarova, E. A., Dashkevich, S. N. and Luk'yanets, E. A. Synthesis and electronic absorption spectra of

unsubstituted tetrabenzoporphins. Chemistry of Heterocyclic Compounds. 24 (1988): 630-637. 101-105.

[59] Vorotnikov, A. M., Kopranenkov, V. N. and Luk'yanets, E. A. Dimeric covalently-bonded analogs of tetrabenzoporphyrin. Chemistry of Heterocyclic Compounds. 30 (1994): 31-34.

[60] Koehorst, R. B. M., Kleibeuker, J. F., Schaafsma, T. J., De Bie, D. A., Geurtsen, B., Henrie, R. N. and Van Der Plas, H. C. Preparation and spectroscopic properties of pure tetrabenzoporphyrins. Journal of the Chemical Society, Perkin Transactions 2. (1981): 1005-1009.

[61] Vicente, M. G. H., Tomé, A. C., Walter, A. and Cavaleiro, J. A. S. Synthesis and cycloaddition reactions of pyrrole-fused 3-sulfolenes: A new versatile route to tetrabenzoporphyrins. Tetrahedron Letters. 38 (1997): 3639-3642.

[62] Arnold, D. P., Burgessdean, L., Hubbard, J. and Rahman, M. A. The Preparation of Pyrrole-2-carboxylates From Vinyl Sulfones. Australian Journal of Chemistry. 47 (1994): 969-974.

[63] Galanin, N. E., Kudrik, E. V. and Shaposhnikov, G. P. 4-Tetraphenyl- and 4-tetraphenoxy-substituted meso- tetraphenyltetrabenzoporphyrins. Synthesis and spectral properties. Russian Journal of Organic Chemistry. 42 (2006): 603-606.

[64] Ichimura, K., Sakuragi, M., Morii, H., Yasuike, M., Fukui, M. and Ohno, O. Reinvestigation of synthetic methods for zinc meso-tetraphenyltetrabenzoporphyrin. Inorganica Chimica Acta. 176 (1990): 31-33.

[65] Finikova, O., Cheprakov, A., Beletskaya, I. and Vinogradov, S. An expedient synthesis of substituted tetraaryltetrabenzoporphyrins. Chemical Communications. (2001): 261-262.

[66] Finikova, O. S., Cheprakov, A. V., Beletskaya, I. P., Carroll, P. J. and Vinogradov, S. A. Novel Versatile Synthesis of Substituted Tetrabenzoporphyrins. Journal of Organic Chemistry. 69 (2004): 522-535.

[67] Finikova, O. S., Cheprakov, A. V. and Vinogradov, S. A. Synthesis and luminescence of soluble meso-unsubstituted tetrabenzo- and tetranaphtho[2,3]porphyrins. Journal of Organic Chemistry. 70 (2005): 9562-9572.

[68] Murashima, T., Tsujimoto, S., Yamada, T., Miyazawa, T., Uno, H., Ono, N. and Sugimoto, N. Synthesis of water-soluble porphyrin and the corresponding highly planar benzoporphyrin without meso-substituents. Tetrahedron Letters. 46 (2005): 113-116.

[69] Yamada, H., Kushibe, K., Okujima, T., Uno, H. and Ono, N. Novel one-pot synthesis of 5-alkenyl-15-alkynylporphyrins and their derivatisation to a butadiyne-linked benzoporphyrin dimer. Chemical Communications. (2006): 383-385.

[70] Filatov, M. A., Cheprakov, A. V. and Beletskaya, I. P. A facile and reliable method for the synthesis of tetrabenzoporphyrin from 4,7-dihydroisoindole. European Journal of Organic Chemistry. (2007): 3468-3475.

[71] Halik, M., Klauk, H., Zschieschang, U., Schmid, G., Ponomarenko, S., Kirchmeyer, S. and Weber, W. Relationship between molecular structure and electrical performance of oligothiophene organic thin film transistors. Advanced Materials. 15 (2003): 917-922.

[72] Doré, K., Dubus, S., Ho, H. A., Lévesque, I., Brunette, M., Corbeil, G., Boissinot, M., Boivin, G., Bergeron, M. G., Boudreau, D. and Leclerc, M. Fluorescent Polymeric Transducer for the Rapid, Simple, and Specific Detection of Nucleic Acids at the Zeptomole Level. Journal of the American Chemical Society. 126 (2004): 4240-4244.

[73] Yu, H. H., Pullen, A. E., Büschel, M. G. and Swager, T. M. Charge-specific interactions in segmented conducting polymers: An approach to selective ionoresistive responses. Angewandte Chemie - International Edition. 43 (2004): 3700-3703.

[74] Frontmatter. In *Handbook of Oligo- and Polythiophenes*; Wiley-VCH Verlag GmbH: 1999.

[75] Guide, M., Dang, X. D. and Nguyen, T. Q. Nanoscale characterization of tetrabenzoporphyrin and fullerene-based solar cells by photoconductive atomic force microscopy. Advanced Materials. 23 (2011): 2313-2319.

[76] Liu, Y., Xiang, N., Feng, X., Shen, P., Zhou, W., Weng, C., Zhao, B. and Tan, S. Thiophene-linked porphyrin derivatives for dye-sensitized solar cells. Chemical Communications. (2009): 2499-2501.

[77] Zhou, W., Zhao, B., Shen, P., Jiang, S., Huang, H., Deng, L. and Tan, S. Multi-alkylthienyl appended porphyrins for efficient dye-sensitized solar cells. Dyes and Pigments. 91 (2011): 404-412.

[78] Brückner, C., Foss, P. C., Sullivan, J. O., Pelto, R., Zeller, M., Birge, R. R. and Crundwell, G. Origin of the bathochromically shifted optical spectra of meso-tetrathien-2'- and 3'-ylporphyrins as compared to meso-tetraphenylporphyrin. Physical chemistry chemical physics : PCCP. 8 (2006): 2402-2412.

[79] Geier Iii, G. R., Ciringh, Y., Li, F., Haynes, D. M. and Lindsey, J. S. A survey of acid catalysts for use in two-step, one-flask syntheses of meso-substituted porphyrinic macrocycles. Organic Letters. 2 (2000): 1745-1748.

[80] Jiao, J., Thamyongkit, P., Schmidt, I., Lindsey, J. S. and Bocian, D. F. Characterization of porphyrin surface orientation in monolayers on Au(111) and Si(100) using spectroscopically labeled molecules. Journal of Physical Chemistry C. 111 (2007): 12693-12704.

[81] Rochford, J., Botchway, S., McGarvey, J. J., Rooney, A. D. and Pryce, M. T. Photophysical and electrochemical properties of meso-substituted thien-2-yl Zn(II) porphyrins. Journal of Physical Chemistry A. 112 (2008): 11611-11618.

[82] Waykole, L., Paquette, L. A. Ethynyl *p*-tolyl sulfone. Organic Syntheses, 67 (1993): 149-151.

[83] Shimidzu, T., Segawa, H., Wu, F. and Nakayama, N. Approaches to conducting polymer devices with nanostructures: photoelectrochemical function of one-dimensional and two-dimensional porphyrin polymers

with oligothienyl molecular wire. Journal of Photochemistry and Photobiology, A: Chemistry. 92 (1995): 121-127.

[84] Bonar-Law, R. P. Porphyrin synthesis in surfactant solution: Multicomponent assembly in micelles. Journal of Organic Chemistry. 61 (1996): 3623-3634.

[85] Back, T. G. The chemistry of acetylenic and allenic sulfones. Tetrahedron. 57 (2001): 5263-5301.

[86] Arjona, O., Csákÿ, A. G., Medel, R. and Plumet, J. First intermolecular Pauson-Khand reaction of 7-azanorbornenes. Control of the regioselectivity by the effect of the substituents attached to the olefinic partner. Tetrahedron Letters. 42 (2001): 3085-3087.

[87] Arjona, O., Iradier, F., Medel, R. and Plumet, J. The Diels-Alder reaction of phenylsulfonylacetylene and furan derivatives. Normal vs. Tandem 'pincer' reactions. Heterocycles. 50 (1999): 653-656.

[88] Vorogushin, A. V., Predeus, A. V., Wulff, W. D. and Hansen, H. J. Diels - Alder reaction - Aromatization approach toward functionalized ring C allocolchicinoids. Enantioselective total synthesis of (-)-7S-allocolchicine. Journal of Organic Chemistry. 68 (2003): 5826-5831.

[89] Lindsey, J. S., Hsu, H. C. and Schreiman, I. C. Synthesis of tetraphenylporphyrins under very mild conditions. Tetrahedron Letters. 27 (1986): 4969-4970.

[90] Sun, X., Zhang, J. and He, B. The synthesis and photochemical characterization of meso-tetra-thienyl porphyrins. Journal of Photochemistry and Photobiology A: Chemistry. 172 (2005): 283-288.

[91] Bhyrappa, P., Sankar, M., Varghese, B. and Bhavana, P. Meso-tetrathienylporphyrins: Steady-state emission and structural properties. Journal of Chemical Sciences. 118 (2006): 393-397.

[92] Diskin-Posner, Y., Balasubramanian, S., Patra, G. K. and Goldberg, I. [5,10,15,20-meso-Tetrakis(2-thienyl)porphyrinato-κ4N]copper(II). Acta Crystallographica Section E. 57 (2001): m346-m348.

[93] Gupta, I. and Ravikanth, M. Spectroscopic properties of meso-thienylporphyrins with different porphyrin cores. Journal of Photochemistry and Photobiology A: Chemistry. 177 (2006): 156-163.

[94] Purushothaman, B., Varghese, B. and Bhyrappa, P. [5,10,15,20-tetrakis(2-thienyl)-porphyrinato]zinc(II). Acta Crystallographica Section C: Crystal Structure Communications. 57 (2001): 252-253.

[95] Harriman, A. and Davila, J. Spectroscopic studies of some zinc meso-tetraaryl porphyrins. Tetrahedron. 45 (1989): 4737-4750.

[96] K.M. Kadish, E.V. Caemelbecke and G. Royal In: K.M. Kadish, K.M. Smith and R. Guilard, Editors, *The Porphyrin Handbook*, **Vol.18,** Acedemic Press, New York (2003) ch. 113.

[97] Gomer, R. and Tryson, G. An experimental determination of absolute half-cell emf's and single ion free energies of solvation. The Journal of Chemical Physics. 66 (1977): 4413-4424.

[98] Cardona, C. M., Li, W., Kaifer, A. E., Stockdale, D. and Bazan, G. C. Electrochemical Considerations for Determining Absolute Frontier Orbital Energy Levels of Conjugated Polymers for Solar Cell Applications. Advanced Materials. 23 (2011): 2367-2371.

[99] Baran, D., Balan, A., Celebi, S., Meana Esteban, B., Neugebauer, H., Sariciftci, N. S. and Toppare, L. Processable Multipurpose Conjugated Polymer for Electrochromic and Photovoltaic Applications. Chemistry of Materials. 22 (2010): 2978-2987.

APPENDICES

APPENDIX A

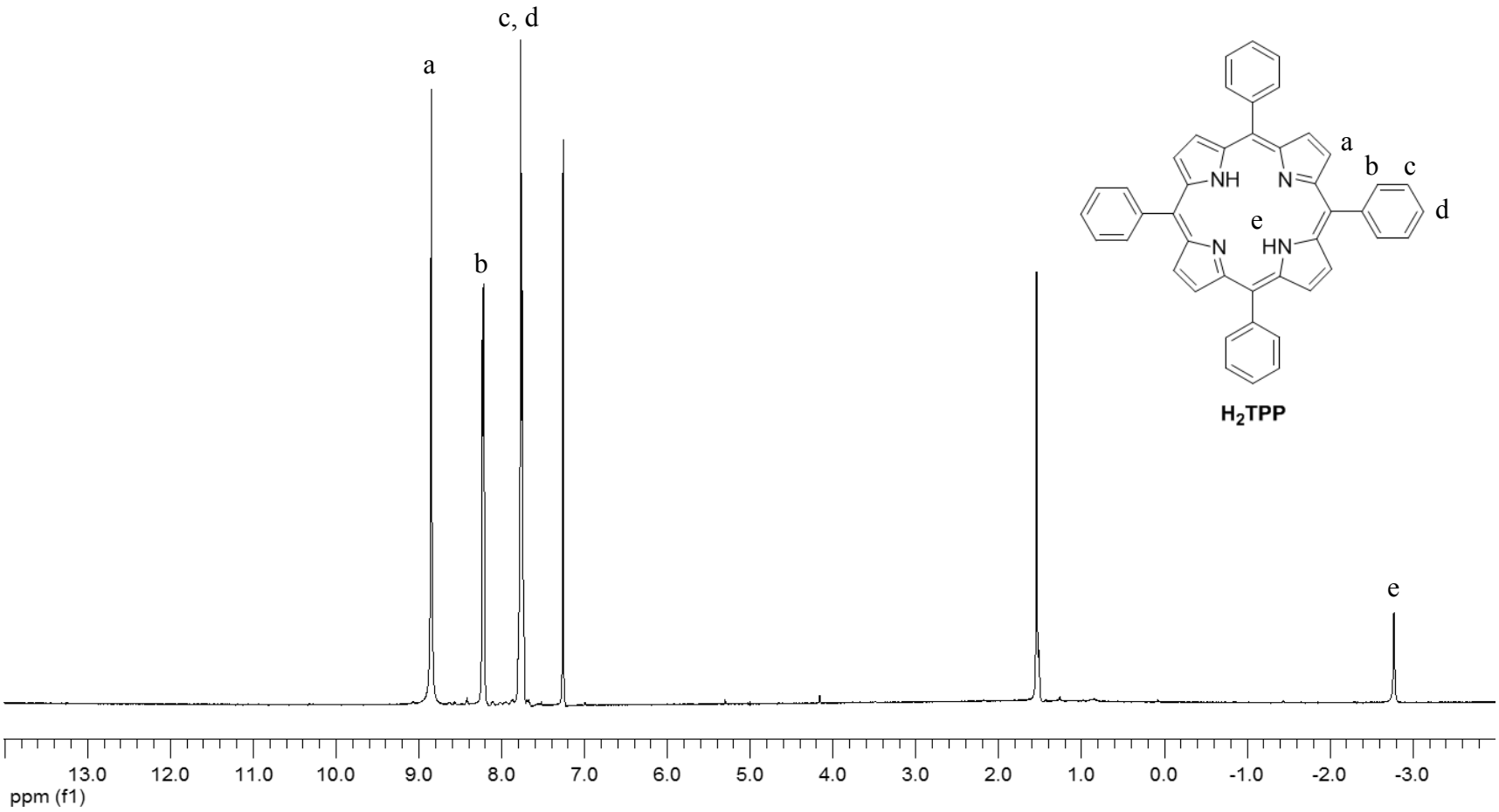

Figure A-1: ^{1}H-NMR spectrum of compound **H_2TPP**

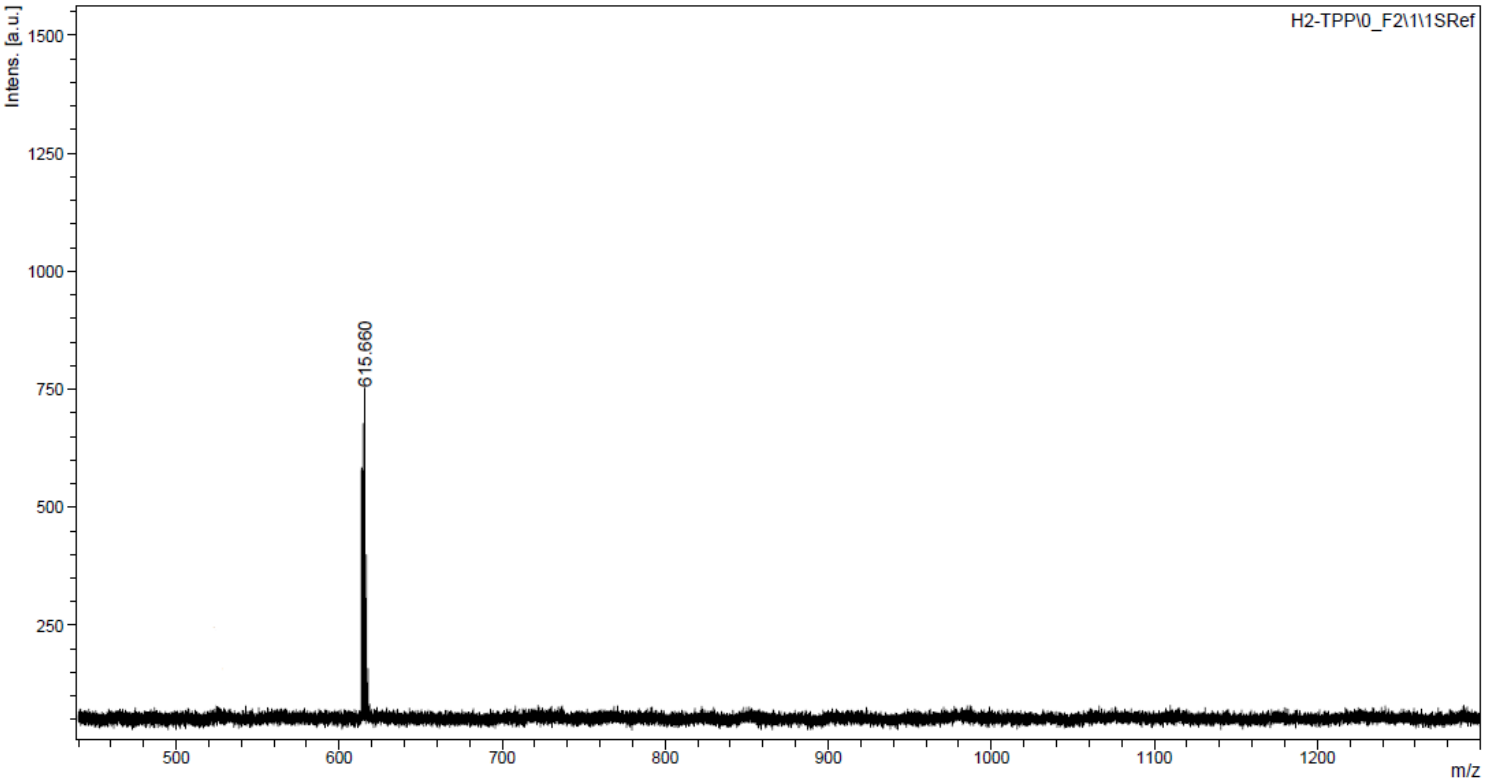

Figure A-2: Mass spectrum of compound **H_2TPP**

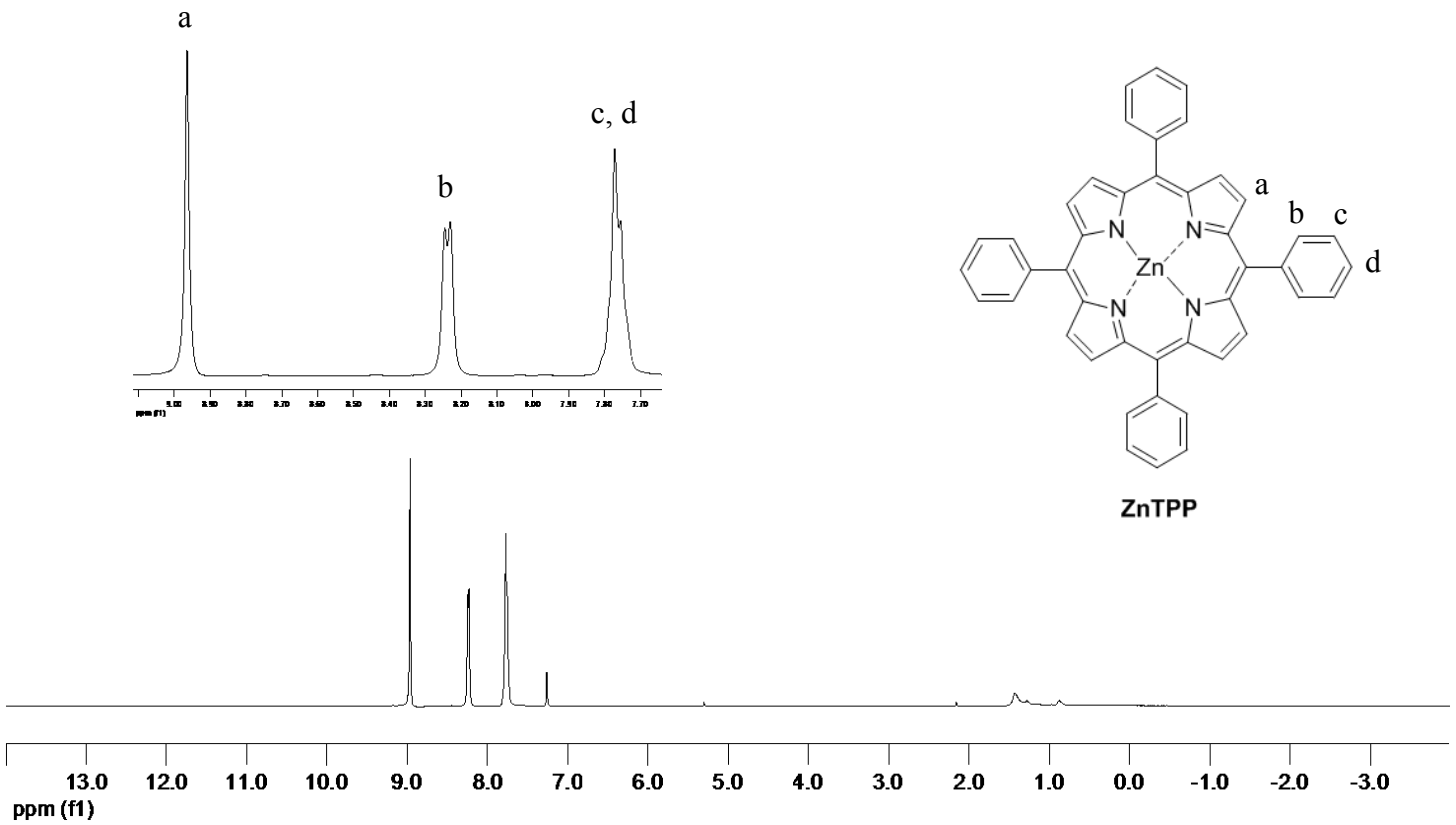

Figure A-3: ^{1}H-NMR spectrum of compound **ZnTPP**

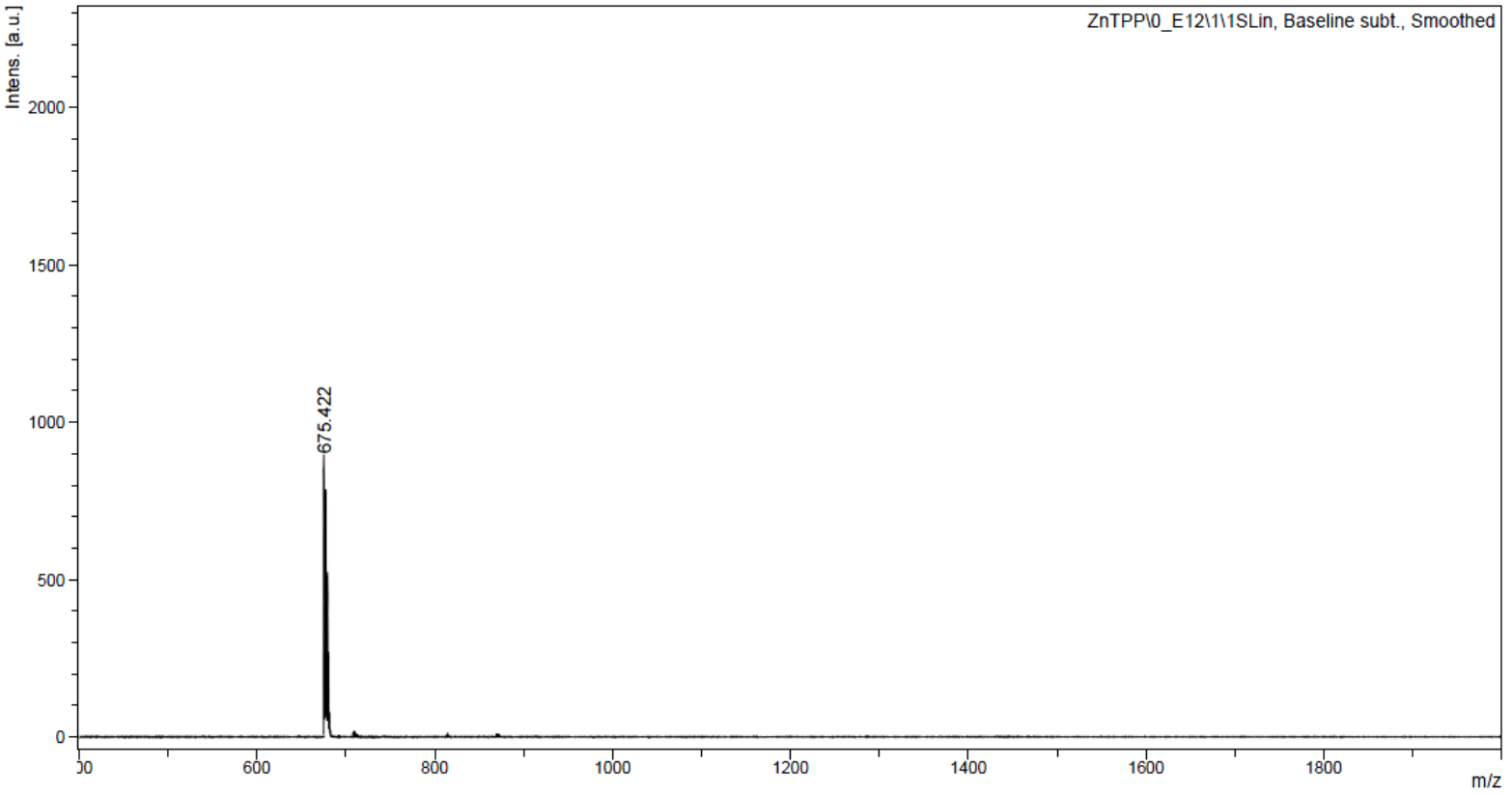

Figure A-4: Mass spectrum of compound **ZnTPP**

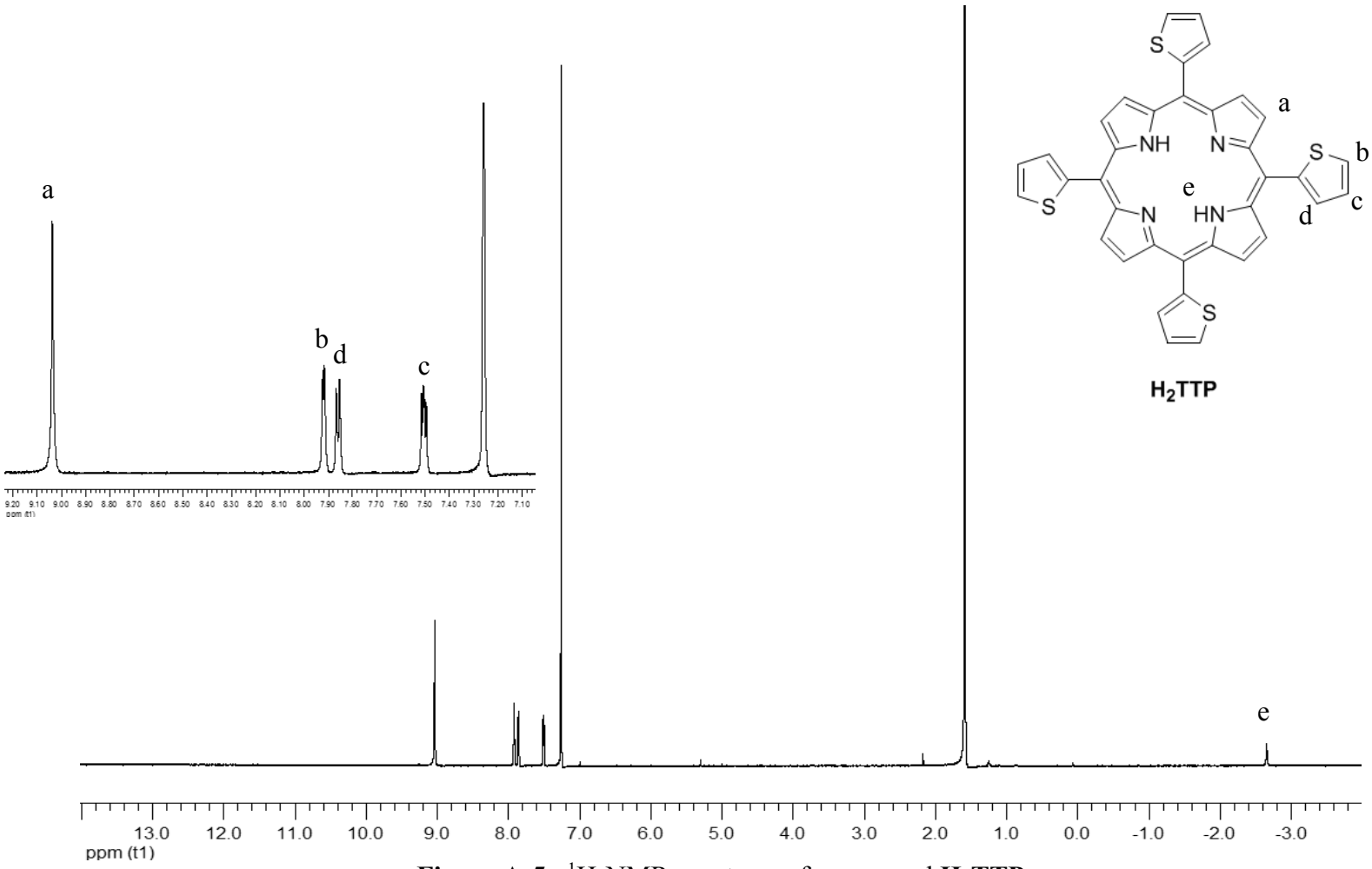

Figure A-5: ^{1}H-NMR spectrum of compound **H_2TTP**

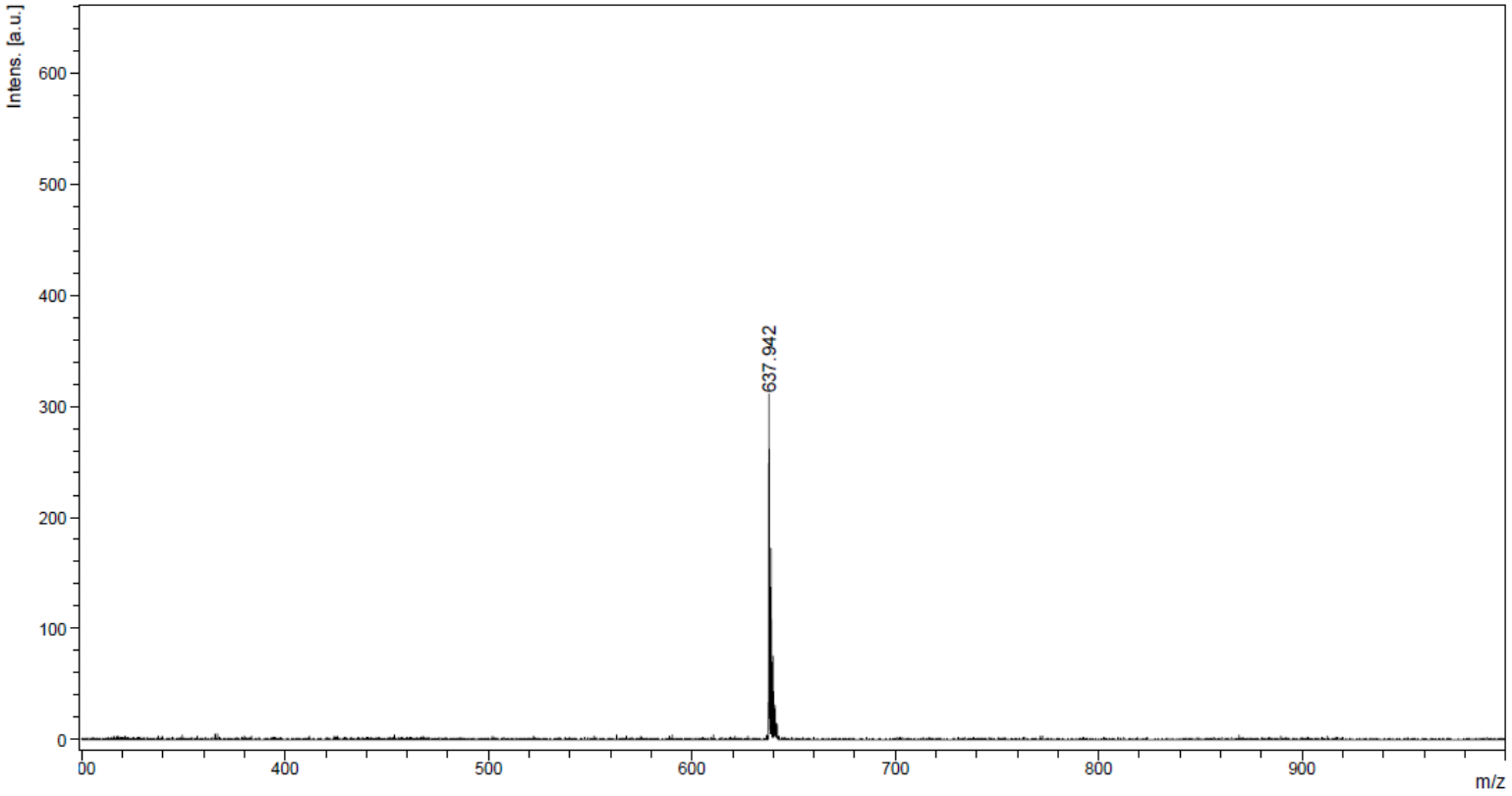

Figure A-6: Mass spectrum of compound **H_2TTP**

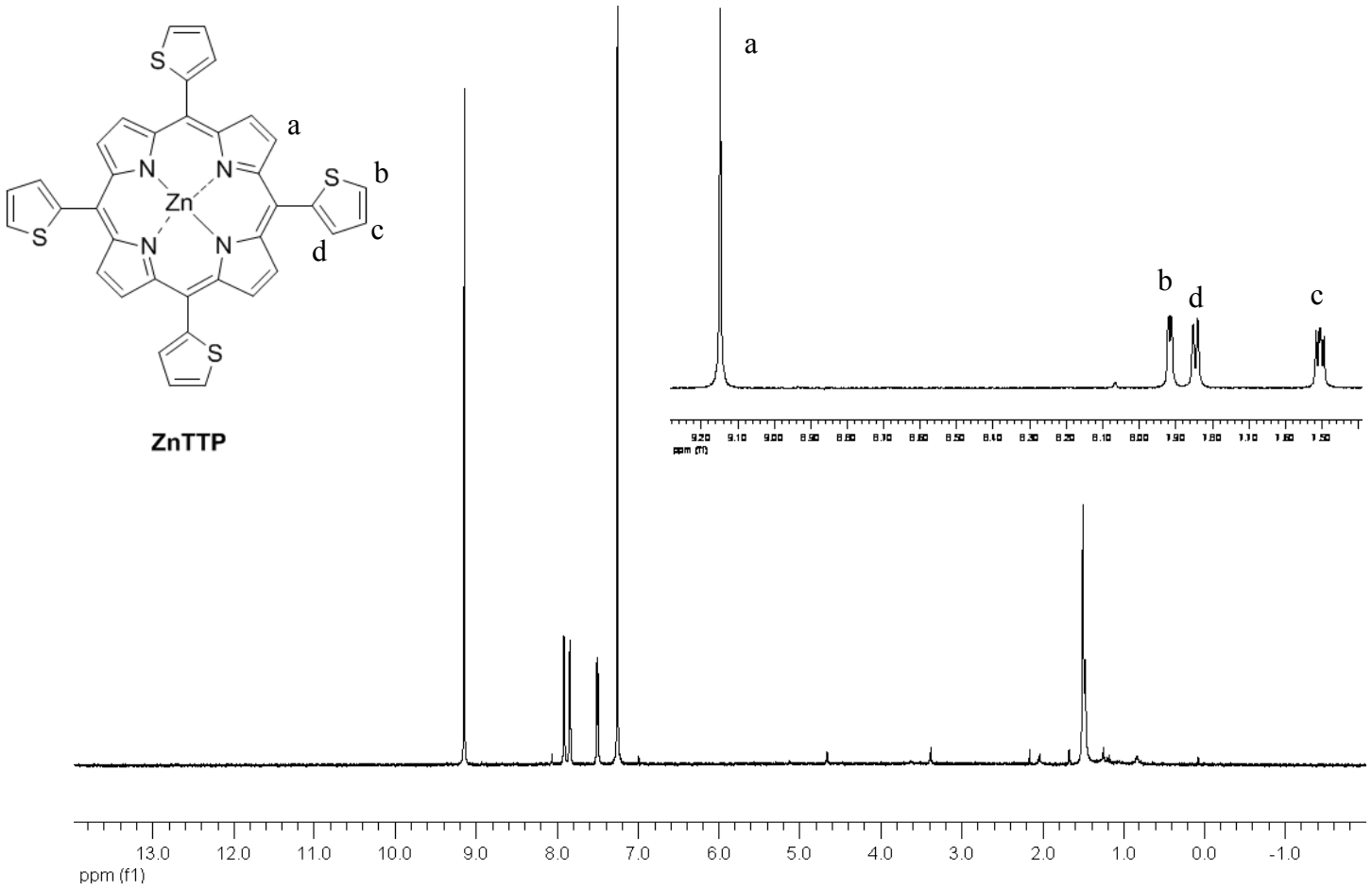

Figure A-7: ^{1}H-NMR spectrum of compound **ZnTTP**

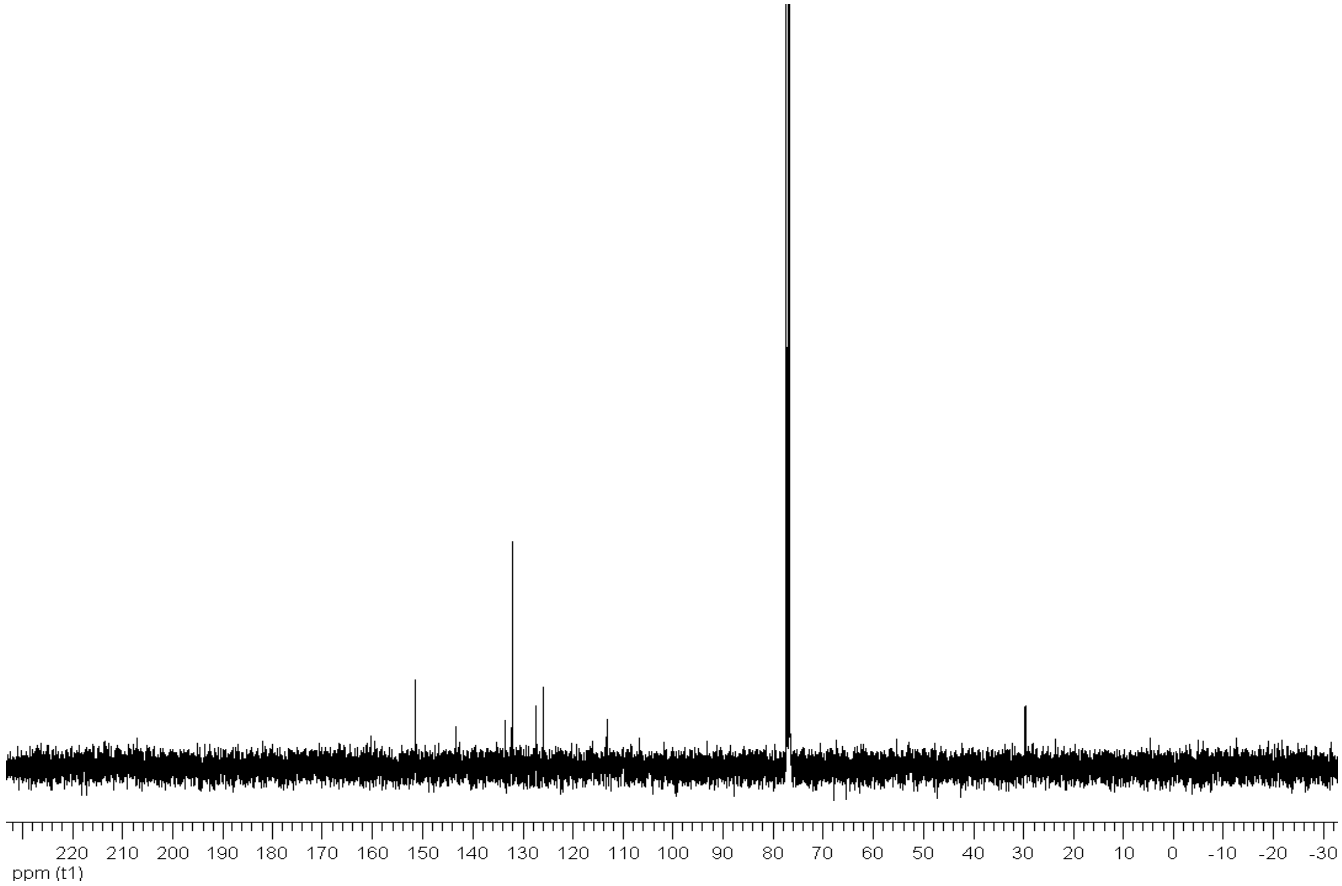

Figure A-8: ^{13}C-NMR spectrum of compound **ZnTTP**

Mass Spectrum List Report

Analysis Info

Analysis Name	CUPT560207003.d	Acquisition Date	2/7/2013 3:06:44 PM
Method	MKE_tune_wide_20130204.m	Operator	Administrator
Sample Name	Zn-TTP	Instrument	micrOTOF 72
	Zn-TTP		

Acquisition Parameter

Source Type	ESI	Ion Polarity	Positive	Set Corrector Fill	45 V
Scan Range	n/a	Capillary Exit	150.0 V	Set Pulsar Pull	385 V
Scan Begin	50 m/z	Hexapole RF	800.0 V	Set Pulsar Push	385 V
Scan End	3000 m/z	Skimmer 1	45.0 V	Set Reflector	1300 V
		Hexapole 1	25.0 V	Set Flight Tube	9000 V
				Set Detector TOF	2450 V

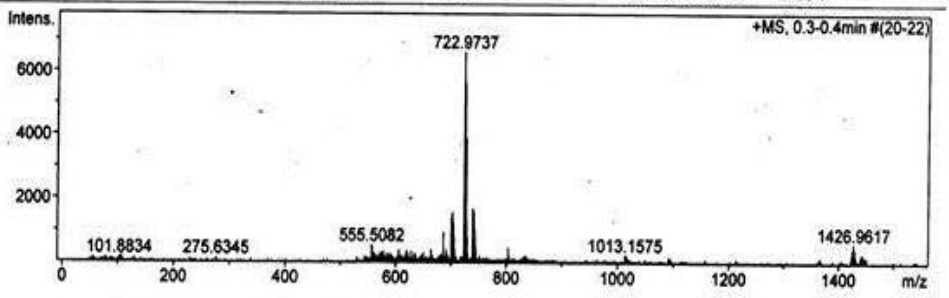

#	m/z	I	I %	S/N	FWHM	Res.
1	555.5082	554	8.4	45.0	0.0546	10183
2	557.5185	486	7.3	39.1	0.0593	9405
3	685.4344	962	14.5	53.7	0.0693	9894
4	686.4384	493	7.4	26.9	0.0643	10677
5	699.9856	1421	21.5	77.2	0.0704	9950
6	700.9909	1400	21.2	75.8	0.0725	9671
7	701.4039	534	8.1	28.1	0.0648	10820
8	701.9844	1570	23.7	85.0	0.0719	9768
9	702.9880	1290	19.5	69.4	0.0726	9684
10	703.9823	1241	18.8	66.6	0.0725	9708
11	704.9837	820	12.4	43.5	0.0720	9787
12	705.9852	441	6.7	22.8	0.0723	9768
13	722.9737	6618	100.0	345.4	0.0715	10116
14	723.9751	2996	45.3	155.3	0.0669	10825
15	724.9718	5639	85.2	292.8	0.0690	10511
16	725.9747	2495	37.7	128.6	0.0750	9681
17	726.9710	3892	58.8	200.8	0.0695	10462
18	727.9712	1351	20.4	68.8	0.0774	9408
19	728.9678	811	12.3	40.7	0.0752	9690
20	738.9450	1695	25.6	85.7	0.0684	10796
21	739.9488	729	11.0	36.2	0.0727	10178
22	740.9461	1581	23.9	80.1	0.0717	10327
23	741.9480	725	11.0	36.1	0.0723	10263
24	742.9427	1057	16.0	53.3	0.0728	10204
25	743.9437	529	8.0	26.1	0.0650	11437
26	803.5397	470	7.1	25.4	0.0760	10579
27	1424.9630	440	6.7	39.6	0.1495	9533
28	1426.9617	619	9.4	56.3	0.1366	10443
29	1427.9579	513	7.8	46.4	0.1140	12521
30	1428.9496	455	6.9	41.0	0.1144	12496

Figure A-9: High resolution mass spectrum of compound **ZnTTP**

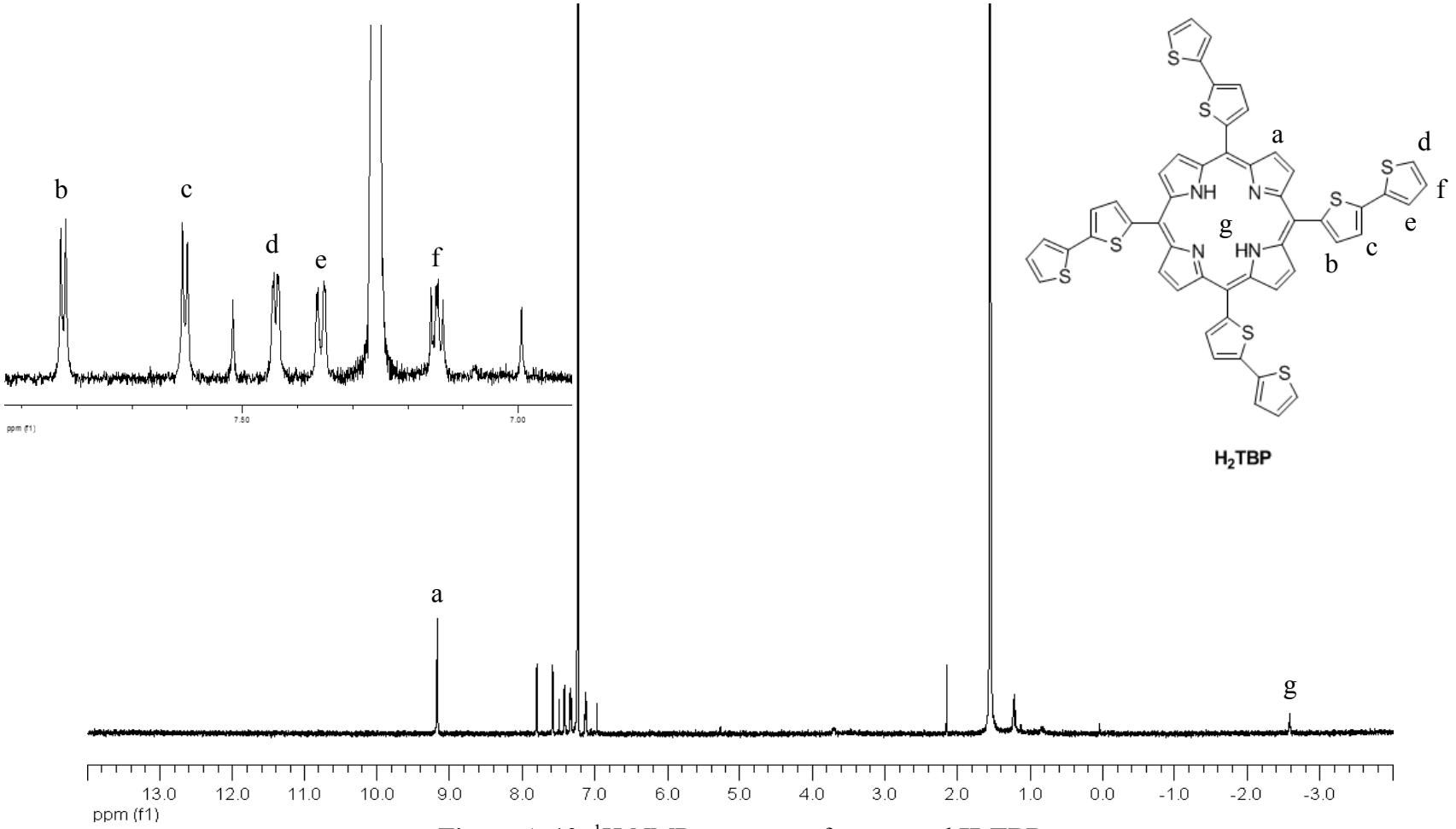

Figure A-10: ^{1}H-NMR spectrum of compound **H_2TBP**

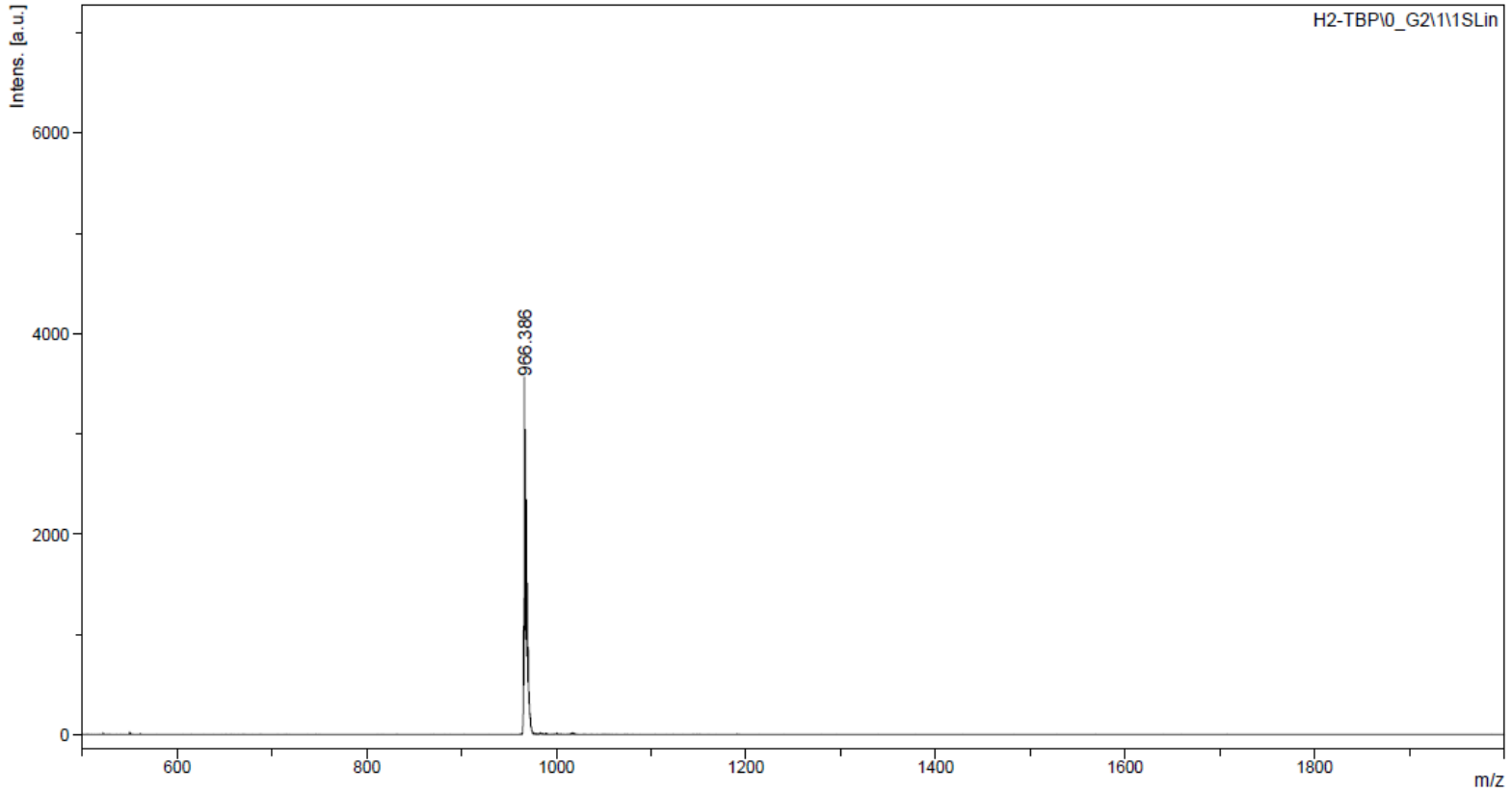

Figure A-11: Mass spectrum of compound **H_2TBP**

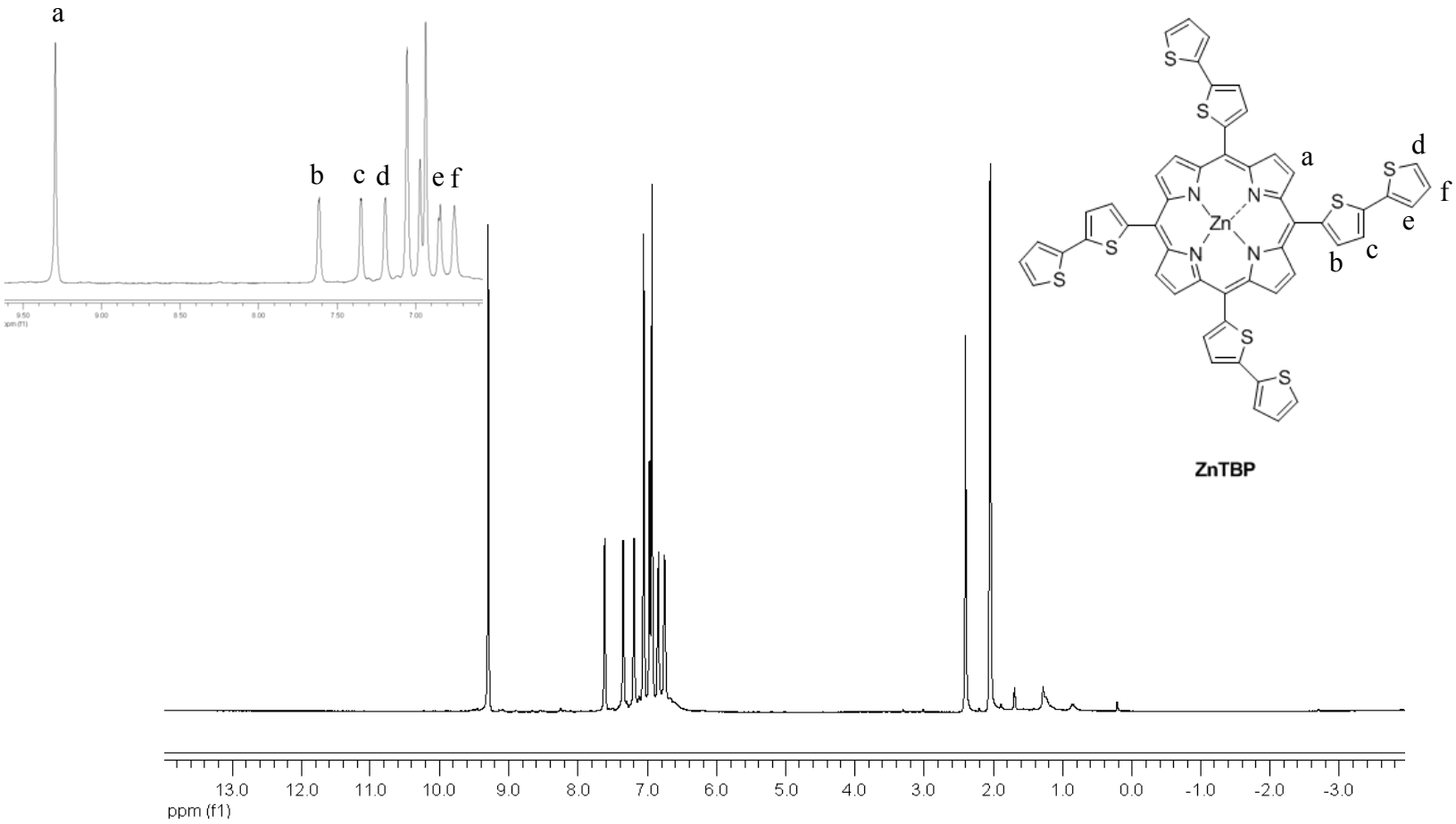

Figure A-12: ^{1}H-NMR spectrum of compound **ZnTBP**

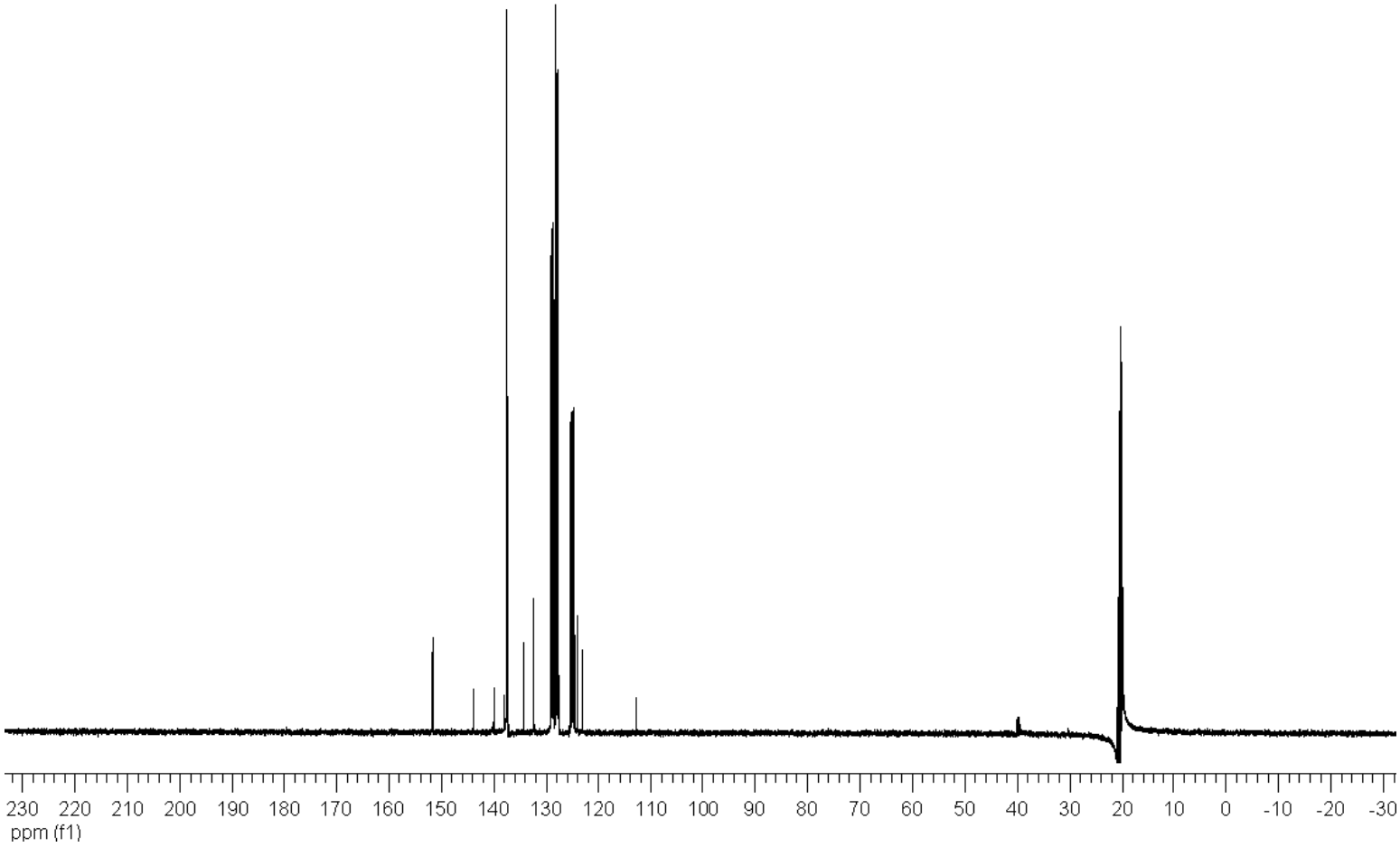

Figure A-13: ^{13}C-NMR spectrum of compound **ZnTBP**

Mass Spectrum List Report

Analysis Info

Analysis Name	CUPT560207005.d	Acquisition Date	2/7/2013 3:30:20 PM
Method	MKE_tune_wide_20130204.m	Operator	Administrator
Sample Name	Zn-TBP	Instrument	micrOTOF 72
	Zn-TBP		

Acquisition Parameter

Source Type	ESI	Ion Polarity	Positive	Set Corrector Fill	45 V
Scan Range	n/a	Capillary Exit	400.0 V	Set Pulsar Pull	385 V
Scan Begin	50 m/z	Hexapole RF	800.0 V	Set Pulsar Push	385 V
Scan End	3000 m/z	Skimmer 1	45.0 V	Set Reflector	1300 V
		Hexapole 1	30.0 V	Set Flight Tube	9000 V
				Set Detector TOF	2450 V

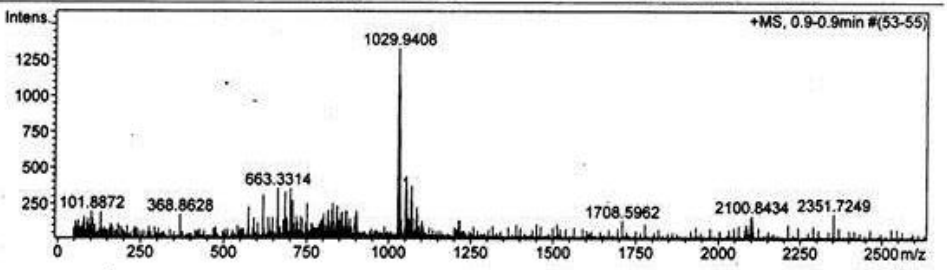

#	m/z	I	I %	S/N	FWHM	Res.
1	575.2767	217	12.9	23.9	0.0711	8086
2	619.3010	352	21.0	36.6	0.0700	8846
3	661.2333	203	12.1	19.2	0.0171	38758
4	663.3318	357	21.3	34.6	0.0687	9660
5	685.4321	253	15.1	23.3	0.0612	11200
6	701.4032	353	21.1	32.3	0.0661	10611
7	707.3497	320	19.1	28.9	0.0785	9016
8	751.3743	239	14.2	20.4	0.0813	9237
9	899.9804	247	14.7	20.7	0.0719	12513
10	900.9873	245	14.6	20.6	0.0991	9092
11	901.9861	211	12.6	17.5	0.0940	9596
12	1027.9294	1404	83.7	119.8	0.0881	11662
13	1028.9376	1527	91.0	130.3	0.0905	11371
14	1029.9353	1678	100.0	143.2	0.1059	9730
15	1030.9382	1528	91.1	130.3	0.0940	10964
16	1031.9350	1469	87.5	125.1	0.0917	11256
17	1032.9350	1021	60.8	86.5	0.1019	10132
18	1033.9298	631	37.6	52.9	0.1073	9637
19	1034.9294	362	21.6	29.8	0.0983	10532
20	1050.9217	351	20.9	28.7	0.1040	10103
21	1051.9214	255	15.2	20.4	0.0975	10788
22	1052.9227	432	25.7	35.6	0.0959	10979
23	1053.9204	288	17.1	23.2	0.0870	12108
24	1054.9195	323	19.3	26.3	0.0913	11559
25	1066.8968	277	16.5	22.3	0.1032	10335
26	1068.8939	343	20.4	27.8	0.0887	12057
27	1069.8970	197	11.7	15.4	0.0893	11983
28	1070.8944	238	14.2	18.9	0.1016	10541
29	1084.9060	212	12.6	16.6	0.0935	11604
30	2351.6123	211	12.6	24.7	0.0342	68732

#	m/z	I	I %	S/N	FWHM	Res.
1	575.2755	228	17.1	23.8	0.0723	7953
2	619.3034	310	23.3	30.0	0.0715	8667
3	663.3314	358	26.9	32.1	0.0631	10516
4	685.4341	333	25.0	28.6	0.0655	10473

Figure A-14: High resolution mass spectrum of compound **ZnTBP**

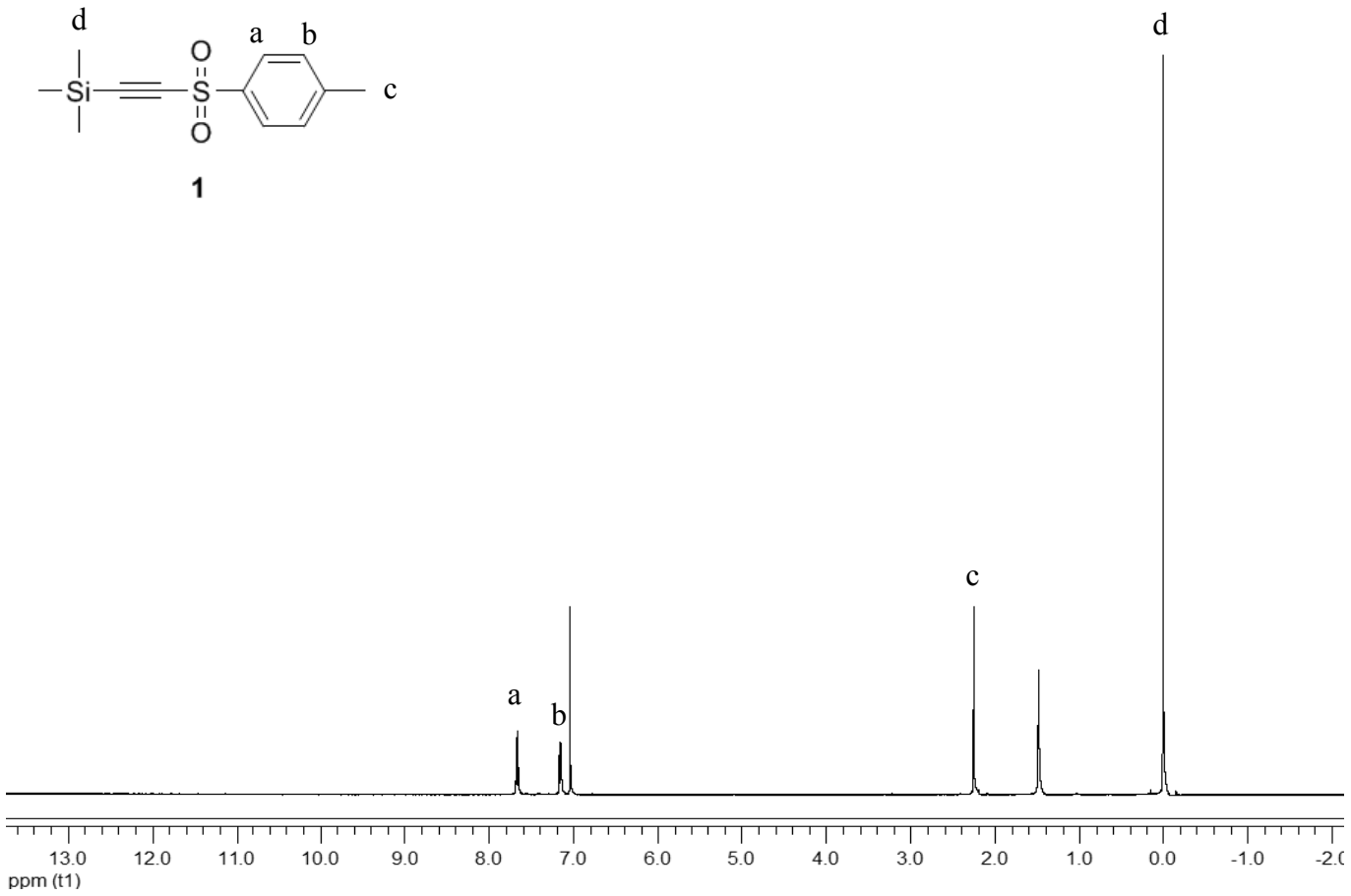

Figure A-15: ^{1}H-NMR spectrum of compound **1**

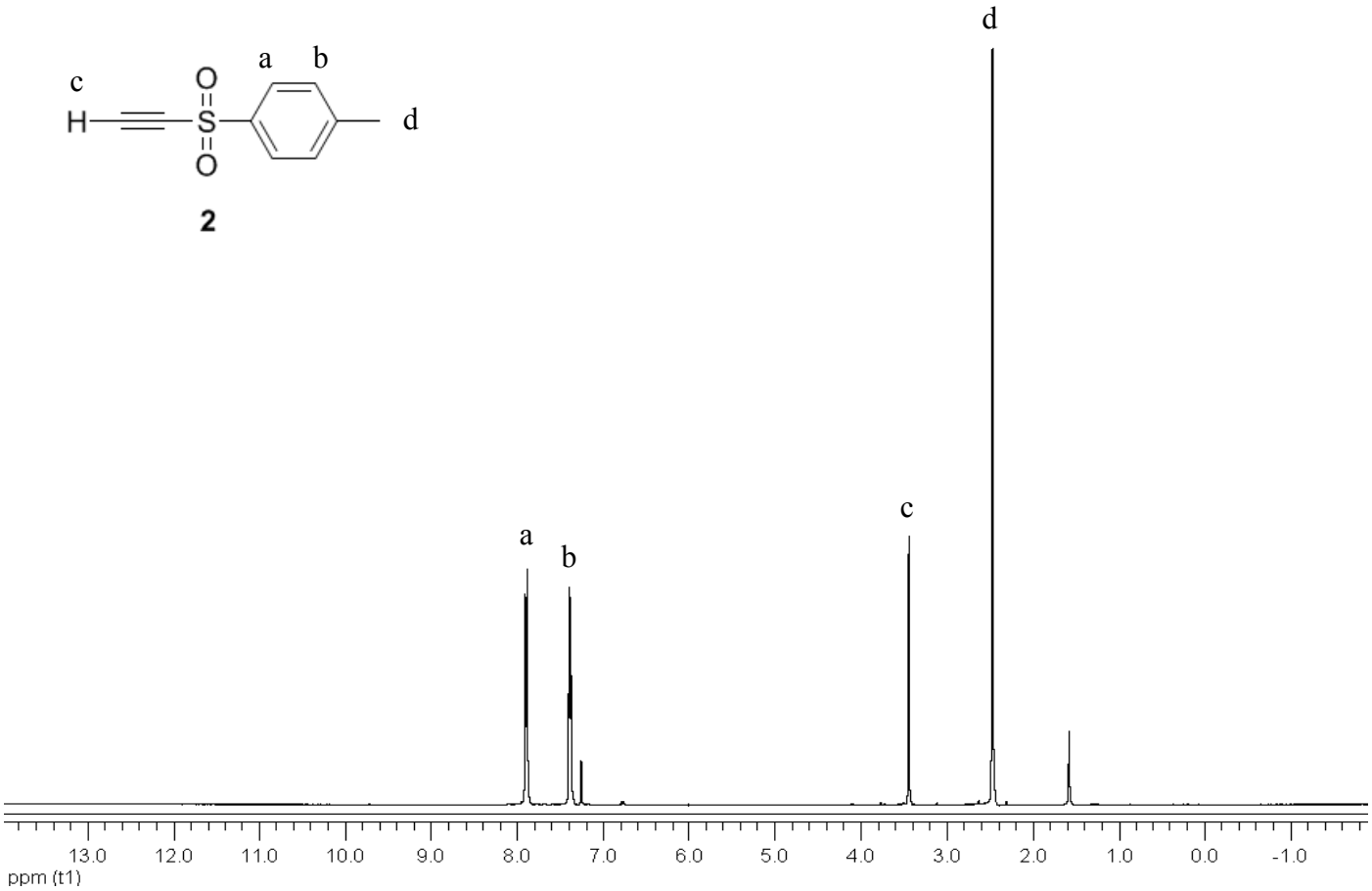

Figure A-16: ^{1}H-NMR spectrum of compound **2**

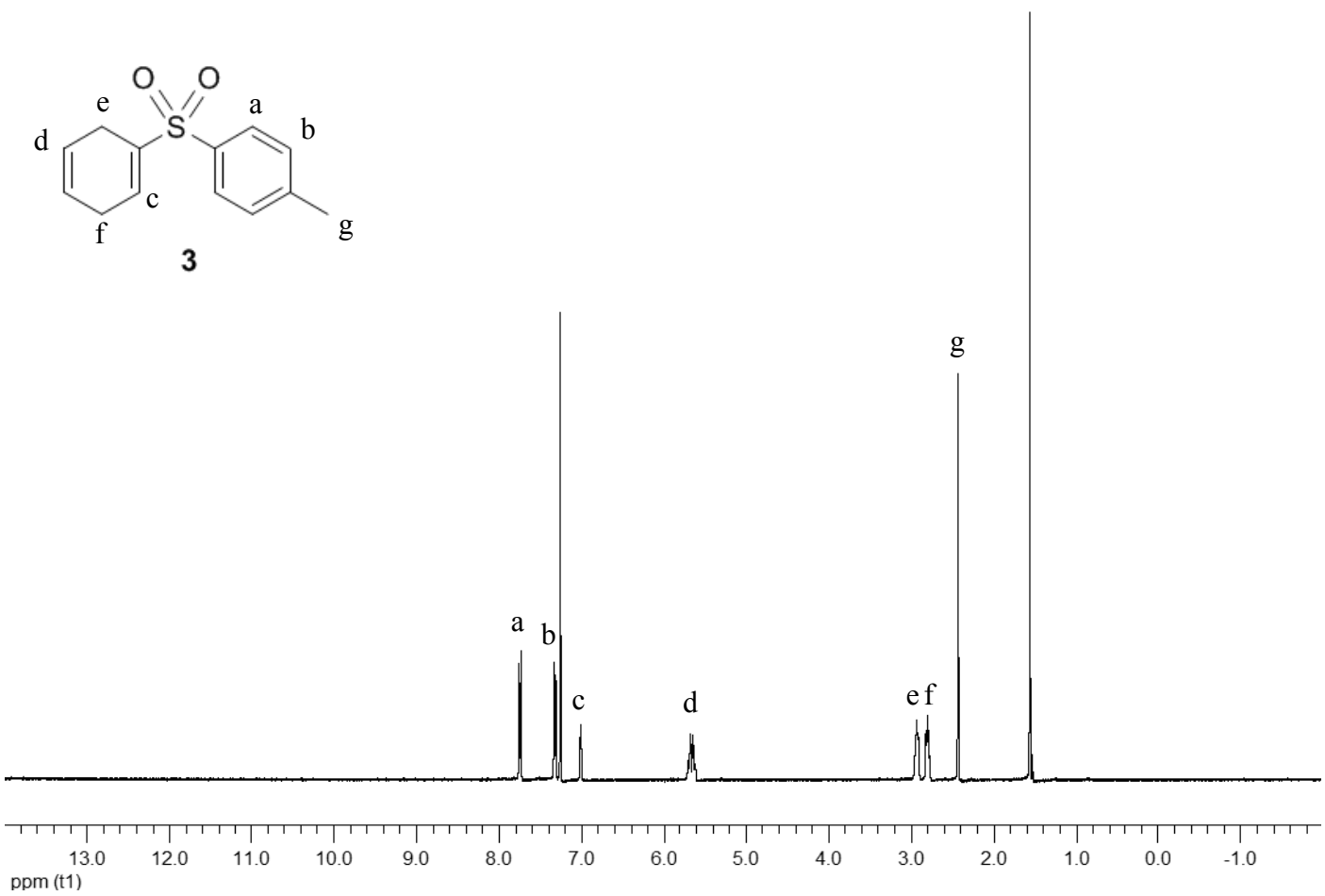

Figure A-17: ^{1}H-NMR spectrum of compound **3**

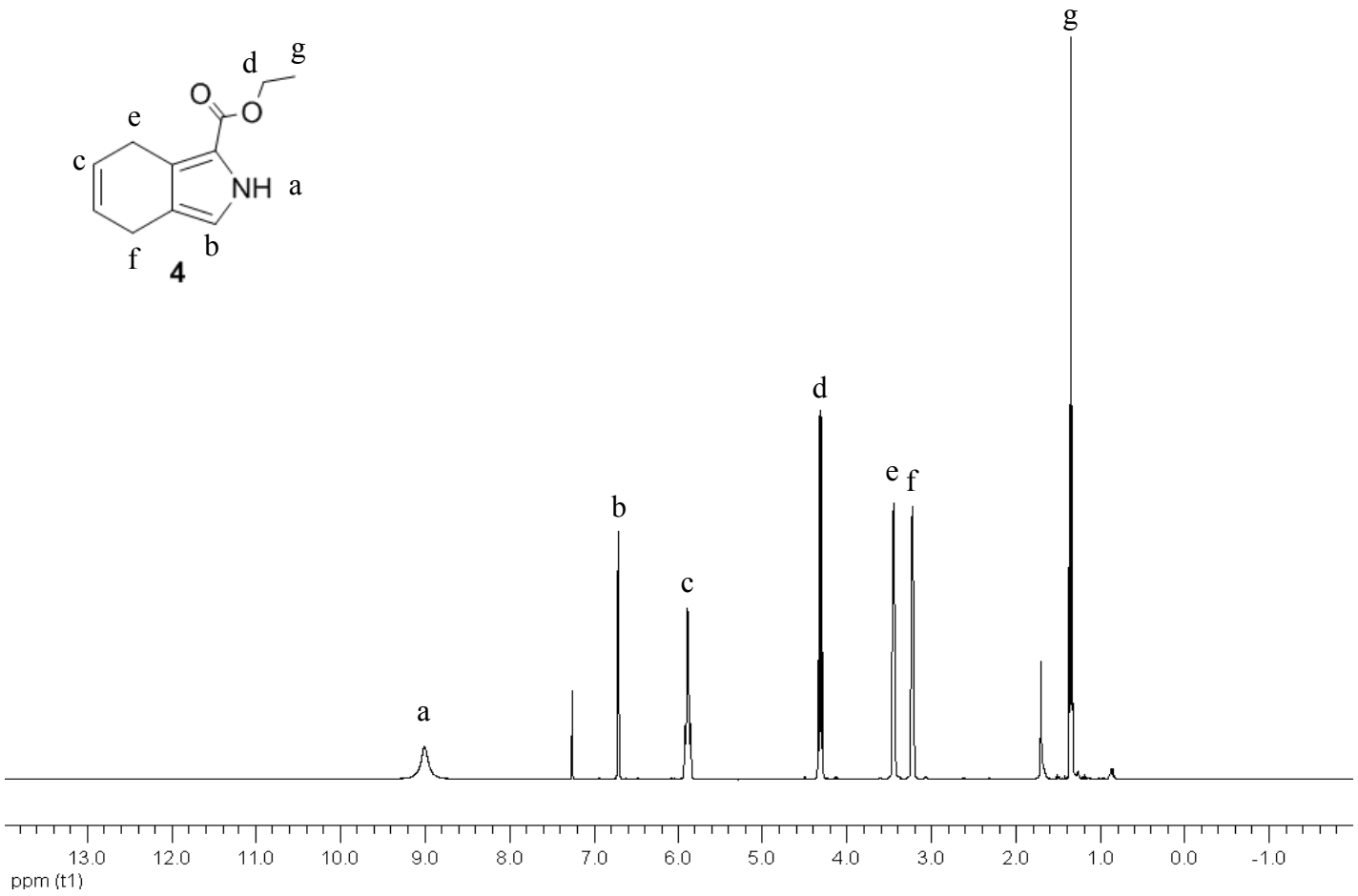

Figure A-18: ^{1}H-NMR spectrum of compound **4**

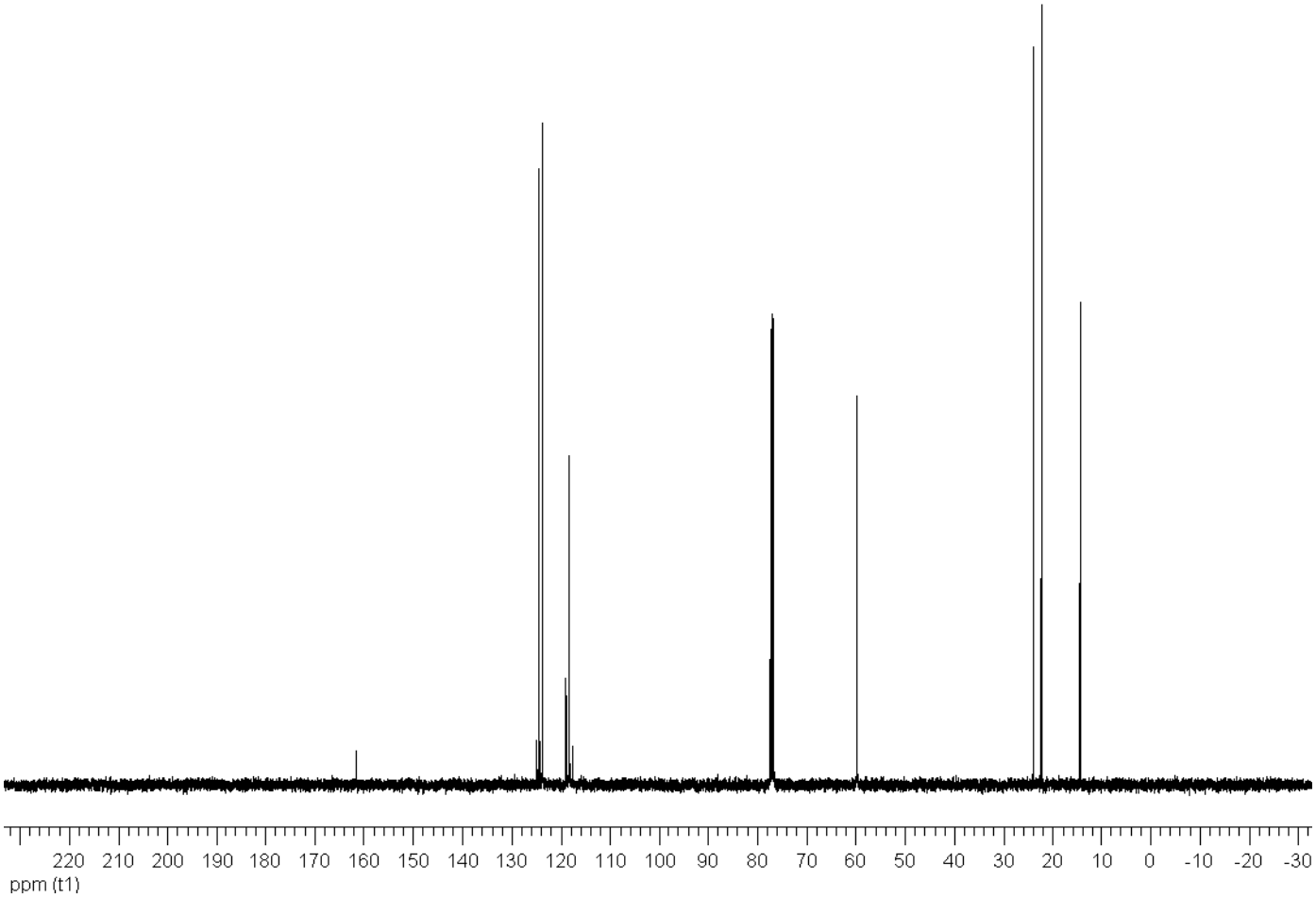

Figure A-19: ^{13}C-NMR spectrum of compound **4**

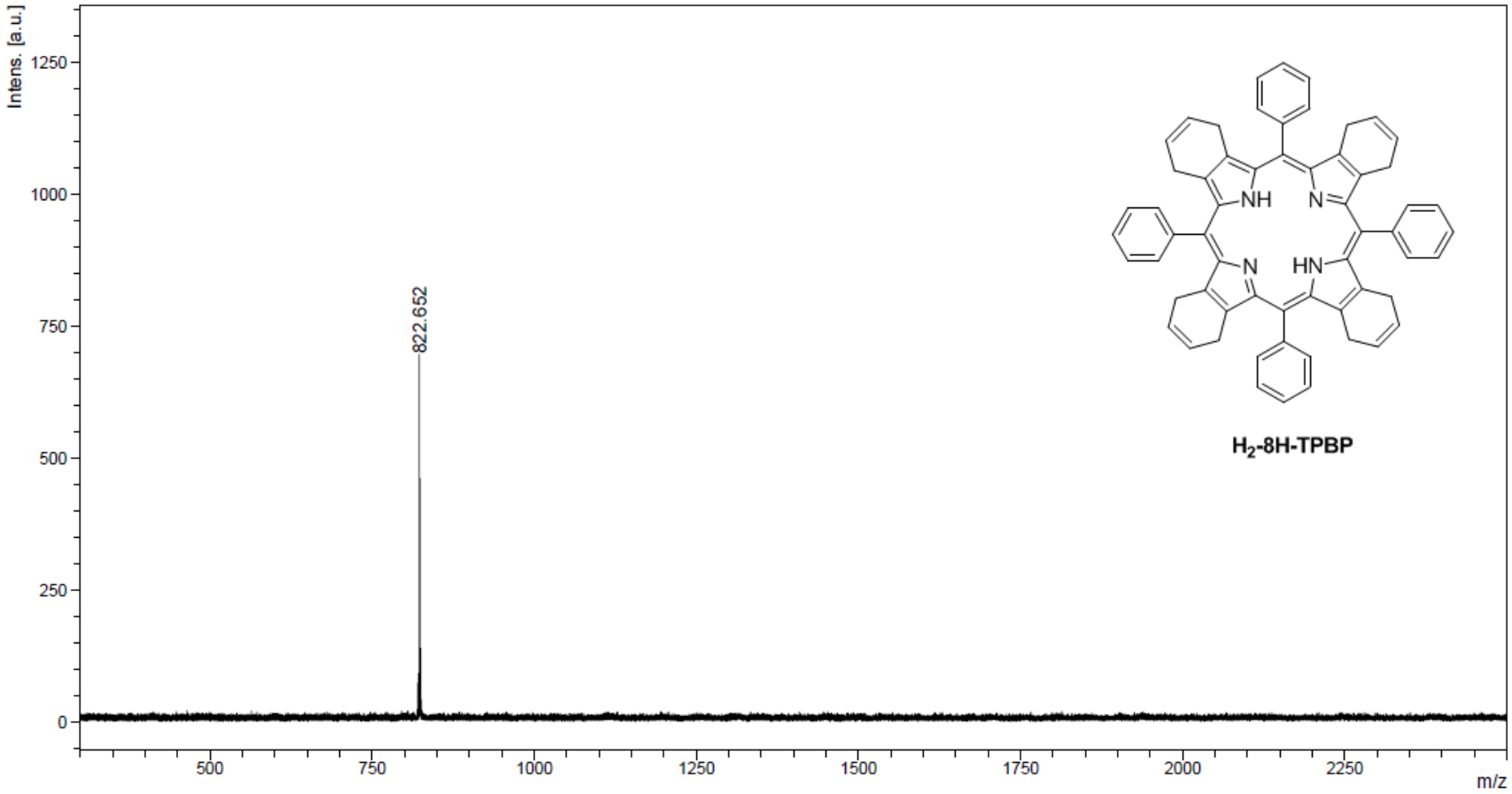

Figure A-20: Mass spectrum of compound **H_2-8H-TPBP**

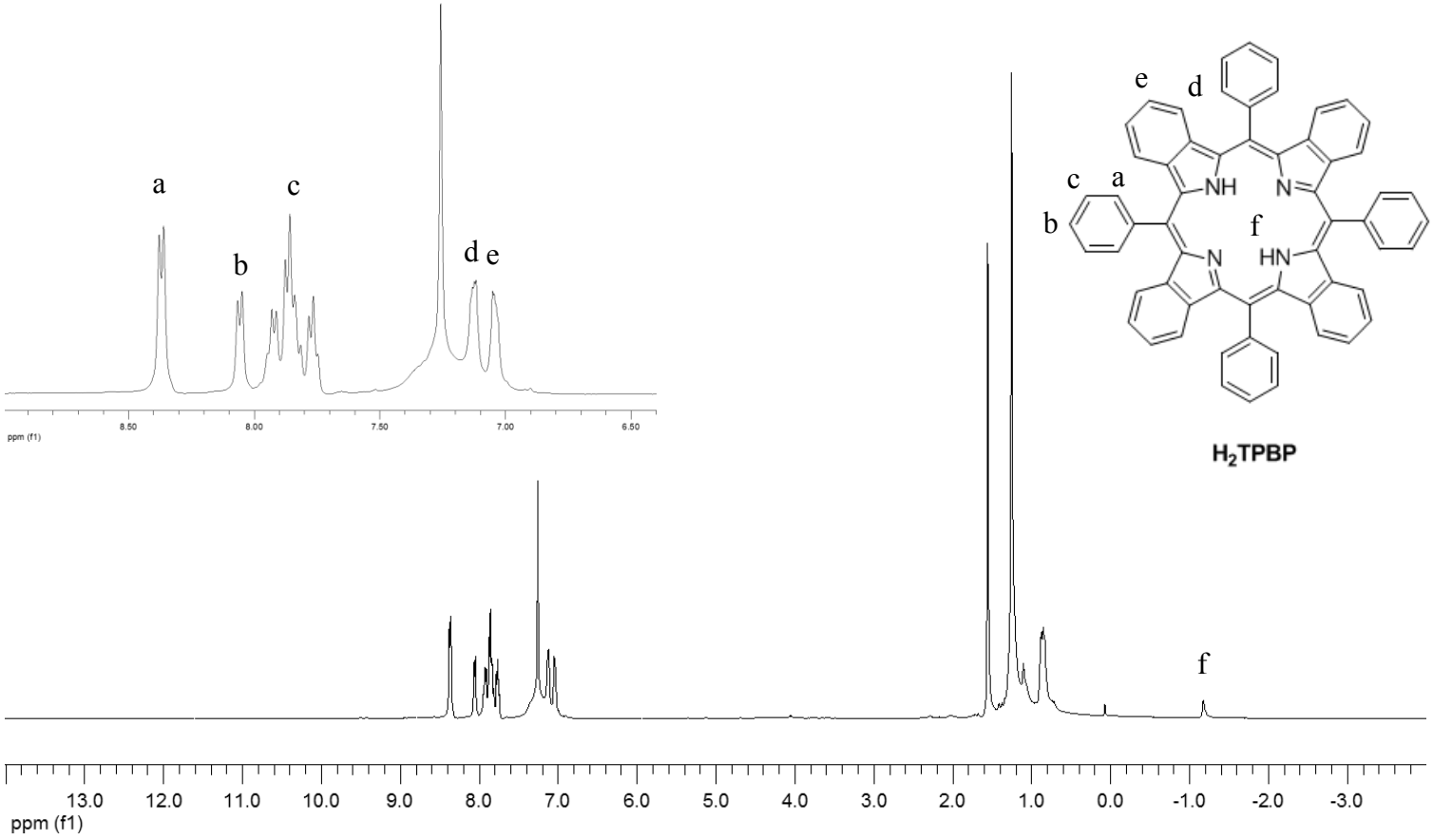

Figure A-21: ^{1}H-NMR spectrum of **H_2TPBP**

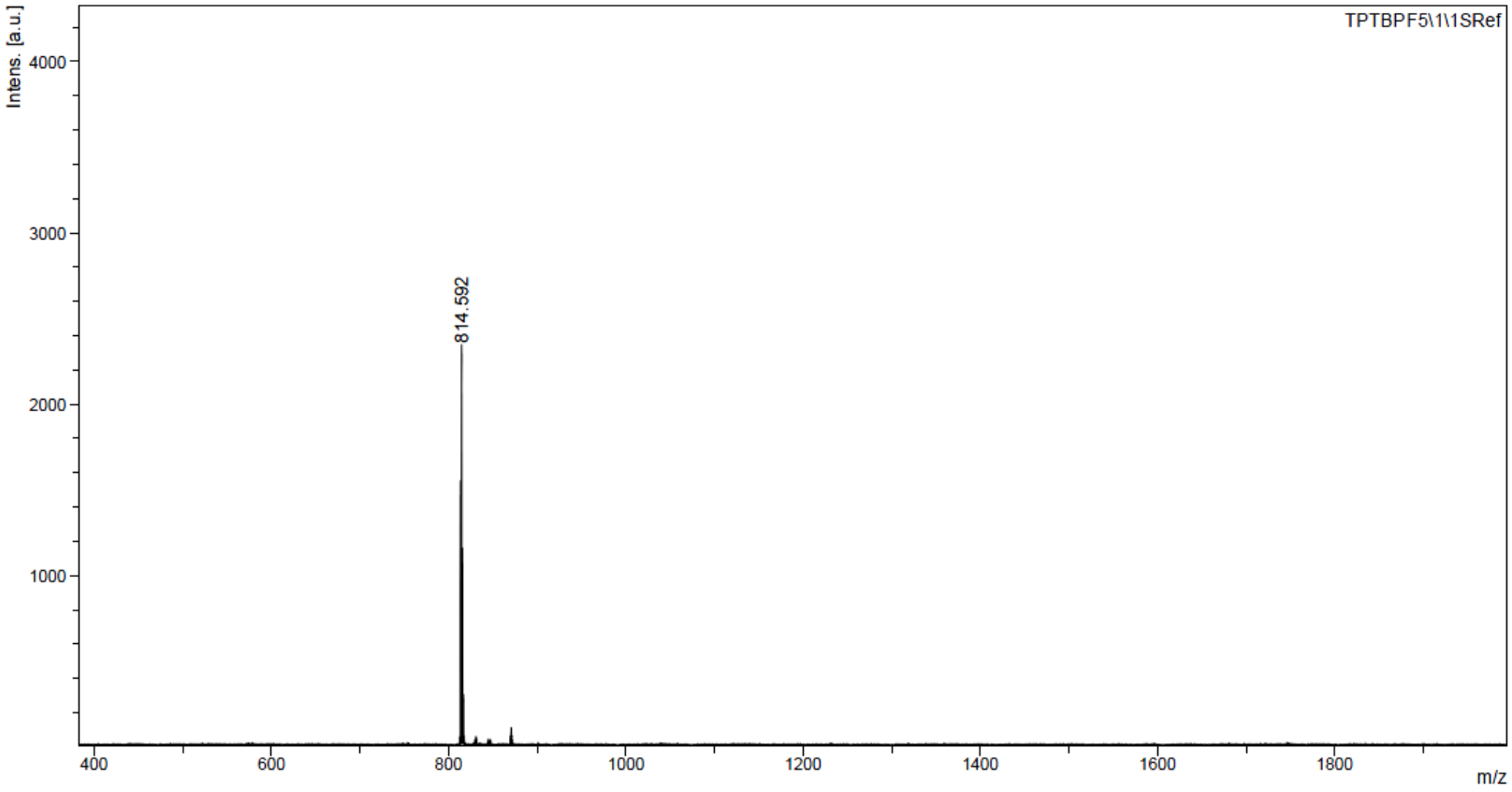

Figure A-22: Mass spectrum of compound **H_2TPBP**

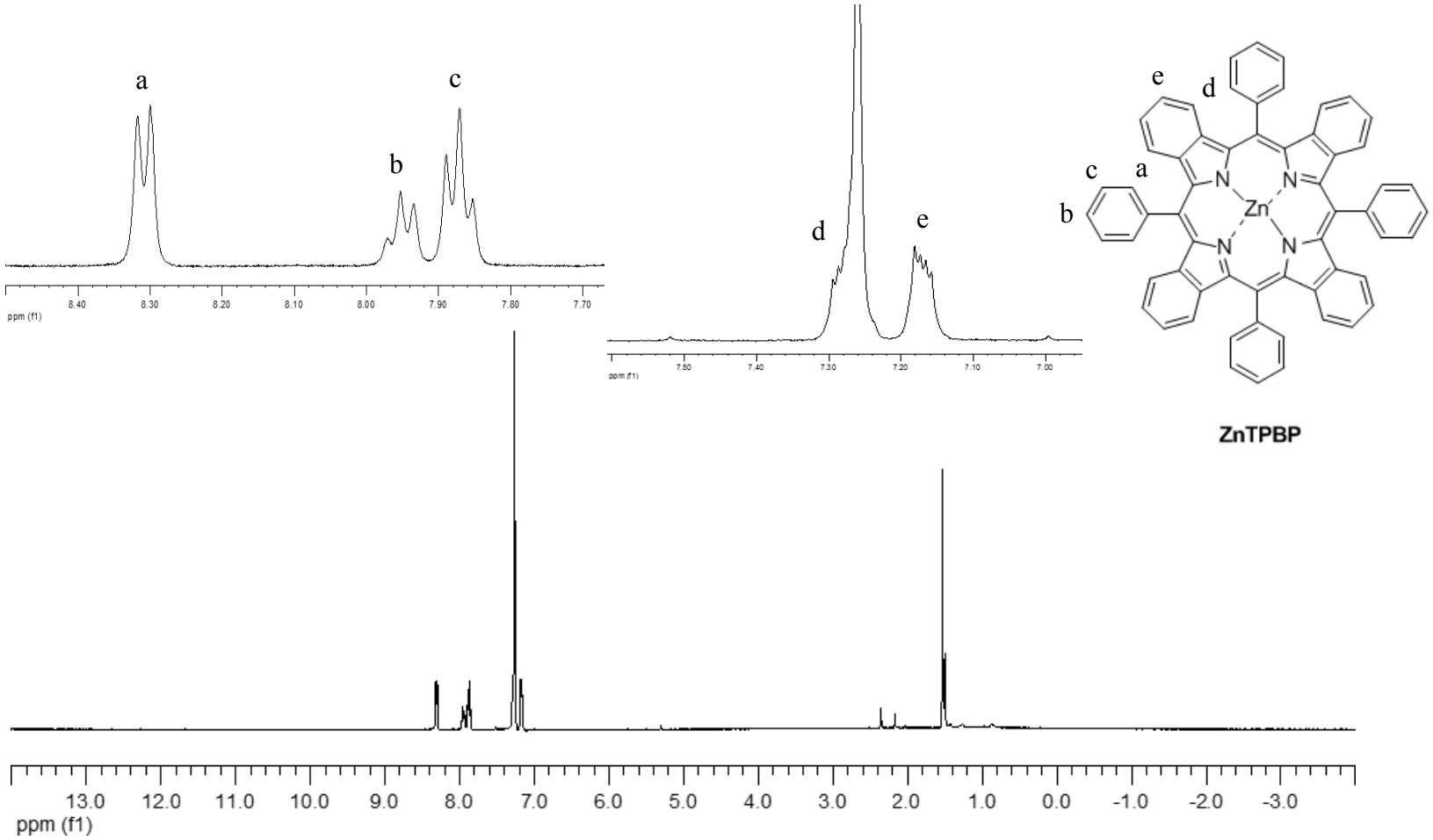

Figure A-23: ^{1}H-NMR spectrum of **ZnTPBP**

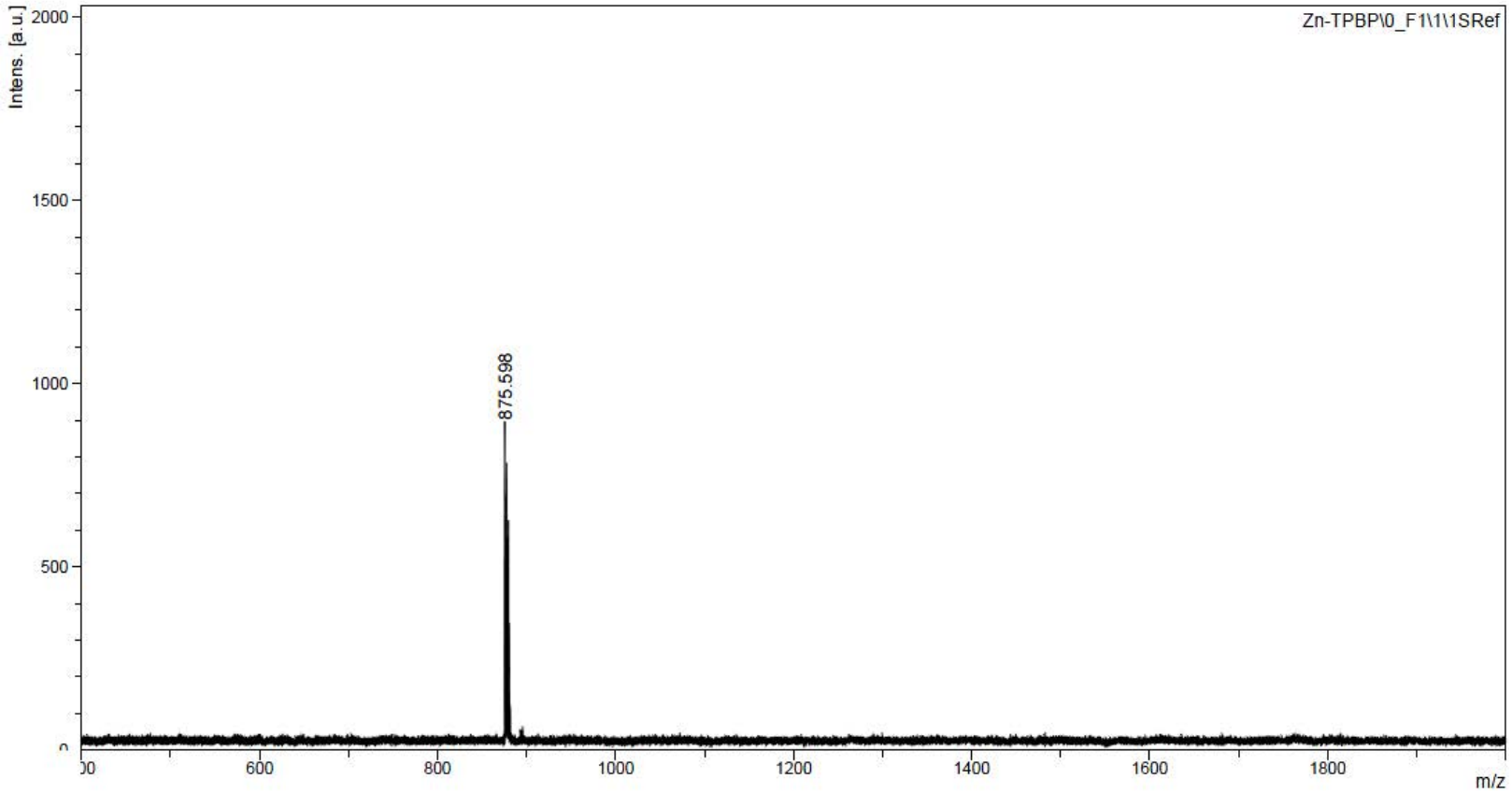

Figure A-24: Mass spectrum of **ZnTPBP**

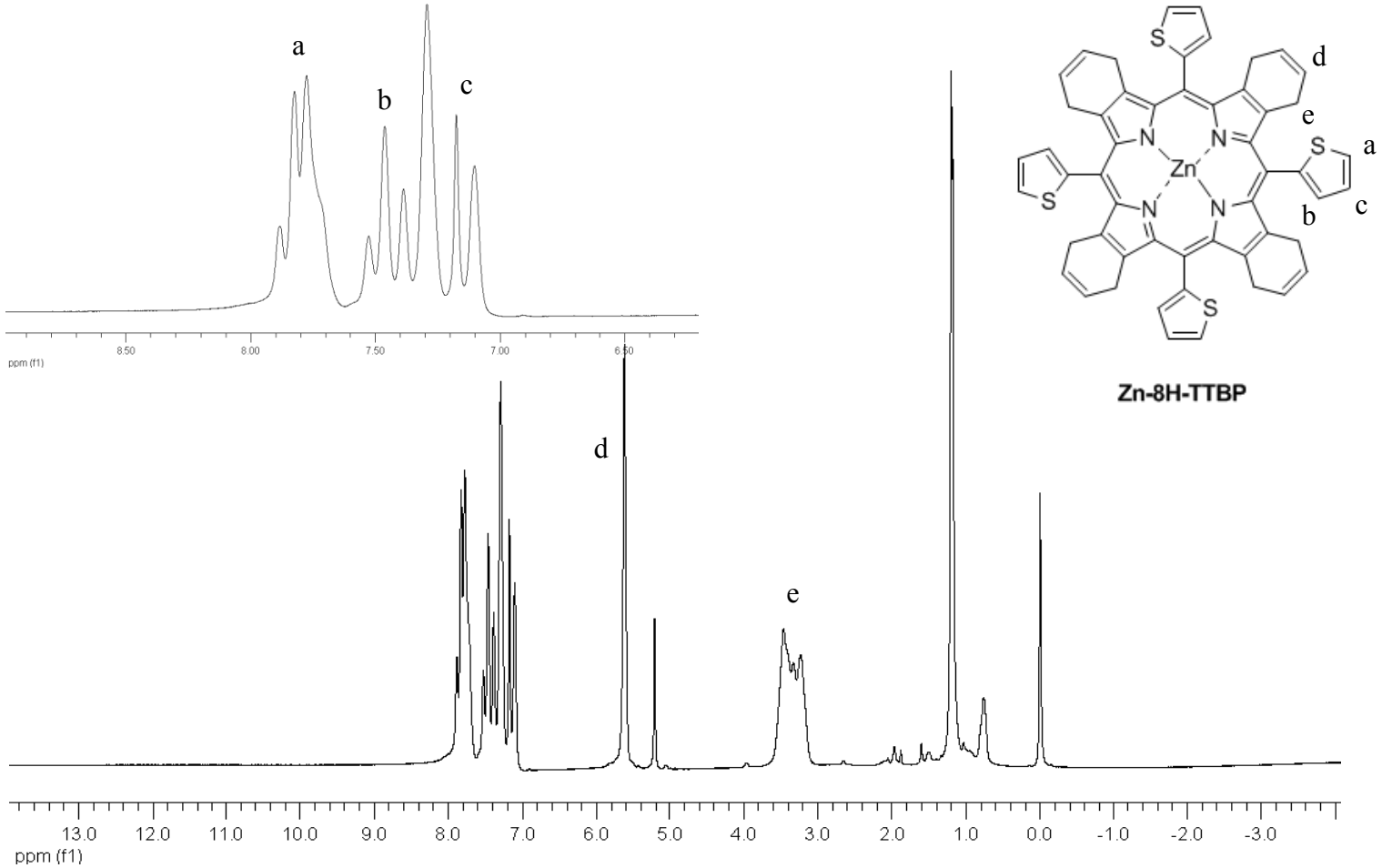

Figure A-25: ^{1}H-NMR spectrum of **Zn-8H-TTBP**

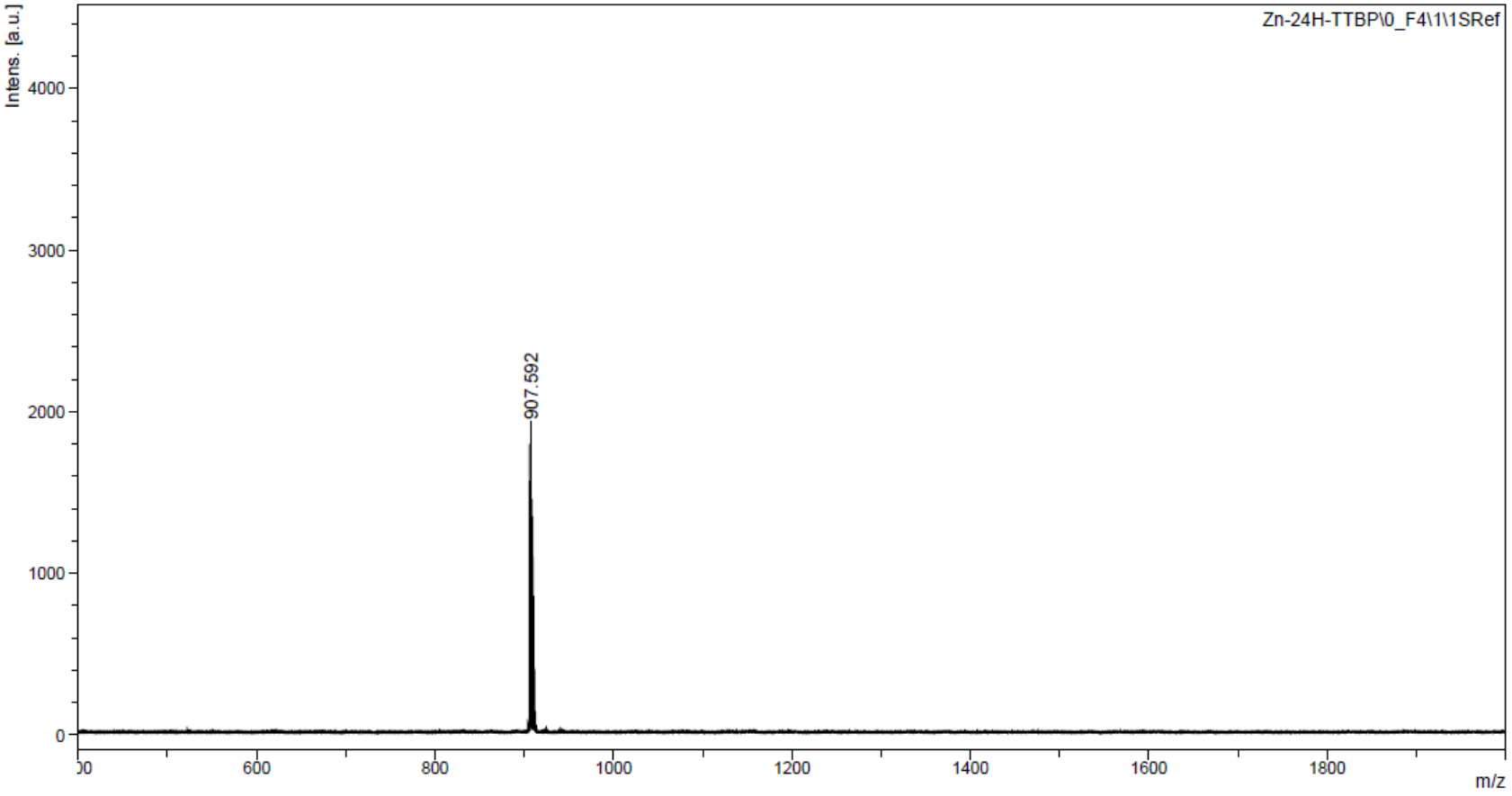

Figure A-26: Mass spectrum of **Zn-8H-TTBP**

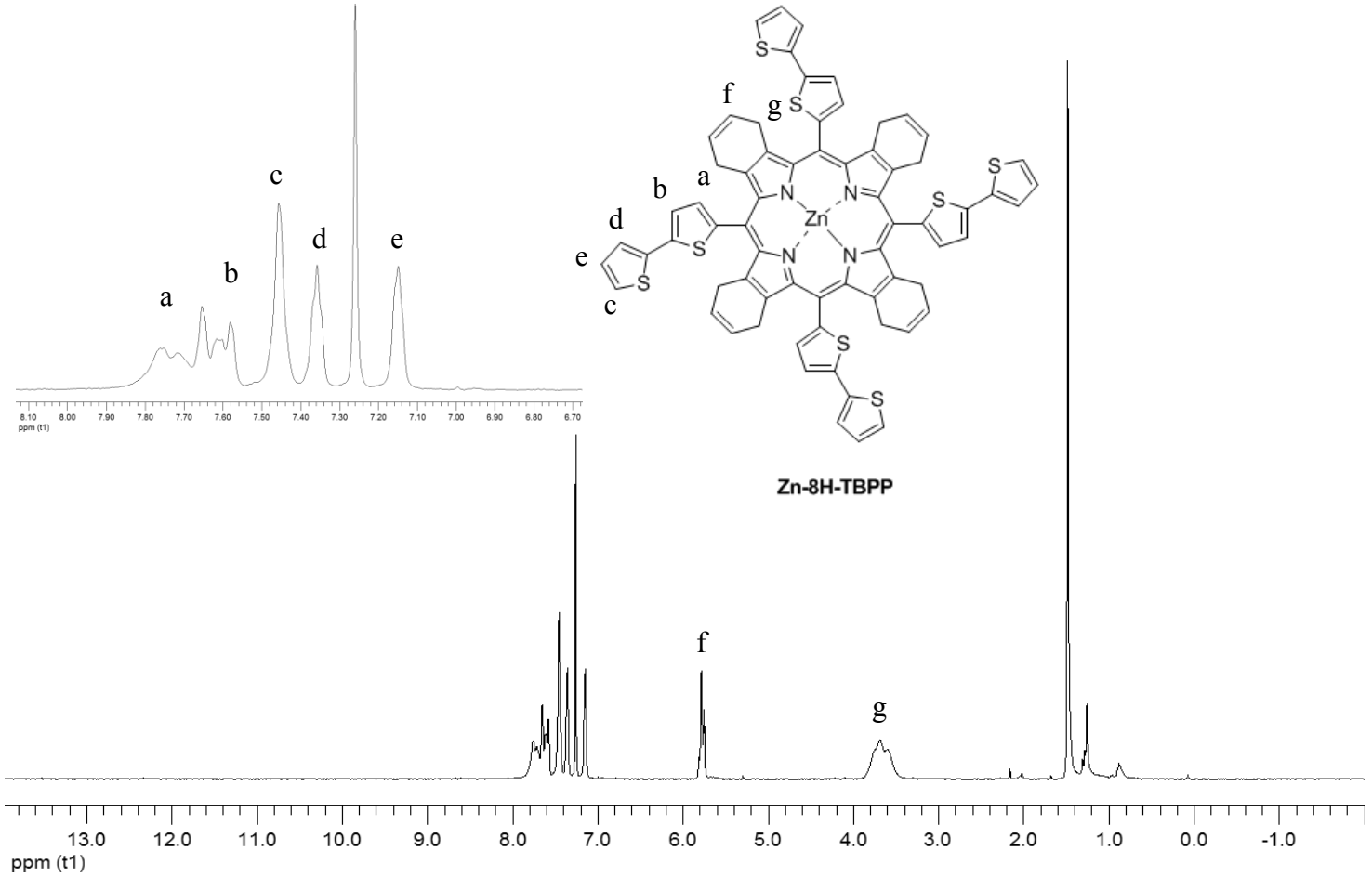

Figure A-27: ^{1}H-NMR spectrum of **Zn-8H-TBBP**

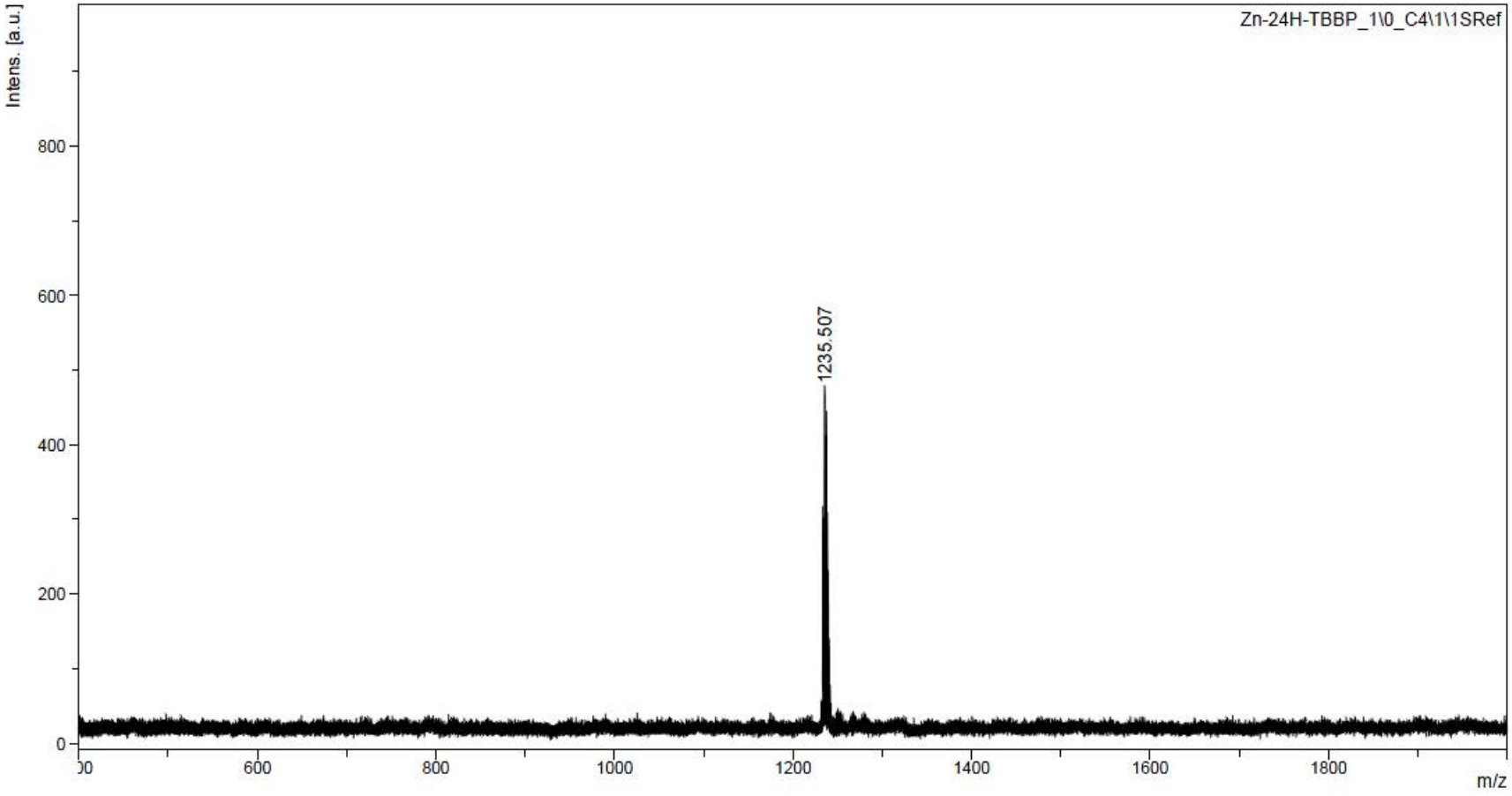

Figure A-28: Mass spectrum of **Zn-8H-TBBP**

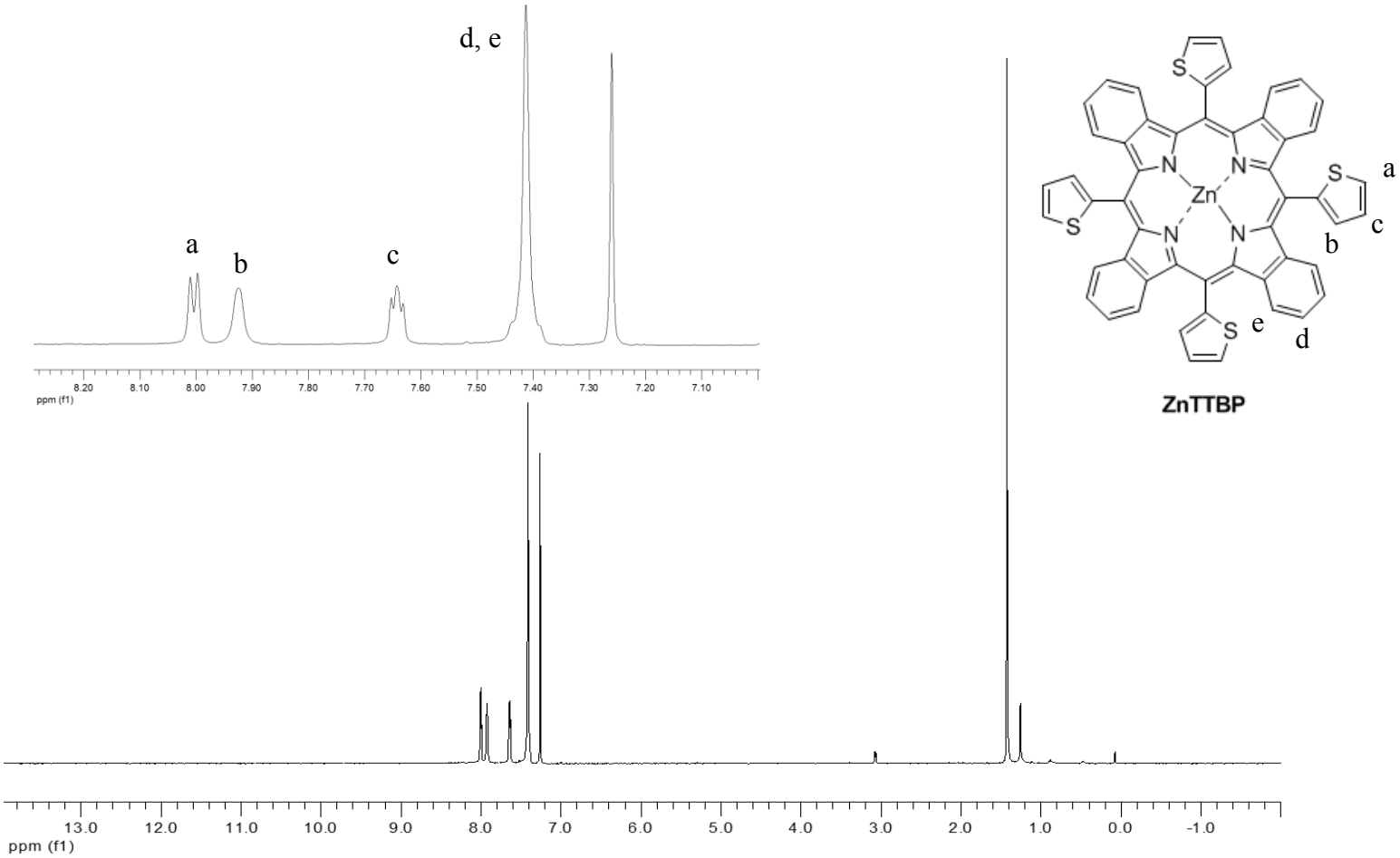

Figure A-29: ^{1}H-NMR spectrum of **ZnTTBP**

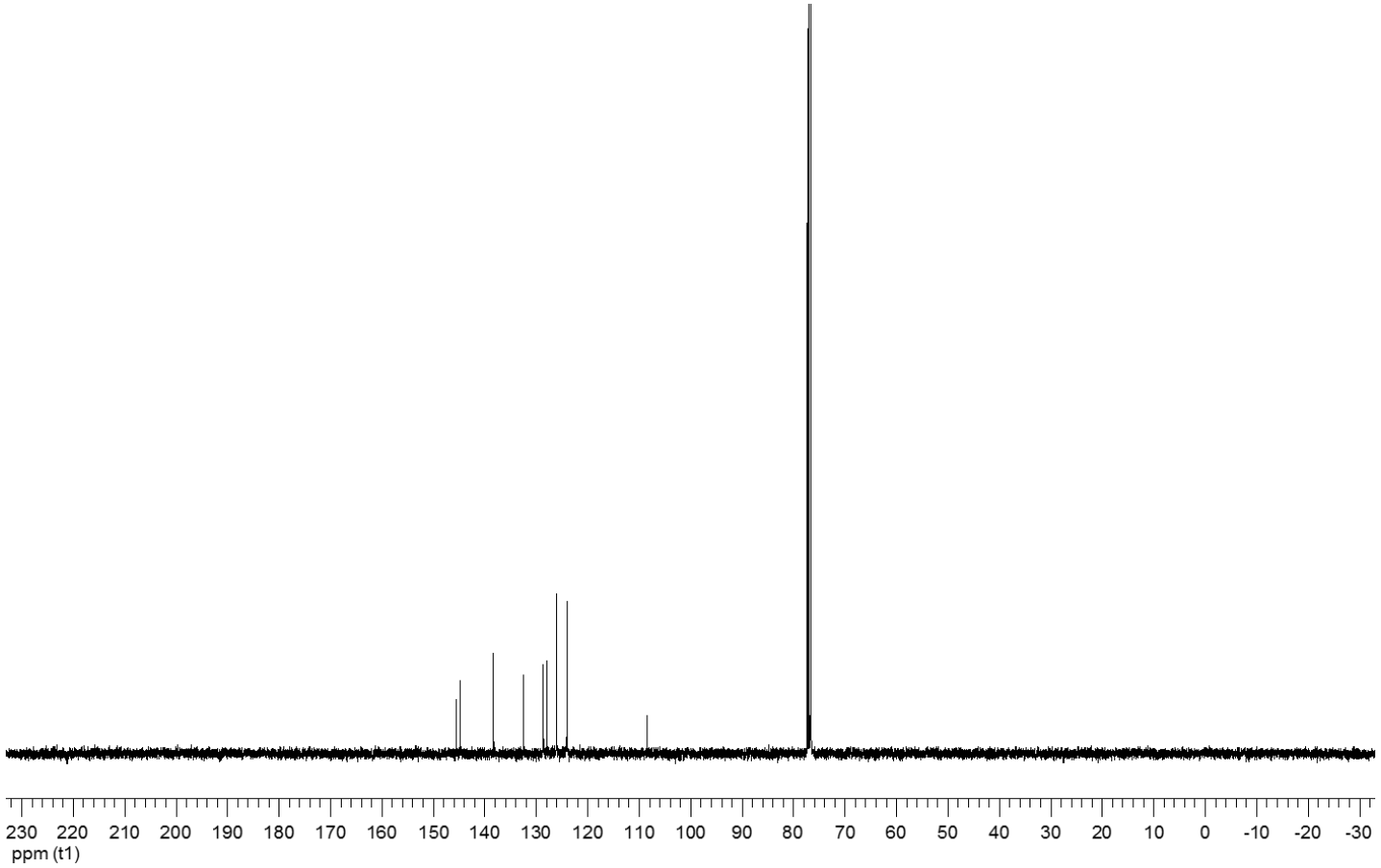

Figure A-30: ^{13}C-NMR spectrum of **ZnTTBP**

Mass Spectrum List Report

Analysis Info

Analysis Name	OSGK56071004.d	Acquisition Date	7/10/2013 6:41:05 PM
Method	Tune_wide_POS_Natee20130403.m	Operator	Administrator
Sample Name	Zn-TTBP	Instrument	micrOTOF 72
	Zn-TTBP		

Acquisition Parameter

Source Type	ESI	Ion Polarity	Positive	Set Corrector Fill	33 V
Scan Range	n/a	Capillary Exit	250.0 V	Set Pulsar Pull	386 V
Scan Begin	50 m/z	Hexapole RF	300.0 V	Set Pulsar Push	368 V
Scan End	3000 m/z	Skimmer 1	45.0 V	Set Reflector	1300 V
		Hexapole 1	24.3 V	Set Flight Tube	9000 V
				Set Detector TOF	2450 V

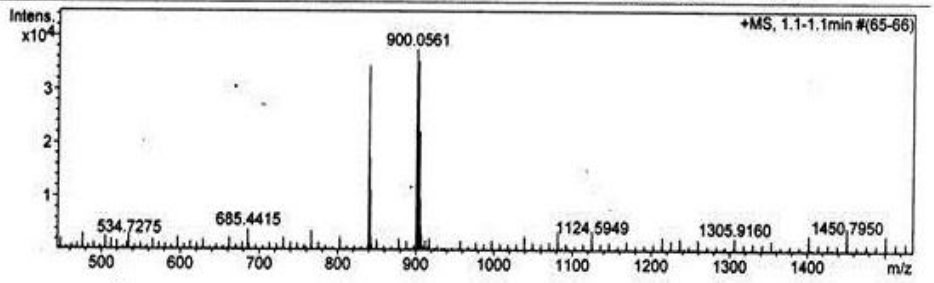

#	m/z	I	I %	S/N	FWHM	Res.
1	56.3726	4298	11.4	16.5	0.0089	6366
2	58.8167	3828	10.2	14.7	0.0063	9267
3	61.3371	3182	8.5	12.2	0.0073	8395
4	130.2382	2813	7.5	10.8	0.0451	2888
5	161.5947	3078	8.2	12.0	0.0172	9407
6	234.5839	2862	7.6	12.0	0.0100	23345
7	298.1621	3417	9.1	15.3	0.0535	5576
8	321.0893	3043	8.1	14.0	0.0368	8728
9	421.1354	2920	7.8	14.4	0.0332	12677
10	685.4415	4084	10.9	21.1	0.0876	7826
11	839.1505	34447	91.7	167.0	0.1039	8077
12	840.1523	17290	46.0	83.7	0.1149	7312
13	841.1546	11394	30.3	55.0	0.0933	9016
14	900.0561	37548	100.0	175.6	0.1215	7411
15	901.0587	21691	57.8	101.3	0.1123	8021
16	902.0540	35361	94.2	165.2	0.1137	7934
17	903.0552	19050	50.7	88.8	0.1311	6891
18	904.0540	22120	58.9	103.1	0.1235	7322
19	905.0589	9703	25.8	45.1	0.1342	6745
20	906.0543	4841	12.9	22.4	0.1023	8858
21	907.0573	2801	7.5	12.8	0.0720	12590
22	1124.5949	2870	7.6	14.4	0.1317	8539
23	1450.7449	3086	8.2	15.3	0.0745	19464
24	1450.7950	3185	8.5	15.8	0.0420	34569
25	1551.3241	2934	7.8	14.3	0.0266	58323
26	2289.5475	2867	7.6	13.1	0.0448	51117
27	2351.8446	5230	13.9	24.2	0.0334	70474
28	2352.1358	3131	8.3	14.5	0.0521	45147
29	2545.3942	3234	8.6	15.5	0.0869	29301
30	2745.7527	2795	7.4	12.8	0.0354	77481

Figure A-31: High resolution mass spectrum of compound **ZnTTBP**

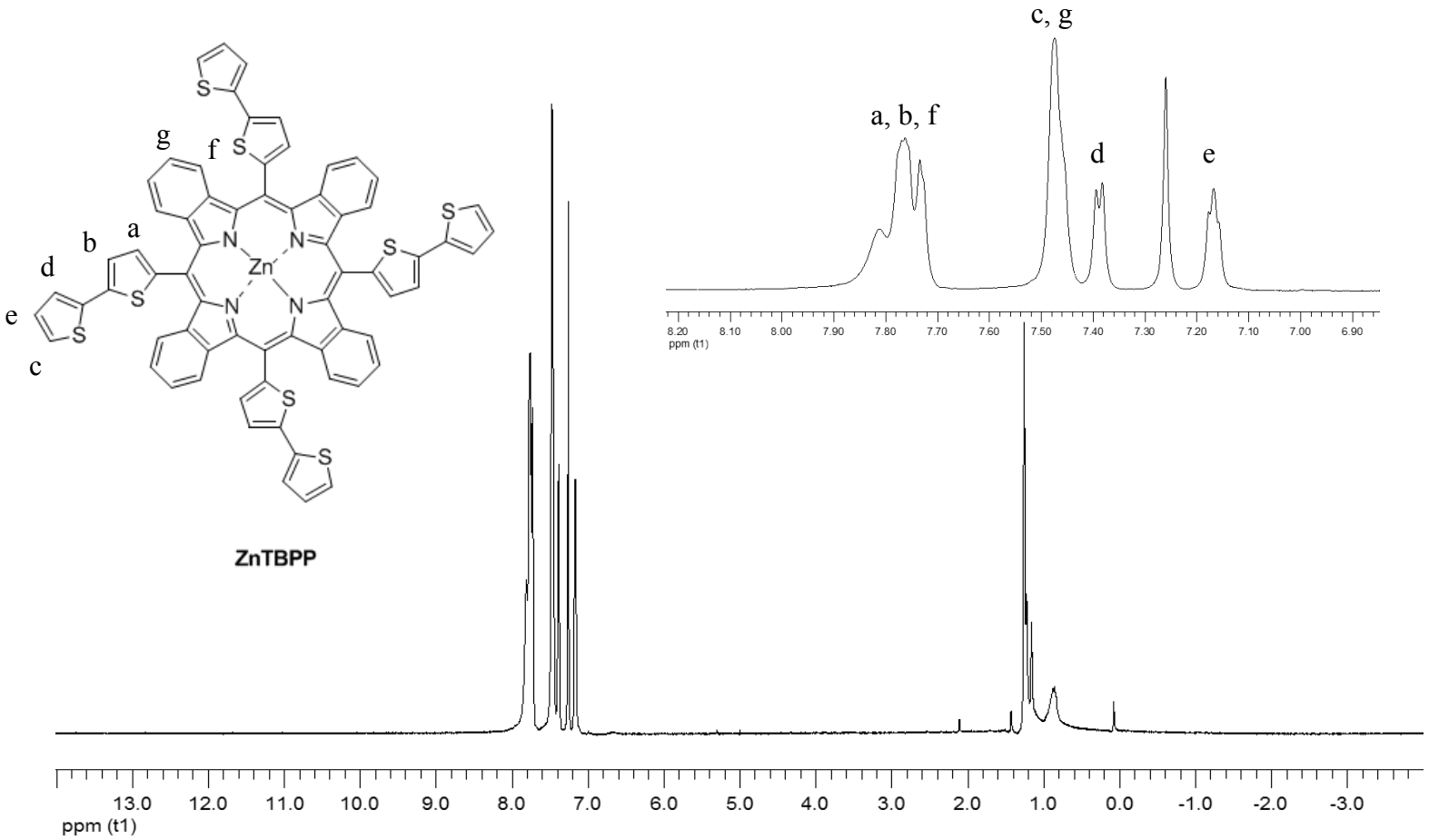

Figure A-32: ^{1}H-NMR spectrum of **ZnTBBP**

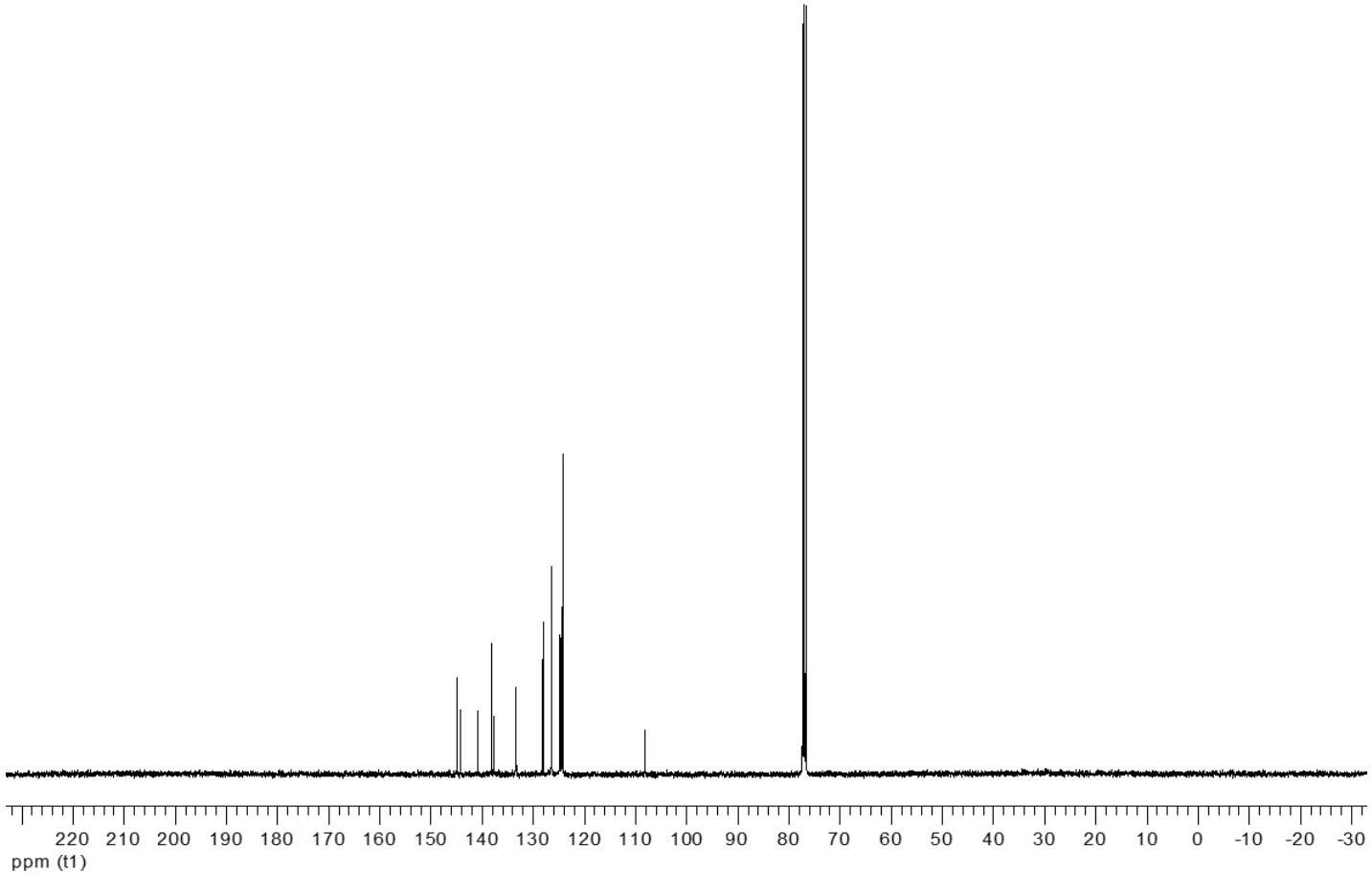

Figure A-33: ^{13}C-NMR spectrum of **ZnTBBP**

Mass Spectrum List Report

Analysis Info

Analysis Name	OSCUGK56082001.d	Acquisition Date	8/20/2013 4:56:51 PM
Method	MKE_tune_wide_20130204.m	Operator	Administrator
Sample Name	Zn-TBBP	Instrument	micrOTOF 72
	Zn-TBBP		

Acquisition Parameter

Source Type	ESI	Ion Polarity	Positive	Set Corrector Fill	75 V
Scan Range	n/a	Capillary Exit	400.0 V	Set Pulsar Pull	398 V
Scan Begin	50 m/z	Hexapole RF	800.0 V	Set Pulsar Push	380 V
Scan End	3000 m/z	Skimmer 1	45.0 V	Set Reflector	1300 V
		Hexapole 1	25.0 V	Set Flight Tube	9000 V
				Set Detector TOF	1910 V

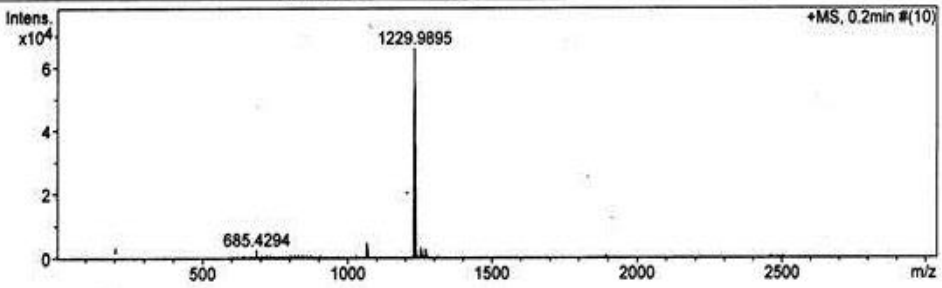

#	m/z	I	I %	S/N	FWHM	Res.
1	685.4294	2607	3.9	109.7	0.0671	10208
2	1064.0131	4373	6.6	180.2	0.0975	10909
3	1065.0183	3354	5.1	137.7	0.0944	11283
4	1066.0141	4753	7.2	196.3	0.0960	11110
5	1067.0141	3226	4.9	132.5	0.0982	10862
6	1068.0106	3681	5.6	151.6	0.0990	10792
7	1069.0115	2365	3.6	96.6	0.0932	11466
8	1070.0116	1473	2.2	59.2	0.0922	11606
9	1227.9895	52494	79.5	1799.4	0.1091	11252
10	1228.9924	45643	69.1	1560.9	0.1077	11406
11	1229.9895	66031	100.0	2254.1	0.1104	11140
12	1230.9908	51199	77.5	1743.5	0.1069	11518
13	1231.9879	54334	82.3	1846.4	0.1092	11286
14	1232.9885	35460	53.7	1201.7	0.1086	11355
15	1233.9870	22449	34.0	758.4	0.1104	11179
16	1234.9878	11526	17.5	387.6	0.1133	10900
17	1235.9854	5687	8.6	189.8	0.1112	11114
18	1236.9873	2477	3.8	81.4	0.1075	11503
19	1250.9806	2664	4.0	85.1	0.1040	12030
20	1251.9829	1985	3.0	62.8	0.1108	11297
21	1252.9761	3085	4.7	98.5	0.1052	11915
22	1253.9813	2270	3.4	71.8	0.1102	11377
23	1254.9765	2572	3.9	81.5	0.1100	11409
24	1255.9813	1625	2.5	50.7	0.1140	11016
25	1266.9558	2401	3.6	74.1	0.1116	11352
26	1267.9538	1957	3.0	59.9	0.1058	11984
27	1268.9526	2762	4.2	85.2	0.1091	11633
28	1269.9543	2036	3.1	62.2	0.1143	11106
29	1270.9529	2322	3.5	71.0	0.1123	11321
30	1271.9549	1570	2.4	47.4	0.1111	11447

Figure A-34: High resolution mass spectrum of compound **ZnTBBP**

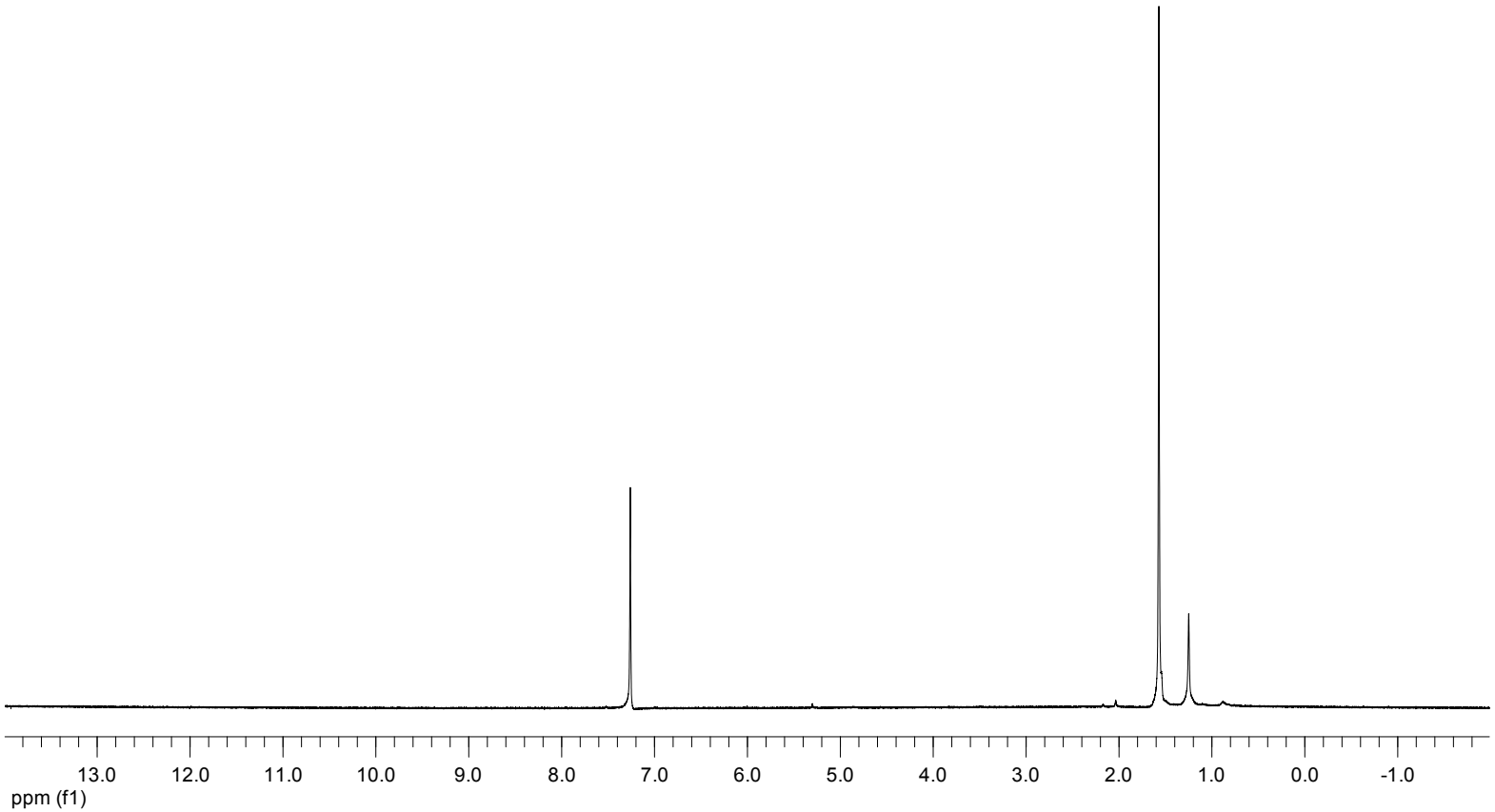

Figure A-35: ^{1}H-NMR spectrum of $CDCl_3$

APPENDIX B

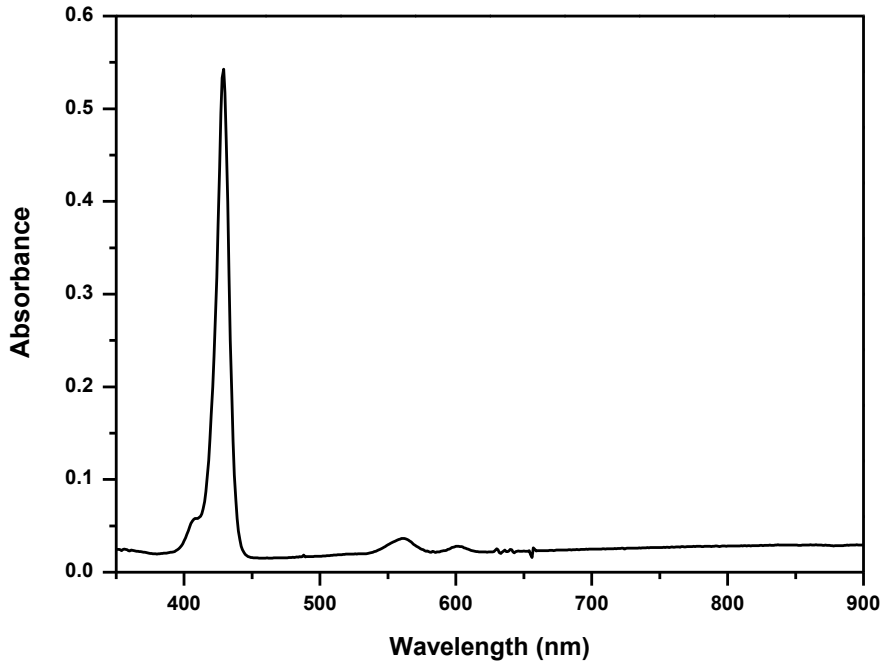

Figure B-1: Absorption spectrum of compound **ZnTPP** in toluene

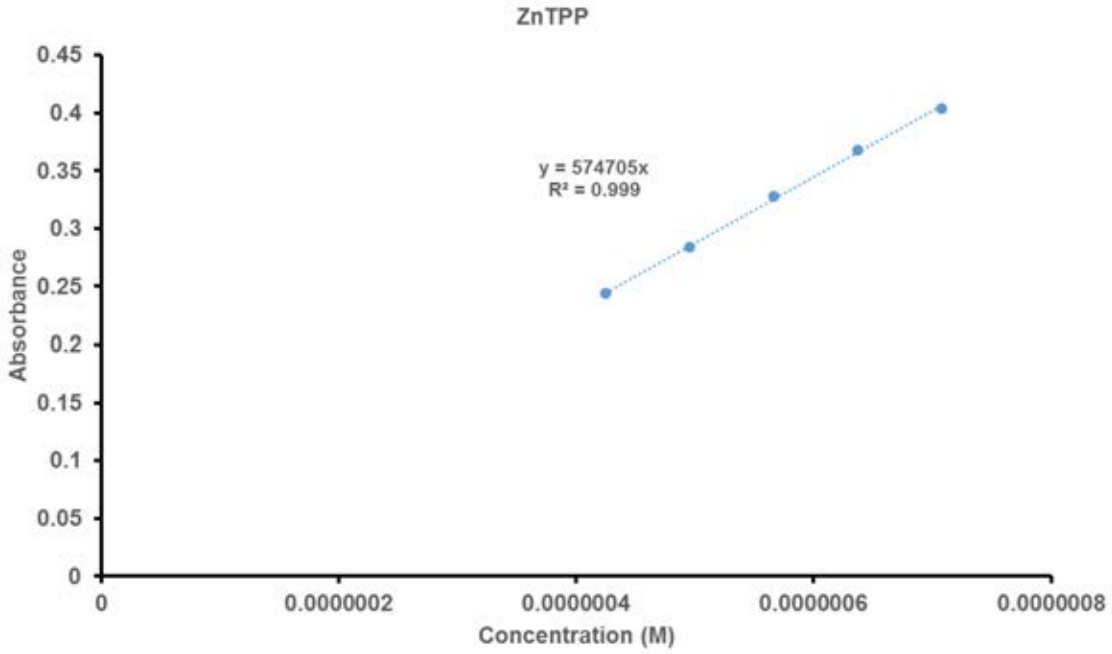

Figure B-2: Calibration curve for quantitative determination of compound **ZnTPP** in toluene (λ_{abs} = 429 nm)

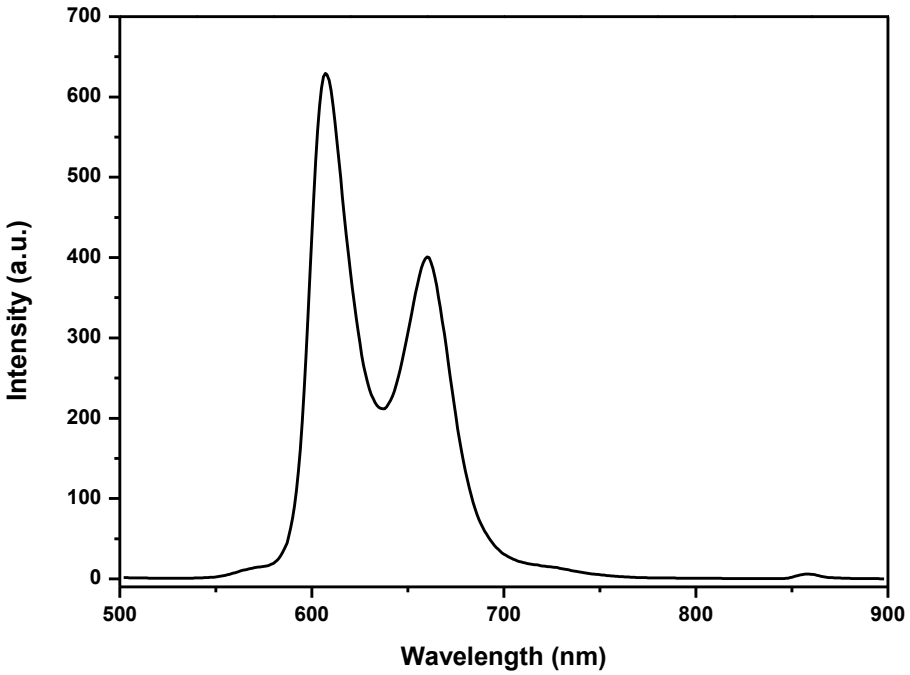

Figure B-3: Emission spectrum of compound **ZnTPP** in toluene (λ_{ex} = 429 nm)

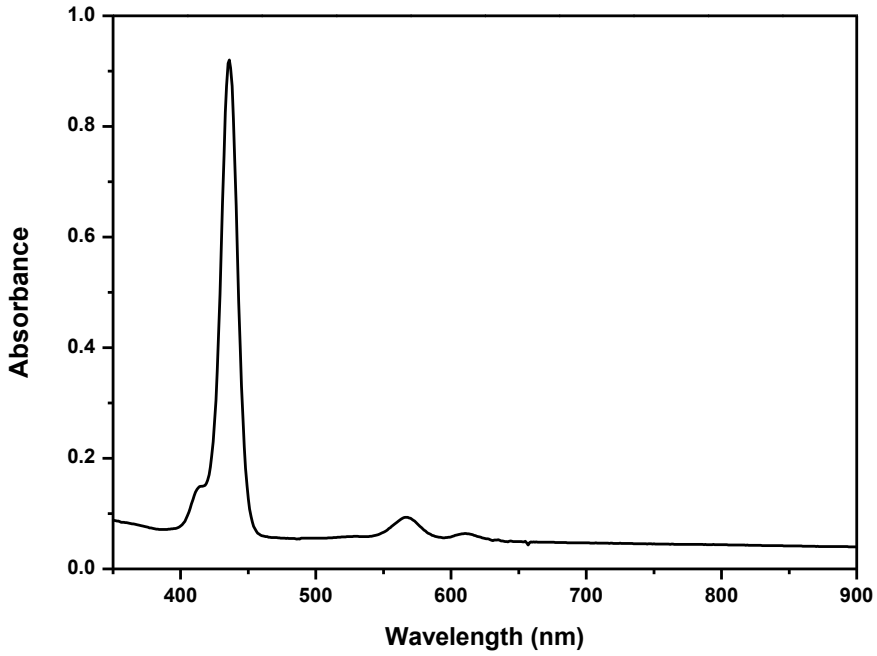

Figure B-4: Absorption spectrum of compound **ZnTTP** in toluene

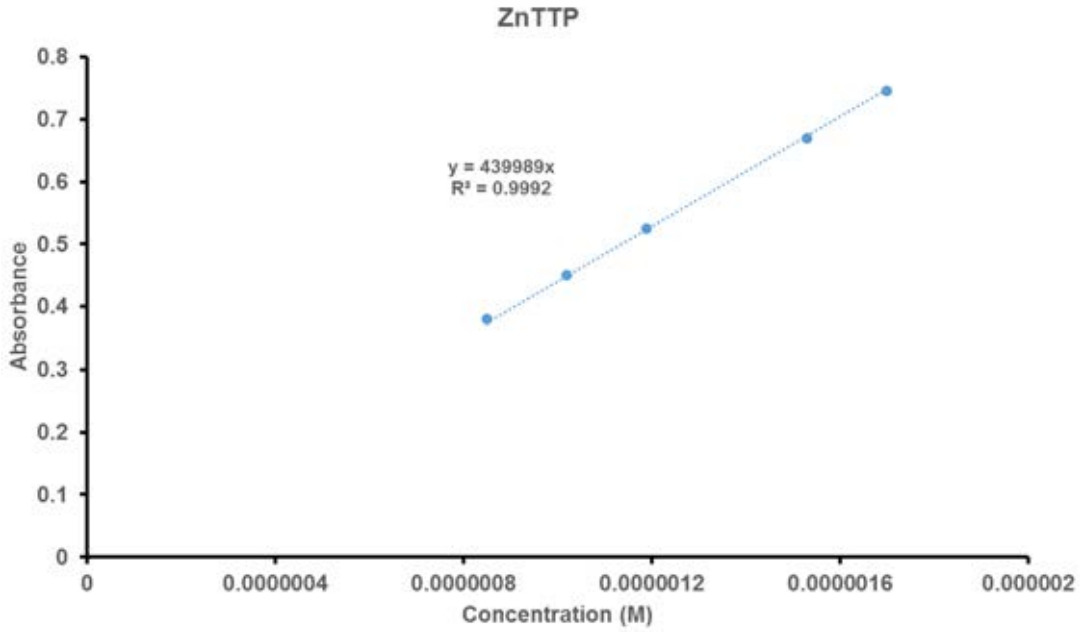

Figure B-5: Calibration curve for quantitative determination of compound **ZnTTP** in toluene (λ_{abs} = 436 nm)

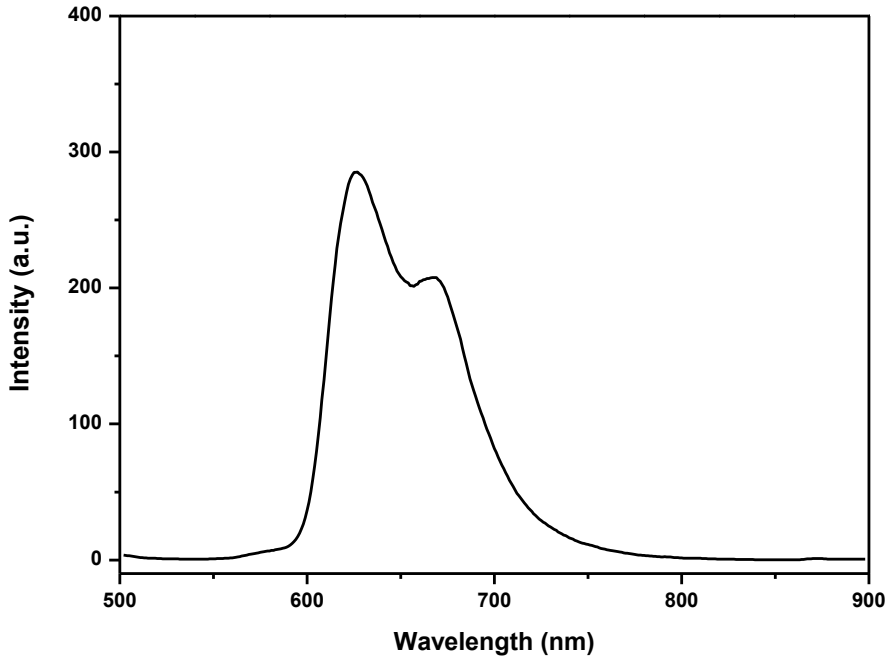

Figure B-6: Emission spectrum of compound **ZnTTP** in toluene (λ_{ex} = 436 nm)

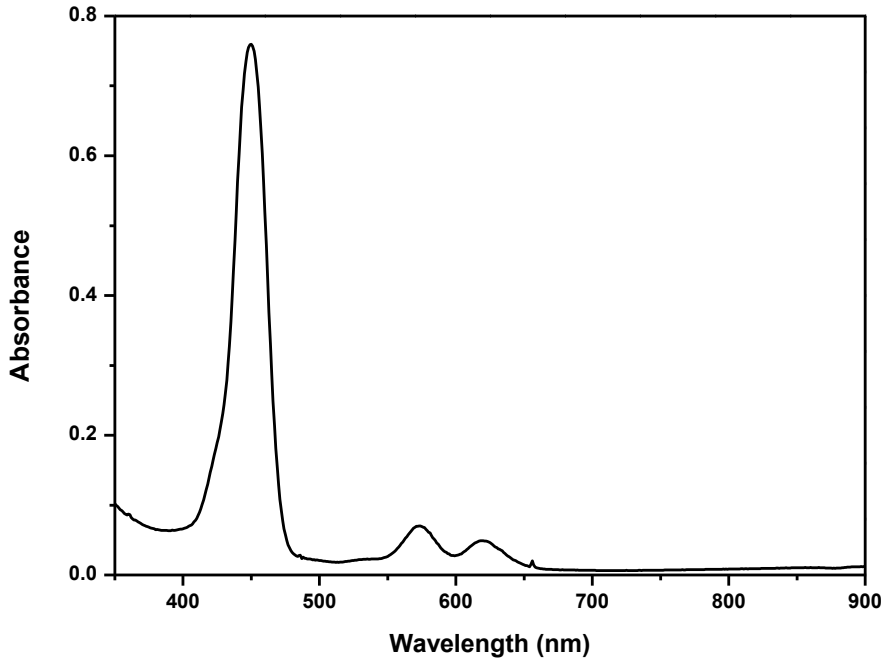

Figure B-7: Absorption spectrum of compound **ZnTBP** in toluene

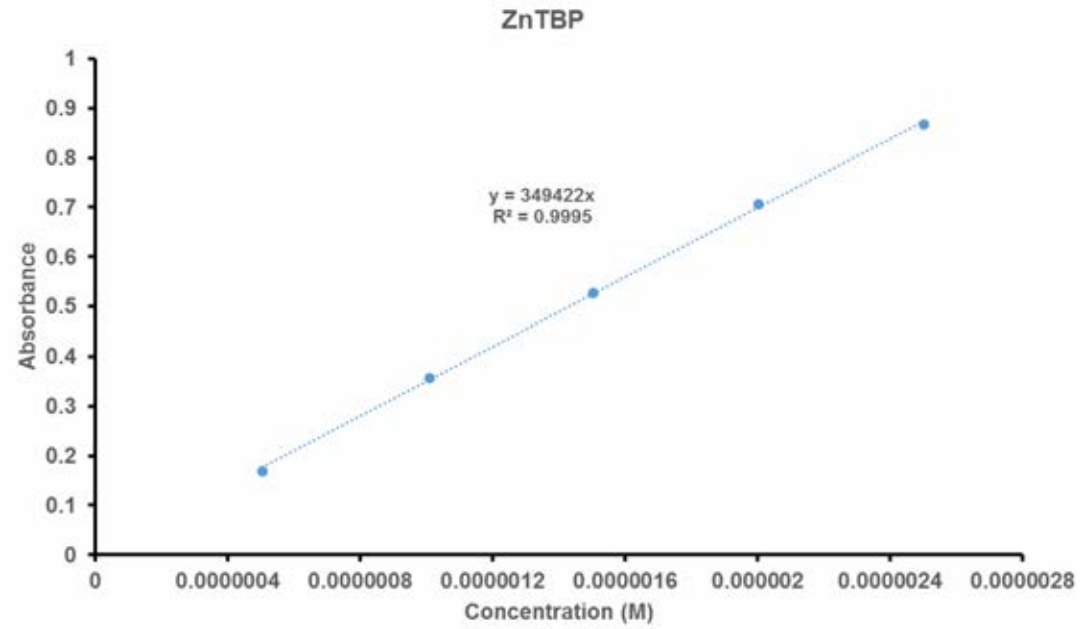

Figure B-8: Calibration curve for quantitative determination of compound **ZnTTP** in toluene (λ_{abs} = 450 nm)

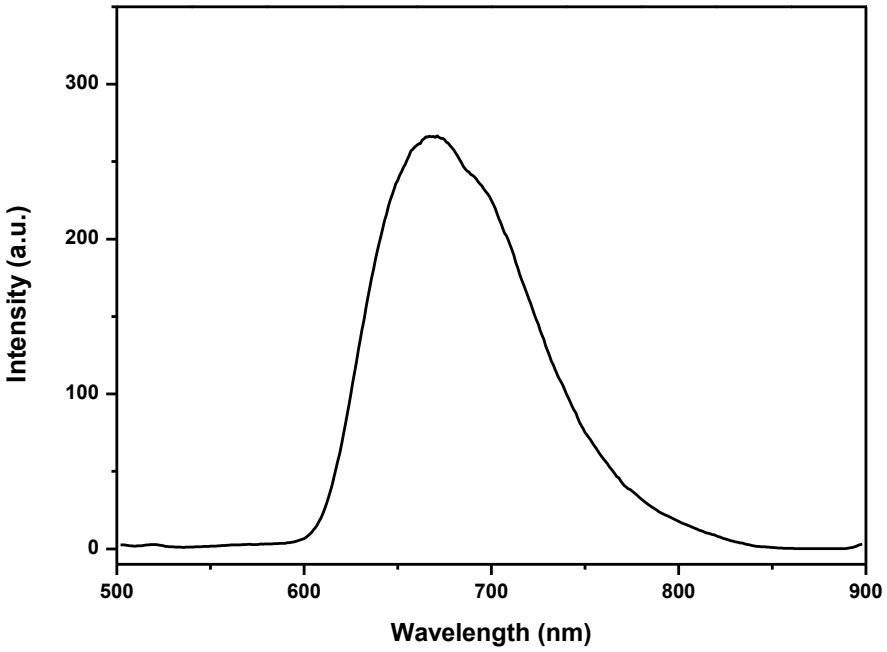

Figure B-9: Emission spectrum of compound **ZnTBP** in toluene (λ_{ex} = 450 nm)

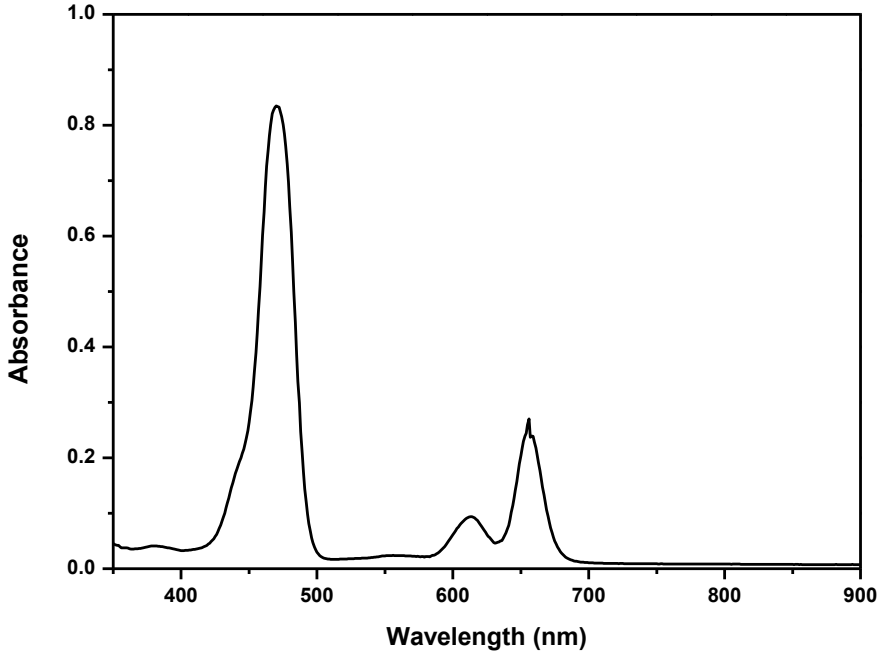

Figure B-10: Absorption spectrum of compound **ZnTPBP** in toluene

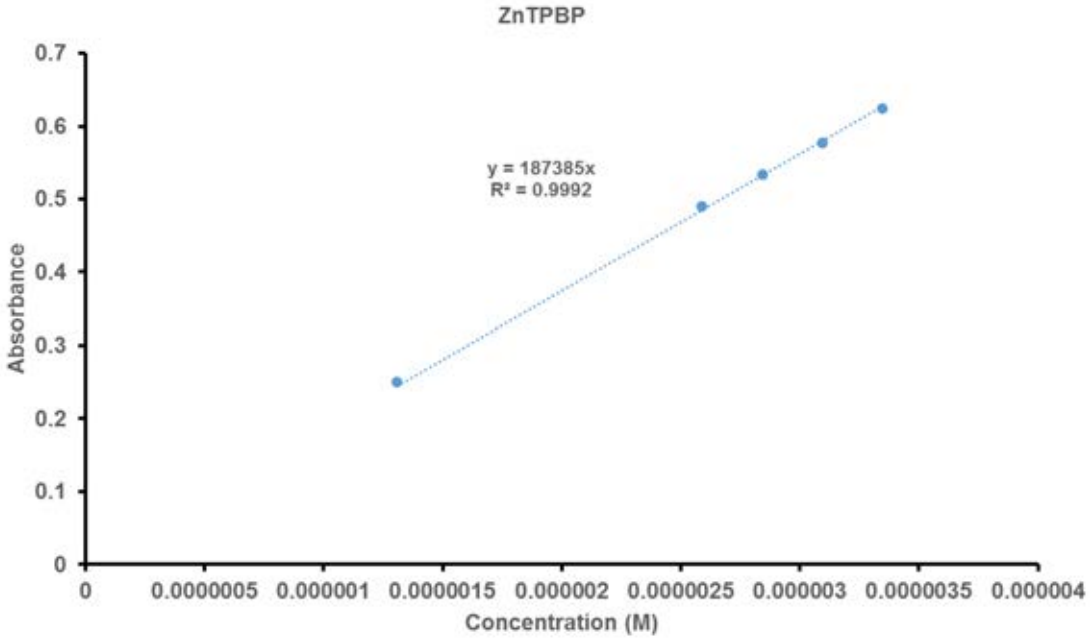

Figure B-11: Calibration curve for quantitative determination of compound **ZnTPBP** in toluene (λ_{abs} = 470 nm)

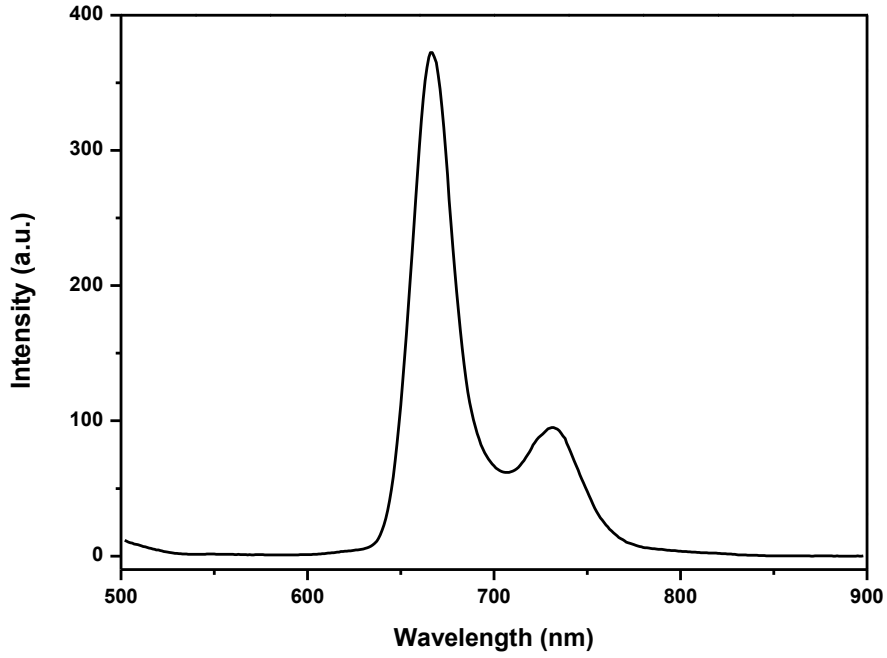

Figure B-12: Emission spectrum of compound **ZnTPBP** in toluene (λ_{ex} = 471 nm)

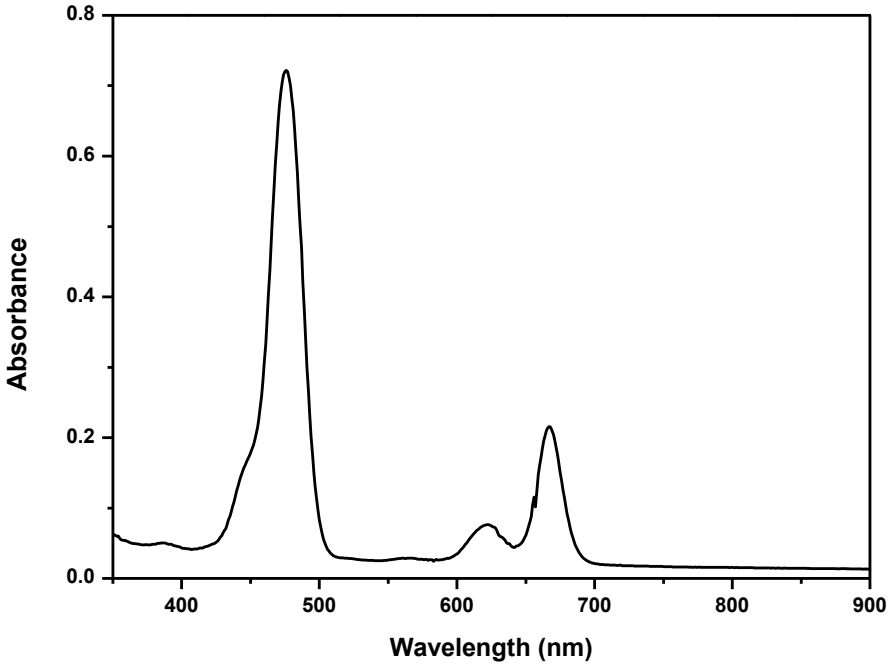

Figure B-13: Absorption spectrum of compound **ZnTTBP** in toluene

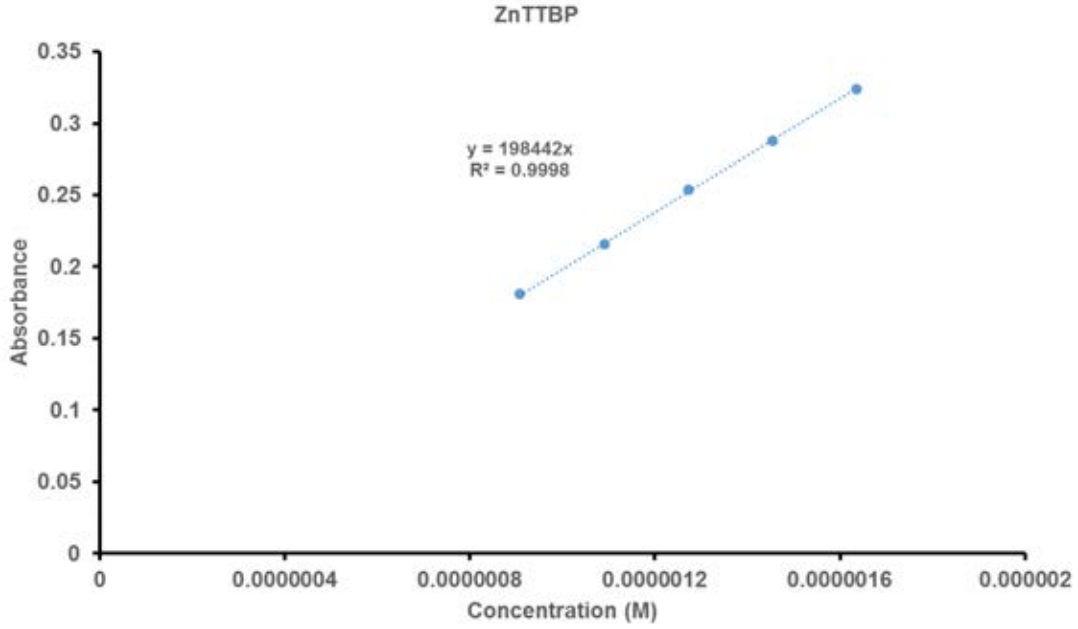

Figure B-14: Calibration curve for quantitative determination of compound **ZnTTBP** in toluene (λ_{abs} = 476 nm)

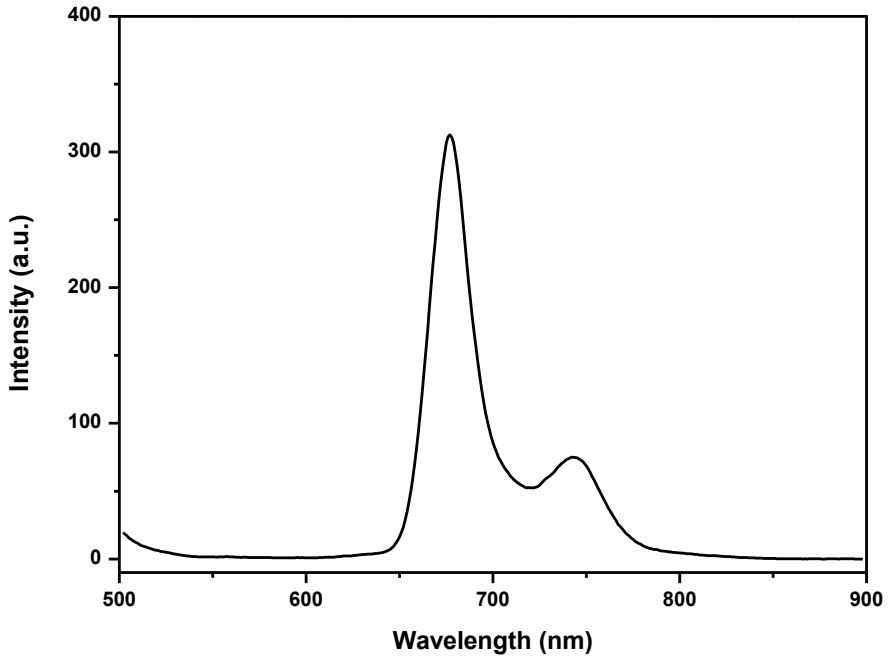

Figure B-15: Emission spectrum of compound **ZnTTBP** in toluene (λ_{ex} = 476 nm)

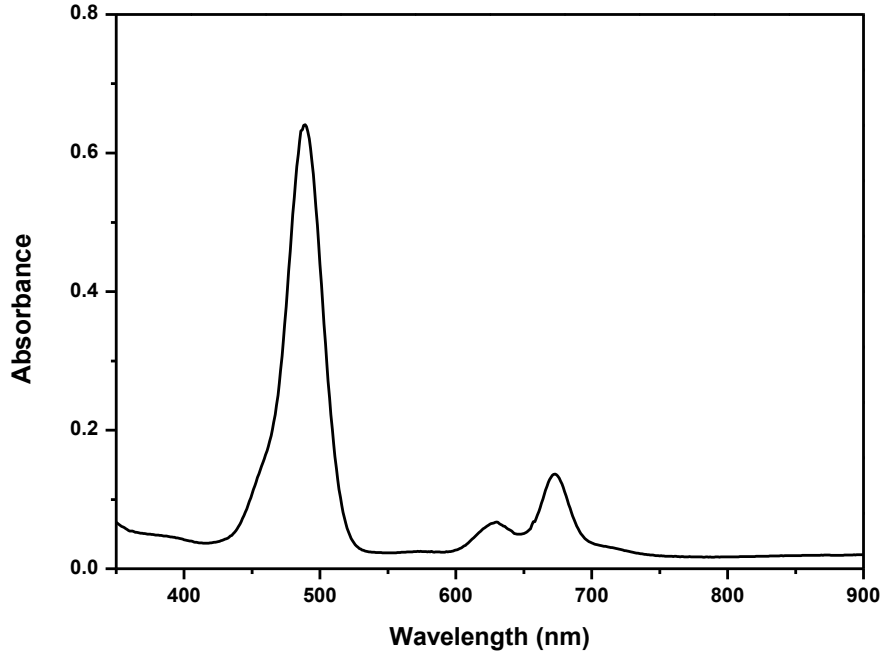

Figure B-16: Absorption spectrum of compound **ZnTBBP** in toluene

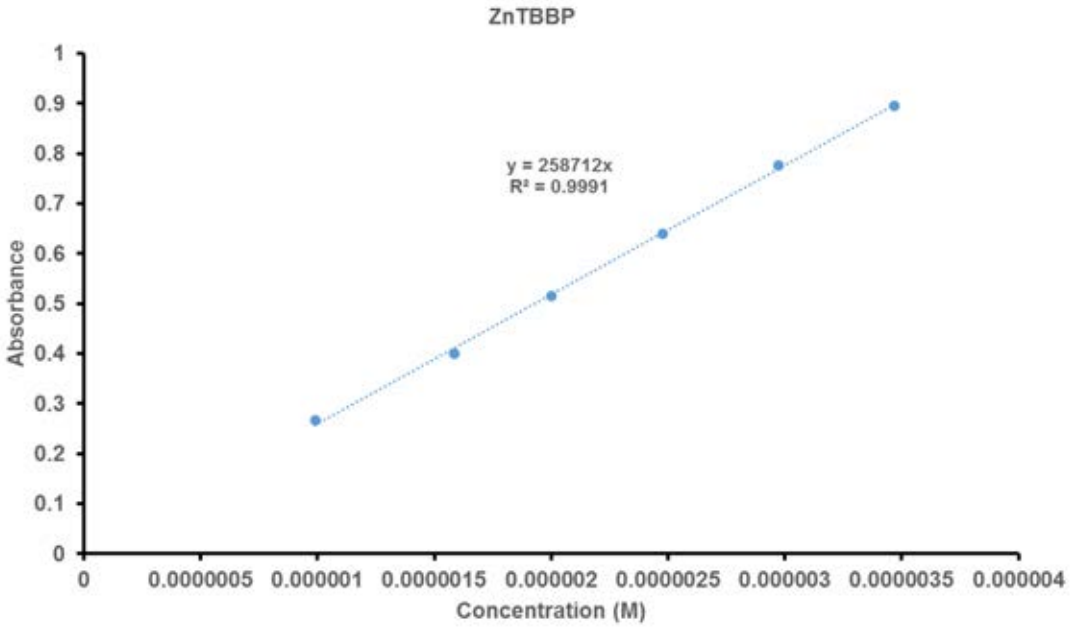

Figure B-17: Calibration curve for quantitative determination of compound **ZnTBBP** in toluene (λ_{abs} = 487 nm)

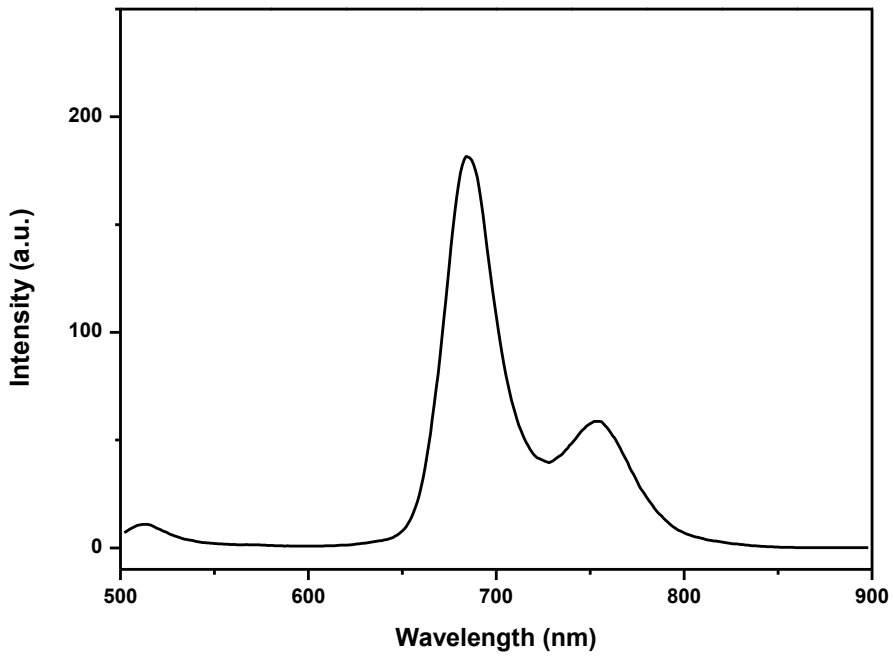

Figure B-18: Emission spectrum of compound **ZnTTBP** in toluene (λ_{ex} = 489 nm)

VITA

Mister Wittawat Keawsongsaeng was born on May 17, 1988 in Nakhonsawan, Thailand. He got a Bachelor Degree of Chemistry from Faculty of Science at Chulalongkorn University, Bangkok in 2009. Then, he was admitted into a Master Degree in the major of Chemistry, Faculty of Science, Chulalongkorn University, Bangkok in 2009 and completed the program in 2013.